rec'd with letter dtd. 2/12/93

Raytheon Services Nevada	**DESIGN ANALYSIS** Number: ST-MN-216 Rev: 0 Page 1 of 106

WBS No. 1.2.6	PRINT NAME	SIGNATURE	TITLE	DATE
ORIGINATOR:	SAEED BONABIAN	Saeed Bonabian	Sr. Engineer	10-12-92
CHECKER:	Edward F. Fitch	Edward F. Fitch	Principal Engineer	10/12/92
APPROVAL - LDE:	W. R. KENNEDY	W R Kennedy	LEAD MINING ENGR	10/13/92
APPROVAL - SCDM:	Bruce T. Stanley	Bruce T. Stanley	DESIGN MANAGER	10/13/92
QA CONCURRENCE:	DJ TUNNEY	DJ Tunney	MGR. QA Engr. YMP	10/13/92

SUBJECT: SEISMIC ANALYSIS

TITLE: SEISMIC EFFECTS ON STABILITY OF PORTAL OPENING

QAG Reference: RSN-GR-027 REV. 0

9303040156 930204
PDR WASTE
WM-11 PDR

102.8

ENCLOSURE

1.0 PURPOSE

The main purpose of this study is to assess the stability of the North Portal Starter tunnel and the Highwall when subjected to seismic loads. Seismic load sources considered include earthquakes, Underground Nuclear Explosions (UNEs), and construction activities (i.e., excavation by drilling and blasting). The rock properties used in the analysis are the best available data from the RSN Basis For Design (BFD). Assumptions have been made when a parameter was not available.

2.0 METHOD

The analytical method is used in this study.

3.0 DESIGN INPUTS

RSN-BFD-001, Rev. 0, 1.2.6.5.1, FR1
RSN-BFD-001, Rev. 0, 1.2.6.0, F PC 13d,e
RSN-BFD-001, Rev. 0, 1.2.6.5, PC 9a,d; 10bi,bii; 13a,b; 18a
RSN-BFD-001, Rev. 0, 1.2.6.6, PC 19b; 20d
RSN-BFD-001, Rev. 0, 1.2.6.5.1, C1,2
RSN-BFD-001, Rev. 0, 1.2.6.0, J18,23
RSN-BFD-001, Rev. 0, 1.2.6.0, F C21
Technical Directive: RSN-92-002 Rev. 0

4.0 CODES AND STANDARDS

N/A

5.0 ASSUMPTIONS

It is assumed that all North Portal soil and rock property data will be included in the RSN BFD. The following rock properties have been assumed based on engineering experience and after reviewing related documents on the project. These assumptions need to be verified upon completion of the north portal soil and rock study:

Tensile Strength of the rock mass = 10 MPa
Joint Tensile Strength = 0.5 MPa
Joint Cohesion = 1 MPa

Joint Friction Angle = 30.96° (Coefficient of Friction = 0.6)
Joint Angle = 80°
Joints are assumed to be healed.

These assumptions have been used throughout the analysis.

6.0 REFERENCE MATERIAL

6.1 DOE (U.S. Department of Energy), "Salt Repository Project Shaft Design," DOE/CH/46656-16, Revision 0, Prepared by Fluor Technology, Inc. and Parsons Brinckerhoff/PB-KBB in Conjunction with Morrison-Knudsen Engineers, Inc., Science Applications International Corporation, Woodward-Clyde Consultants, and Rockwell International, Inc. for the U.S. Dept. of Energy, Hereford, TX, 1987.

6.2 Dowding, C. H., and Rozen, A., "Damage to Rock Tunnels from Earthquake Shaking," Journal of the Geotechnical Engineering Division, ASCE, Vol. 104, No. GT2, pp. 175-191, February 1978.

6.3 For Computer Analysis Presented in this Report Refer to RSN Certified Runs of ACL- 34, ACL-35, ACL-36, ACL-37, ACL-38, ACL-39, AND ACL-40 at the RSN Design Records Center.

6.4 Goodman, R. E., Introduction to Rock Mechanics, 1980, New York, Wiley.

6.5 Hardy, M. P., and Bauer, S. J., "Design of Underground Repository Openings in Hard Rock to Accommodate Vibratory Ground Motions," Draft, SAND91-2381C, Sandia National Laboratories, Albuquerque, NM, May 1992.

6.6 Hendron, A. J., Jr., and Fernandez, G., "Dynamic and Static Design Considerations for Underground Chambers," Seismic Design of Embankments and Caverns, Proceedings of a Symposium Sponsored by ASCE Geotechnical Engineering Division, Philadelphia, PA, May 1983, T. R. Howard, Ed., pp. 157-197.

6.7 Nolting, R., and Schmidt, B., "Methodology for Design of Ground Support for ESF and Repository Openings," SAND89-7022, September 1990.

6.8 Owen, G. N., and Scholl, R. E., "Earthquake Engineering of Large Underground Structures," Federal Highway Administration, Report No. FHWA/RD-80/195, January 1981.

6.9 Phillips, J. S. and Luke, B. A., "Tunnel Damage Resulting from Seismic Loading," Proceedings, 2nd International Conference on Recent Advances in Geotechnical Earthquake Engineering and Soil Dynamics, 1991.

6.10 Reference Information Base (RIB), Version 4, Revision 4, dated 04/08/1991.

6.11 Richardson, A. M., "Preliminary Shaft Liner Design Criteria and Methodology Guide," SAND88-7060, April 1990.

6.12 RSN Report, ST-MN-035, Rev. 1, "Preliminary Opening Stability Analyses," Originator: S. Bonabian, 1991.

6.13 RSN Report, ST-SA-201, Rev. 0, "North Portal Concrete," Originator: S. Nordick, 1992.

6.14 RSN Report, ST-MN-218, Rev. 0, "Ground Support System Identification for the Highwall," Originator: S. Bonabian, 1992.

6.15 RSN Report, ST-MN-219, Rev. 0, "Ground Support System Identification System for Portal Opening," Originator: S. Bonabian, 1992.

6.16 St. John, C. M., and Zahra, T. E., "A Seismic Design of Underground Structures," Tunneling and Underground Space Technology, 2(2):165-197, Pergamon Journals, Ltd, 1987.

6.17 Subramanian, C. V., King, D. W., Perkins, D. M., Mudd, R. W., Richardson, A. M., Calovini, J. C., Van Eeckhout, E., Emerson, D. O., "Exploratory Shaft Seismic Design Basis Working Group Report," SAND88-1203, August 1990.

6.18 URS/John A. Blume and Associates, "Ground Motion Evaluation at Yucca Mountain, Nevada with Applications to Repository Conceptual Design and Siting," SAND85-7104, Sandia National Laboratories, Albuquerque, NM, 1986.

6.19 U.S. Army, Waterways Experiment Station, Weapons Effect Laboratory, "Tunnel Destruction: A State-of-the-Art Summary," DNAPR 0033/WESMPN-78-1, Vicksburg, MI, 1978.

6.20 User's Manual, Volumes I & II, Fast Lagrangian Analysis of Continua (FLAC) Version 3.0, Itasca Consulting Group, Inc., 1991.

6.21 Yucca Mountain Site Characterization Project Technical Directive, RSN-92-002, Rev. 0, from: Gardiner, J. T., August 18, 1992.

6.22 Sharma, S.; and Judd, W. R., "Underground Opening Damage from Earthquakes," Elsevier Science Publishers B. V., Amsterdam, Engineering Geology 30, 1991, pp. 263-276.

7.0 COMPUTER PROGRAMS

Fast Lagrangian Analysis of Continua (FLAC), Version 3.03 is used for analysis.

Software Configuration Management Log Number: SCML-18-01
Software Certification Number: SCF-18-00
Software Design Description Waiver Number: SDDW-18 Rev. 00
Software Validation Waiver Number: SVW-18 Rev. 00
Software Maintenance Report Number: SMR-1
Computer Hardware: DELL 325
Hardware Certification Form Number: HCR-03-00
Hardware Configuration Management Log Number: SECML-02-00
Certified Runs Used: ACL-34, ACL-35, ACL-36, ACL-37, ACL-38, ACL-39, ACL-40

Software Verification and Validation Report SVVR-18 Rev. 00, Test Applications #1, #3, #7, and #10 provide support for the analyses performed in this report.

Refer to respective ACLs for input and output.

8.0 UNITS

Metric units are used in the analysis.

9.0 CALCULATIONS

9.1 INTRODUCTION

Three types of loads are considered in the design of the North Portal, namely: (1) geostatic loads, (2) seismic loads, and (3) thermal loads. This report addresses the seismic loads by studying the dynamic effects of earthquakes, Underground Nuclear Explosions (UNEs), and those caused by construction activities. The dynamic effects of Exploratory Studies Facility (ESF) activities include effects of construction blasting. Controlled drilling and blasting methods will be used in construction of the North Portal Starter Tunnel and Highwall. Blast design is based on charge weight per meter of blast hole to minimize and enable an estimate of the vibration depth and blast damage. Therefore, the loads due to the blasting are not considered significant at the time of reinforcement installation and will not be introduced as design loads for the opening stability analysis. Only the seismic loads associated with an earthquake or UNE will be considered in the Starter Tunnel and Highwall stability analysis.

The report by the working group for the Exploratory Shaft Design Basis (Subramanian et al., 1990) recommends seismic parameters for the design of the shaft associated with the ESF. The design parameters presented in that report are also recommended for the more general design of components of the ESF and potential high level nuclear waste repository that are not important to public radiological safety. The working group concluded that deterministic methods were appropriate for establishing conservative levels of ground motion for consideration in the ESF design, and probabilistic methods were appropriate for confirming that the resulting motions are unlikely to be exceeded during the operational life of the ESF. The recommendations, which were based on available site-specific seismic and geologic data, include design parameters for both natural earthquakes that may occur at or near the potential repository site and for UNEs that may occur at the Nevada Test Site (NTS).

According to the working group report, the Bare Mountain fault located 16 km west of the ESF, appears to be the most likely source of potentially severe ground shaking. Based on the probability that this fault may have an average Quaternary slip rate of up to 0.15 mm/yr, a magnitude 6.5 earthquake on the Bare Mountain fault was used as the deterministic basis for establishing earthquake ground motion conditions. The design basis UNE was a 700 kt event at a distance of 22.8 km. This event would provide the largest yield at the closest practical point (from the UNE yield point of view) in the Buckboard Mesa area of the NTS. This event results in the worst-case situation for ground motions from a UNE at Yucca Mountain.

The working group recommended the seismic design basis control motions for the ESF as:

- maximum horizontal component of acceleration, 0.3g;
- maximum vertical component of acceleration, 0.3g;
- maximum horizontal component of velocity, 30 cm/sec; and
- maximum vertical component of velocity, 20 cm/sec,

where g is the acceleration due to gravity.

Additionally, to provide further assurance that the design has adequate conservatism or margin to accommodate uncertainties such as site effects, the working group recommended that the performance of the ESF be evaluated using best-estimate conditions when subjected to ground motions a factor of 1.67 larger than the design basis motion, i.e., for a peak horizontal acceleration of 0.5g and a peak horizontal velocity of 50 cm/sec.

The working group further recommended that, for design purposes, until site characteristics are better quantified, surface control motion values apply at all depths (i. e., no attenuation of ground motion with depth is assumed).

The design basis control motions of horizontal and vertical components of acceleration of 0.75g was also considered in the design. This value was based on a technical directive from the Project Office (Reference 6.21). The analyses incorporating .5g loads are performed for comparison purposes.

The analysis presented in this report assesses the potential for damage to the North Portal Starter Tunnel and the Highwall considering the maximum seismic loads recommended by the working group and Project Office directive.

9.2 DAMAGE MECHANISMS

Damage mechanisms from seismic events may include fault slips, ground failure, or shaking. Fault slip across an opening would result in relative displacements that could cause local damage. Because a slip cannot be prevented by engineering measures, analysis of such an event must concentrate on probability of occurrence, magnitude of slip, and consequence of displacement. Several faults have been identified in the area of Yucca Mountain that show evidence of movement during the Quaternary period; hence a possibility of faulting at the ESF location and vicinity must be considered.

The faulting potential at an ESF site in Coyote Wash was examined by the working group report. The report concluded that no known faults with evidence of Quaternary movement are present in the vicinity of the shaft location and the annual probability of fault displacement in excess of a few centimeters is judged to be less than 10E-4. On this basis it was recommended that fault displacement not be considered in ESF shaft design.

The current ESF North Access site is located on the east side of Exile Hill. No faults with evidence of Quaternary movement have been identified in the immediate area to be considered in the present design. However, Quaternary faulting is recognized on the Bow Ridge fault, located about 1000 ft west of the North Portal. At present, investigations are being conducted on the Bow Ridge fault and in the area of the North Portal (Midway Valley Trenching). If the results of these investigations indicate Quaternary faults with potential for fault displacement in excess of a few centimeters in the area of the North Portal Pad and Starter Tunnel, the consequences will be evaluated and appropriate changes made in the design.

The second damage mechanism to be considered is ground failure due to seismic shaking. Included in a broader definition of ground failure are liquefaction, landsliding, and subsidence. At the ESF site the groundwater table is deep, the soil generally dense, and the surface relatively level, therefore ground failure is not expected to occur during any seismic event.

Transient, recoverable deformations of the ground during seismic shaking constitute the third effect on the portal structure. Effects of ground shaking could include distress or failure of portions of ground support systems, rock falls, spalling, or displacements along joints.

In general, a seismic event generates elastic waves that propagate outward from the source. Body waves may be classified as P (dilational or compressional) waves that consist of alternating compression and tension in the transmission medium or S (shear or distortional) waves that consist of oscillating shears. Distortional ground motions are typically resolved into S_H waves with horizontal particle motions and S_V waves with motions in a vertical plane. By definition, particle motions resulting from S_V waves are in a vertical plane but not necessarily in a vertical direction. P waves have an inherently higher velocity of propagation than S waves and will always arrive first at the site location.

The elastic waves from a seismic event induce transient stresses and strains in a rock mass and, hence, in any embedded structure such as a tunnel liner. The effect on the structure will depend on a number of parameters, including the physical properties of the rock and the structure and the frequency, amplitude, and duration of the ground motion. Seismic events may also impose direct shear displacements on the tunnel liner if they cause movement along faults that transect the tunnel axis. No faults intersect the Starter Tunnel, therefore the possibility of shear displacements is not considered in the analysis.

Surface structures such as buildings tend to move and deform independently when excited by earthquake induced ground motions. On the contrary, underground structures such as tunnel and shaft liners move and distort compatibly with the ground in which they are embedded. This implies that ground-structure interaction analysis is required. Providing that the wavelength of the seismic pulse is relatively large with respect to the opening diameter (i.e., if the rise time of the seismic impulse is long relative to the transit time of the wavefront across the opening), such analysis can be based on static methods because dynamic amplification will be small (Richardson, 1990). Hendron and Fernandez (1983) propose that there will be little dynamic amplification if the wavelength is at least eight opening diameters. The wavelength associated with peak ground motions is estimated to be at least eight times the Starter Tunnel diameter. The quasi-static approach was adopted for the design of the shaft for the proposed repository at the Yucca Mountain site (Richardson, 1990) and the Salt repository in Texas (DOE, 1987).

9.3 DESIGN APPROACH

The empirical and analytical methods are usually applied to estimate the potential ground damage from an earthquake. The empirical methods have been applied in the recent past by evaluating the evidences of stability and instability during actual seismic events. Much of this empirical evidence has been summarized by Dowding and Rozen (1978) and Owen and Scholl (1981). The empirical evidence indicates only minor damage in tunnels where the peak ground acceleration measured at the surface was less than 0.5g or where the peak particle velocity was less than 95 cm/sec. In fact, no damage would be expected for events with peak ground accelerations less than 0.2g, or peak velocities less than 0.2 m/sec. New cracks in rocks and local rock falls have occurred on events with surface accelerations between 0.2 and 0.4g (velocity between 0.2 and 0.4 m/sec). Data from the weapons effects testing program at the NTS (U.S. Army/WES, 1978) indicate that no damage to tunnels in relatively weak rock occurs for particle velocities below 0.46 m/sec, and damage is slight (discontinuous slabbing or spalling) for particle velocities below 1.52 m/sec. Phillips and Luke (1991) reported on an instrumented tunnel section 0.5 km from a UNE subjected to a body wave magnitude and a Richter local magnitude of 5.0. This tunnel was subjected to a peak ground acceleration of 27g and a peak particle velocity of 230 cm/sec. Dowding and Rozen (1978) defined the damage as "minor" (cracking and minor roof falls). Other tests of hardened tunnels subjected to ground motion from UNEs have been reported. St. John and Zahra (1987) reported that tunnels hardened by rock bolts may survive peak ground velocities in excess of 900 cm/sec. On a purely empirical basis, then, there appears to be little danger from seismic or underground nuclear events to the stability of the ESF and potential repository openings (Nolting and Schmidt, 1990). Sharma and Judd (1991) presented a summary of worldwide qualitative data regarding the behavior of underground openings during earthquakes. The shallow near-surface portions and portals showed likely to be susceptible to damage from seismic ground motions.

The analytical methods that are used in civilian design projects to accommodate seismic loads include quasi-static and dynamic analysis. The quasi-static approach assesses the maximum impact of the seismic wave on the host medium without concern for dynamic interactions. Dynamic interactions include dynamic stress concentrations, stress gradient effects, body force effects, and stress reflections. Hendron and Fernandez (1983) have shown that the dynamic stress concentrations are insignificant if the wavelength of the seismic event is greater than eight times the diameter of the tunnel. For short wavelengths, the effect of reflections from the tunnel wall, roof, or floor should be considered. The consequence of the reflected stress wave can be spalling and splitting of the rock, resulting in fractures parallel to the opening surface (Reference 6.5).

The frequency content of the earthquake seismic wave estimated by URS/Blume (1986) shows frequencies in the range of 0.2 to 10 Hz. If a seismic velocity of 2 to 3.2 km/sec combined with a conservative upper bound frequency of 20 Hz is used, a seismic wave with a wavelength of approximately 100 m results. The Starter Tunnel opening is approximately 10 m high and 10 m wide; therefore, the wavelength is approximately 10 times greater than the tunnel dimension. This indicates that dynamic stress concentrations due to stress gradient effects should not be significant.

The analyses presented in this report assess the potential for damage to the North Portal Starter Tunnel and the Highwall due to static seismic loads. In these analyses the Highwall or the Starter Tunnel is subjected to two different seismic loads of 0.75g horizontal and vertical and 0.5g horizontal and vertical. The loads were applied for both supported and unsupported Highwall and the Starter Tunnel. A Starter Tunnel with a 61 cm liner was also analyzed for both loads.

Standard engineering practice is to set vertical ground motion values at two thirds of the horizontal values. This approach would probably be adequate for peak accelerations from a magnitude 6.5 earthquake at a distance of about 15 km. In light of the marginal probability of large vertical accelerations from an earthquake on the Bare Mountain fault and the marginal probability of an earthquake on one of the closer faults, working group recommended that equal peak values for horizontal and vertical acceleration be assumed.

For the initial stresses, the vertical in situ stress σ_v at a point is given by

$$\sigma_v = -\rho g h , \qquad (1)$$

where h is the depth of the point relative to surface and ρ is the average density of the rock mass. The horizontal stress can be calculated using the linear elasticity theory, which assumes equal horizontal stress in all directions. In practice, the stress state within the rock masses does not conform exactly to the simple linear elasticity model. The tectonic environment and nonlinear deformation together result in a stress state that typically exceeds that predicted by the elastic model. For ESF underground openings the horizontal in situ stress has been estimated to be 0.3 to 1.0 times the vertical stress (References 6.7 and 6.12). Due to erosion, near the surface the horizontal stress can be greater than the vertical stress. The range of in situ stresses suggested in the BFD (Table 35) also reflects this fact. In order to accommodate all potential in situ stress conditions, for the analyses presented here two loading cases corresponding to smallest (σ_h/σ_v = 1.0) and largest (σ_h/σ_v = 3.0) horizontal stresses are considered. In the remainder of the report, Case 1 represents the smallest (σ_h/σ_v = 1.0) and Case 2 indicates the (σ_h/σ_v = 3.0) largest horizontal stresses. In the analyses the in situ field stresses are calculated using Equation 1 and horizontal to vertical stress ratios of 1.0 (Case 1) and 3.0 (Case 2).

9.4 DESIGN INPUT DATA

The mechanical properties of the rock and the joint characteristic parameters are required to perform the analyses, for which the best available data have been used. These data are representative of the Tiva Canyon Member of the Paintbrush Tuff in which the North Portal is to be located. The mechanical properties of the rock mass for the analyses and their respective sources are presented in Table 1.

TABLE 1

Rock Mass Properties of the TCw Member

	Average	Low	Reference
In Situ Density	2.2 g/cm^3	2.2 g/cm^3	BFD
Young's Modulus	20.0 GPa	20.0 GPa	BFD
Poisson's Ratio	0.1	0.1	BFD
Cohesion	34.2 MPa	14.8 MPa	BFD
Friction Angle	33.8°	18.8°	BFD
Tensile Strength	10 MPa	10 MPa	Assumed

The joint specific data required for the analyses are given in Table 2. The most conservative values (lowest BFD values) have been selected for the analyses. Assumptions have been made when a parameter was not available. Specific input files for each analysis are provided in corresponding certified runs (Reference 6.3). The outputs from the analyses need to be re-evaluated upon availability of the NRG-1 drilling results.

TABLE 2

Joint Parameters of the TCw Member
(All the values are assumed)

Joint Cohesion	1 MPa
Joint Friction Angle	30.96°
Joint Tensile Strength	0.5 MPa
Joint Angle	80°

9.5 COMPUTER ANALYSES

Fast Lagrangian Analysis of Continua (FLAC), version 3.03 computer software has been used for analyses performed in this report. FLAC is based upon a "Lagrangian" scheme which is well suited for large deflections and has been used primarily for analysis and design in mining engineering and underground construction. Several constitutive laws are provided in FLAC from which Mohr-Coulomb plasticity and ubiquitous joint models are used in the analyses presented in this report.

The Mohr-Coulomb model is the conventional model for plasticity in soil and rock mechanics. The model checks for tensile stresses which exceed either the plastic apex limit or the tensile strength.

The ubiquitous joint model is an anisotropic plasticity model which assumes a series of weak planes embedded in a Mohr-Coulomb solid. Yield may occur in either the solid, along slip plane, or both, depending on the material properties of the solid and plane, the stress state, and the angle of the slip planes. In the ubiquitous joint model, the joints are considered to be continuous (i.e., persistent) and very closely spaced. Slip or opening along the vertical planes of weakness is determined by a Mohr-Coulomb criterion for joints. In FLAC, a joint tensile strength is tested. If the stress perpendicular to the joint for the zone overcomes the tension cut-off, the cut-off is set to zero, and the joint is unable to sustain tension in that direction thereafter. A more detailed discussion on general features and fields of applications of FLAC computer software is presented in the User's Manual (Reference 6.20).

10.0 CONCLUSIONS AND RESULTS OF THE ANALYSES

The computer analyses were performed to determine the impact of the quasi-static seismic loads on the stability of the Starter Tunnel and the Highwall. The Mohr-Coulomb models were completed first to indicate potential yield around the tunnel opening or at the Highwall. The ubiquitous joint model was used to predict any joint failure. The results from the analyses were used to estimate ground support requirements.

Analyses of seismic loads with horizontal and vertical components of 0.5g show no indication of any yield zones around the opening or along the Highwall. The results also indicate that seismic loads have a negligible effect on the zones of stress around the opening and along the Highwall. The ubiquitous joint model analyses showed no joint slip for both the high (Case 2) and low (Case 1) horizontal to vertical in situ stress ratios. The results also show that the additional seismic loads have little effect on the axial loads of the rock bolts. The stresses at the Highwall toe increased due to the 0.5g loads but did not reach the yield limits. Around the opening, maximum stress values of 1.72 MPa and 3.26 MPa resulted for Case 1 and Case 2, respectively. Maximum displacements around the opening for both cases were on the order of 1.45 mm.

Analyses incorporating upward loads in vertical direction (upward vertical acceleration) indicated much less stresses at the portal. This is due to the fact that the vertical loads are reduced and in a gravitational model this yields lower final stresses.

Additionally, seismic loads with horizontal and vertical components of 0.75g create small yield zones at the toe of the Highwall. Stress risers at the toe are due to the sharp corner and large radius of curvature. The localized yield zone at the toe can be alleviated by installation of wire mesh and application of shotcrete. No yield zones were detected in the Starter Tunnel analyses when subjected to these loads. Around the opening, maximum principal stress values of 2.08 MPa for Case 1 and 3.42 MPa for Case 2 were detected. Maximum displacements around the opening for 0.75g loads increased to 2.5 mm. The changes on the rock bolt loads from the 0.5g seismic load cases were not significant.

Even though the zone of overstress does not change significantly with the addition of the seismic loads, the displacements are noticeably affected by these loads. Figures 19 through 22 show the maximum displacements due to 0.5 and 0.75g seismic loads. The loads on the rock bolts, shotcrete, and the tunnel liner are presented in Figures 23 through 54. It can be seen that the loads on the liner and the shotcrete are higher for the 0.75g seismic loads.

In conclusion, the Highwall and Starter Tunnel were analyzed by incorporating seismic loads and the use of static methods. The static analysis was determined to be sufficient for the ESF design, because the wavelength associated with peak ground motion from an earthquake is generally larger (10 times) than the opening size. The analyses were conducted by first creating a model in which the Highwall and the opening were excavated and the ground support systems installed and equilibrium reached. Then the seismic loads with 0.5 and 0.75g horizontal and vertical components were applied to the model statically. The resultant loads on the ground reinforcement system components (rock bolts, shotcrete, and liner) were calculated and the stress conditions at the Highwall and Starter Tunnel determined. The Highwall and Starter Tunnel opening analyses indicate tensile stress zones, which could cause joint opening when the seismic pulse passes through. Local spalling due to joint separations is minimized by the installation of wire mesh and application of shotcrete along the Highwall and inside the Starter Tunnel. The rock bolts installed above and to the sides of the opening provide additional support against joint separation and slip along the Highwall. The 20 ft (6.1 m) bolts installed around the opening perpendicular to the Highwall face provide satisfactory rock bolt load bearing capacity. The Starter Tunnel liner is also designed to accommodate seismic loads (Reference 6.13). The possibility of crack generation and local spalling of the shotcrete and the liner always exists in the event of a severe earthquake. This damage would be minimized by the welded wire fabric reinforcing the shotcrete. The recommended reinforcement systems for the Highwall and the Starter Tunnel are discussed in References 14 and 15.

Finally, the analyses performed here must be reevaluated upon completion of the soil and rock study of the North Portal location. It should also be remembered that the design approach adopted here was for ESF purposes and with potential repository requirements in mind. The approach was chosen based on review of previously published documents on the subject. The ESF design recommendations presented here are not detrimental to the potential repository seismic design.

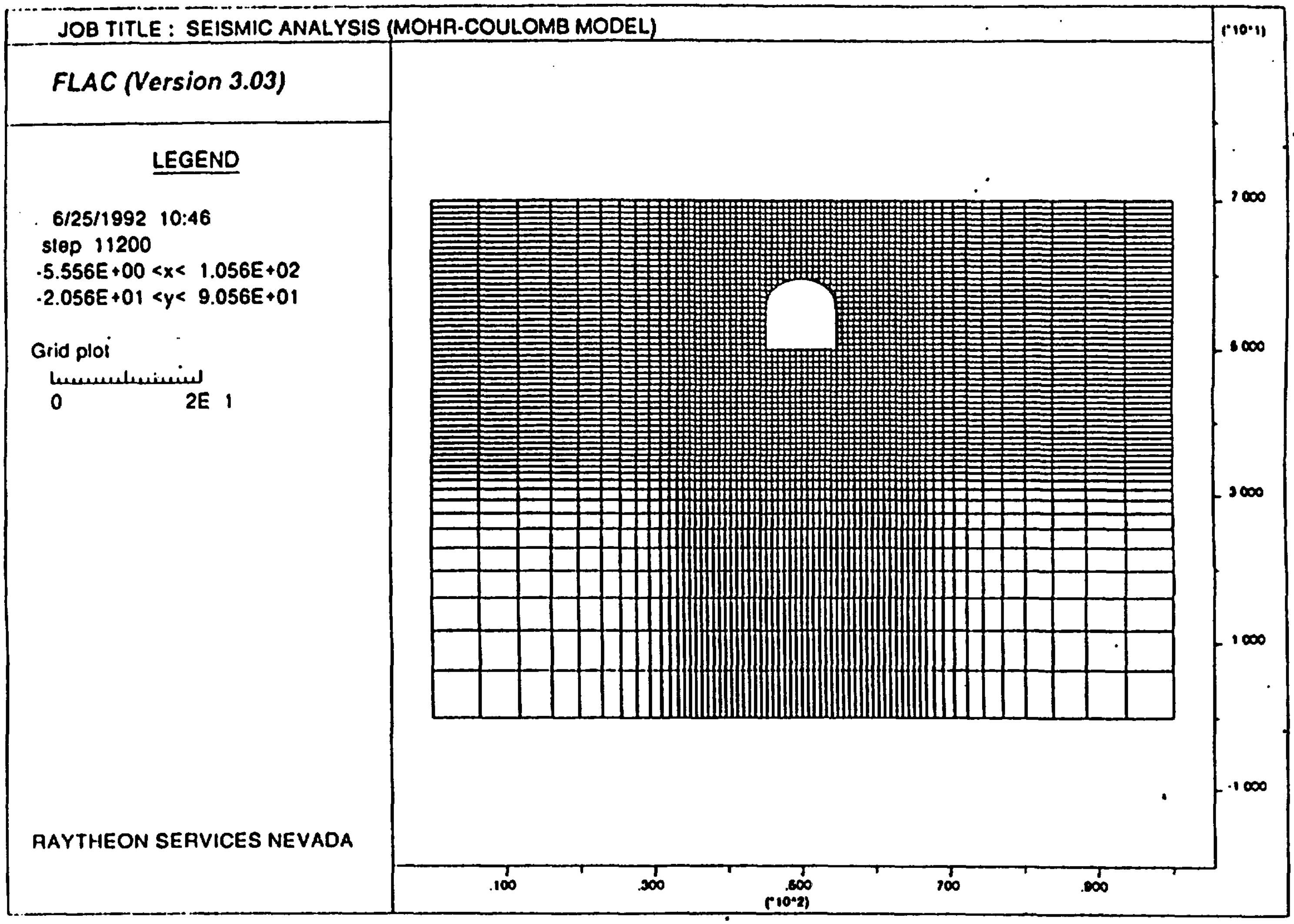

Fig. 1 Finite Difference Mesh Used for the Starter Tunnel Seismic Analyses.

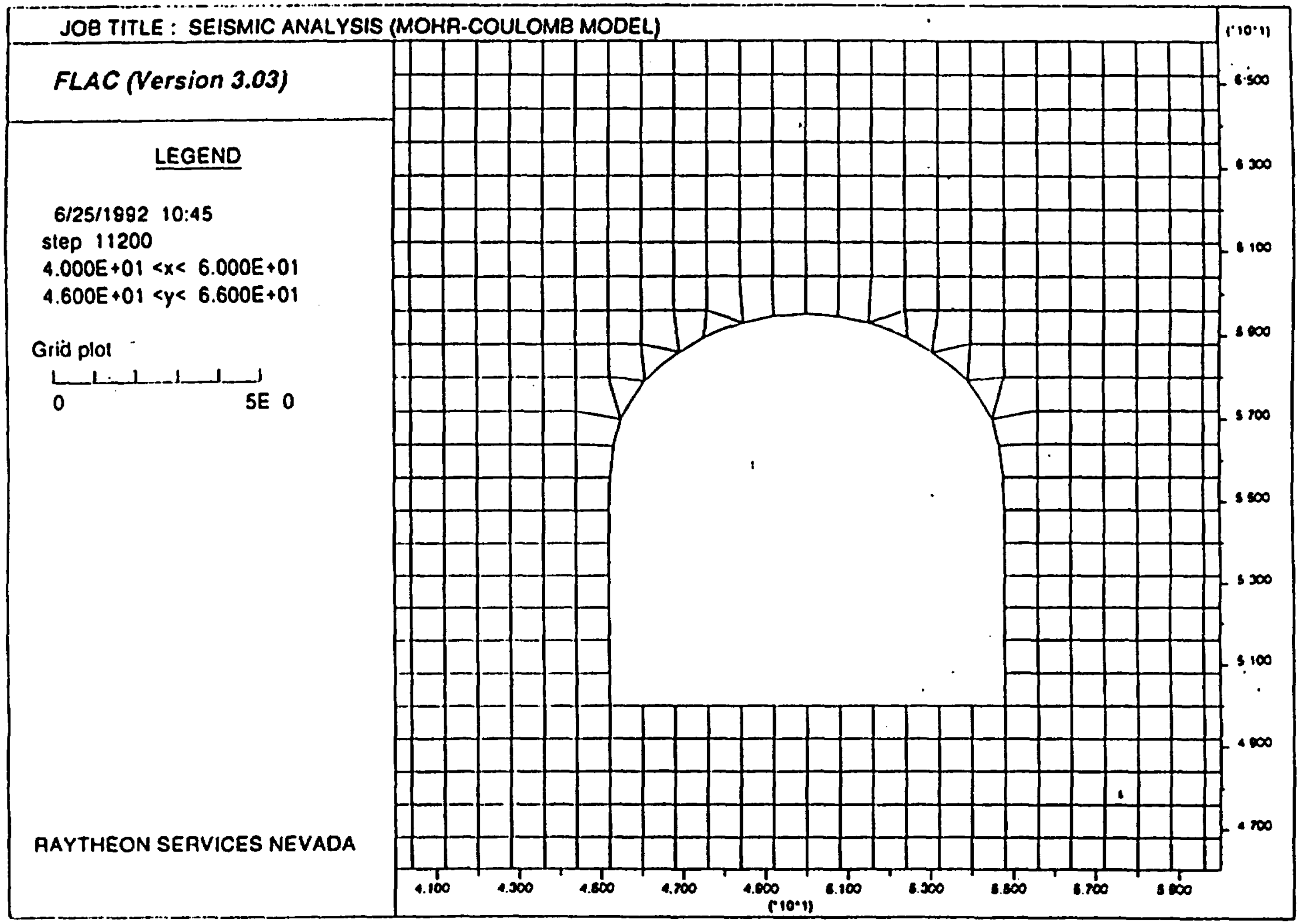

Fig. 2 Close-up of the Grid For the Starter Tunnel.

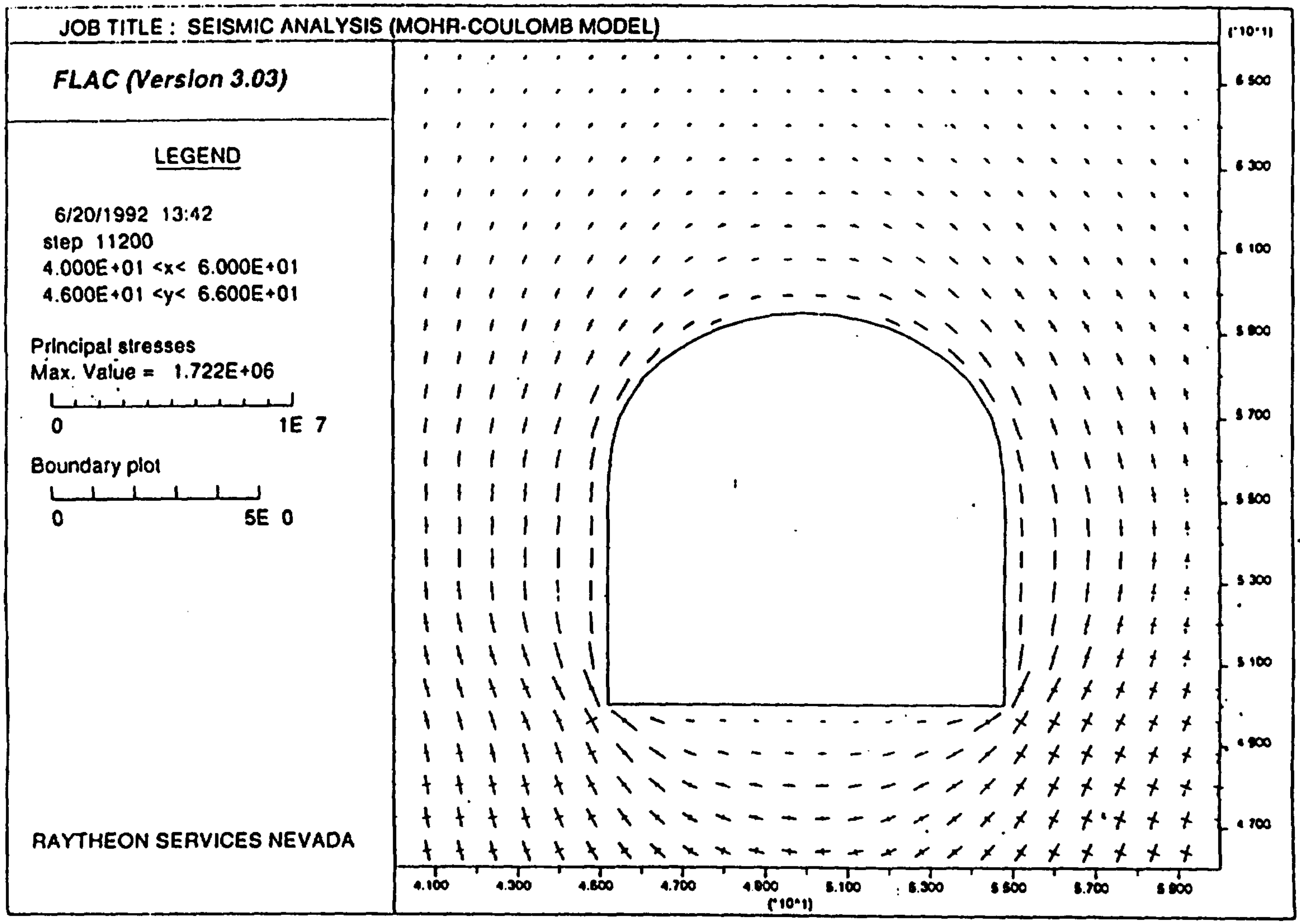

Fig. 3 Principal Stress Vectors around the Tunnel Opening at Seismic Event with Horizontal and Vertical Components of Accelération of 0.5g, Mohr-Coulomb Model (Case 1). Compression is Negative. Stresses are in Pascal.

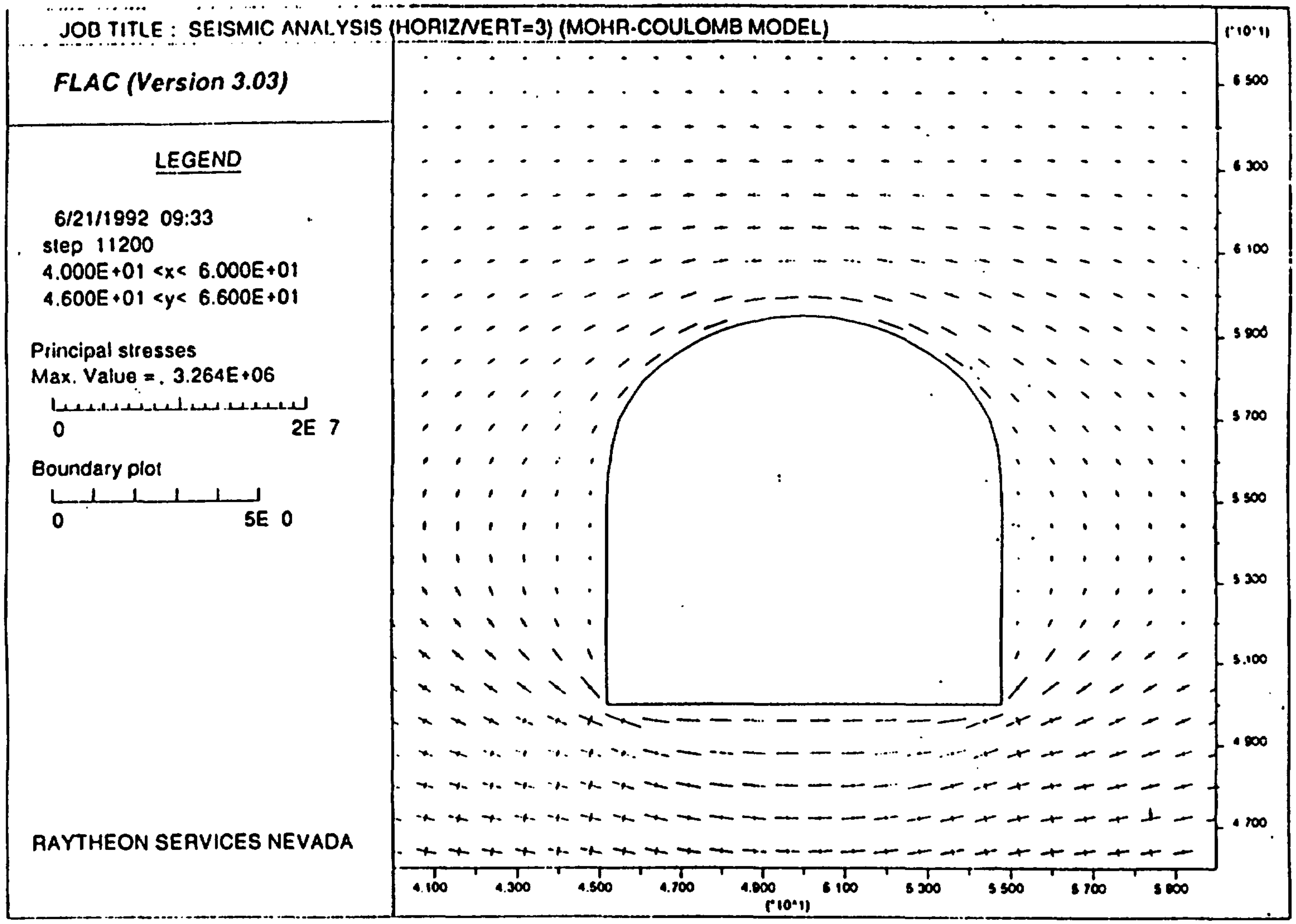

Fig. 4 Principal Stress Vectors around the Tunnel Opening at Seismic Event with Horizontal and Vertical Components of Acceleration of 0.5g, Mohr-Coulomb Model (Case 2). Compression is Negative. Stresses are in Pascal.

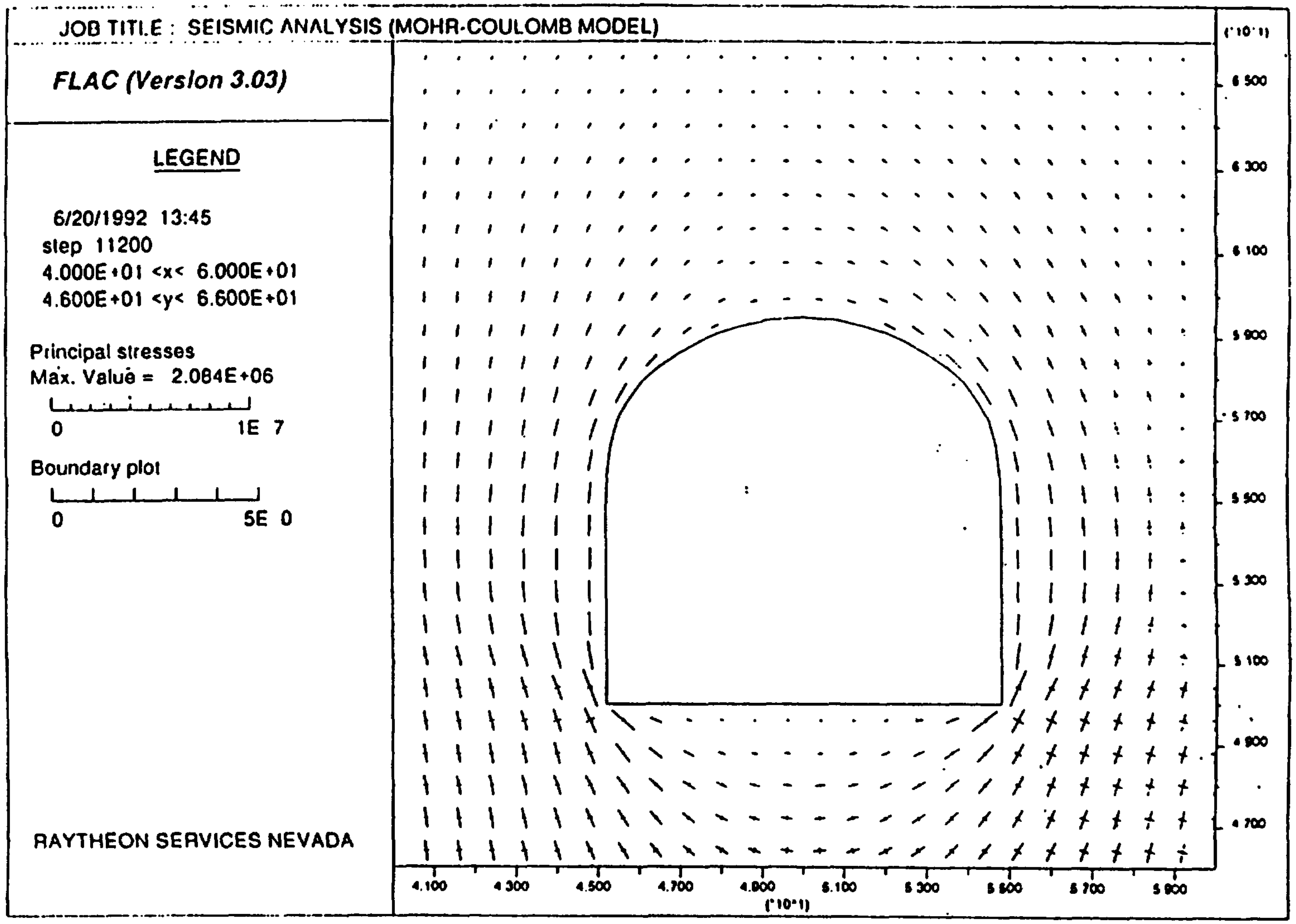

Fig. 5 Principal Stress Vectors around the Tunnel Opening at Seismic Event with Horizontal and Vertical Components of Acceleration of 0.75g, Mohr-Coulomb Model (Case 1). Compression is Negative. Stresses are in Pascal.

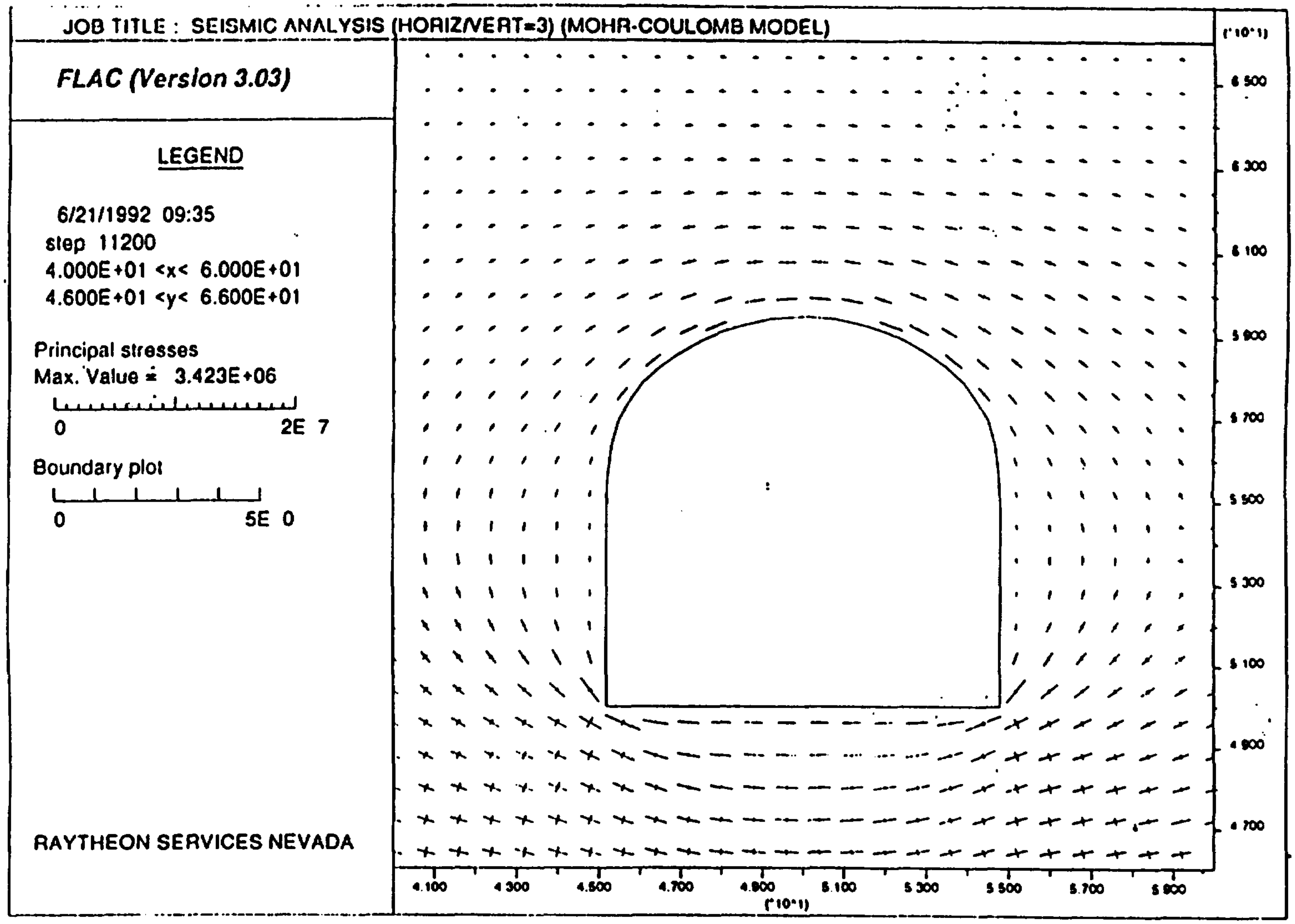

Fig. 6 Principal Stress Vectors around the Tunnel Opening at Seismic Event with Horizontal and Vertical Components of Acceleration of 0.75g, Mohr-Coulomb Model (Case 2). Compression is Negative. Stresses are in Pascal.

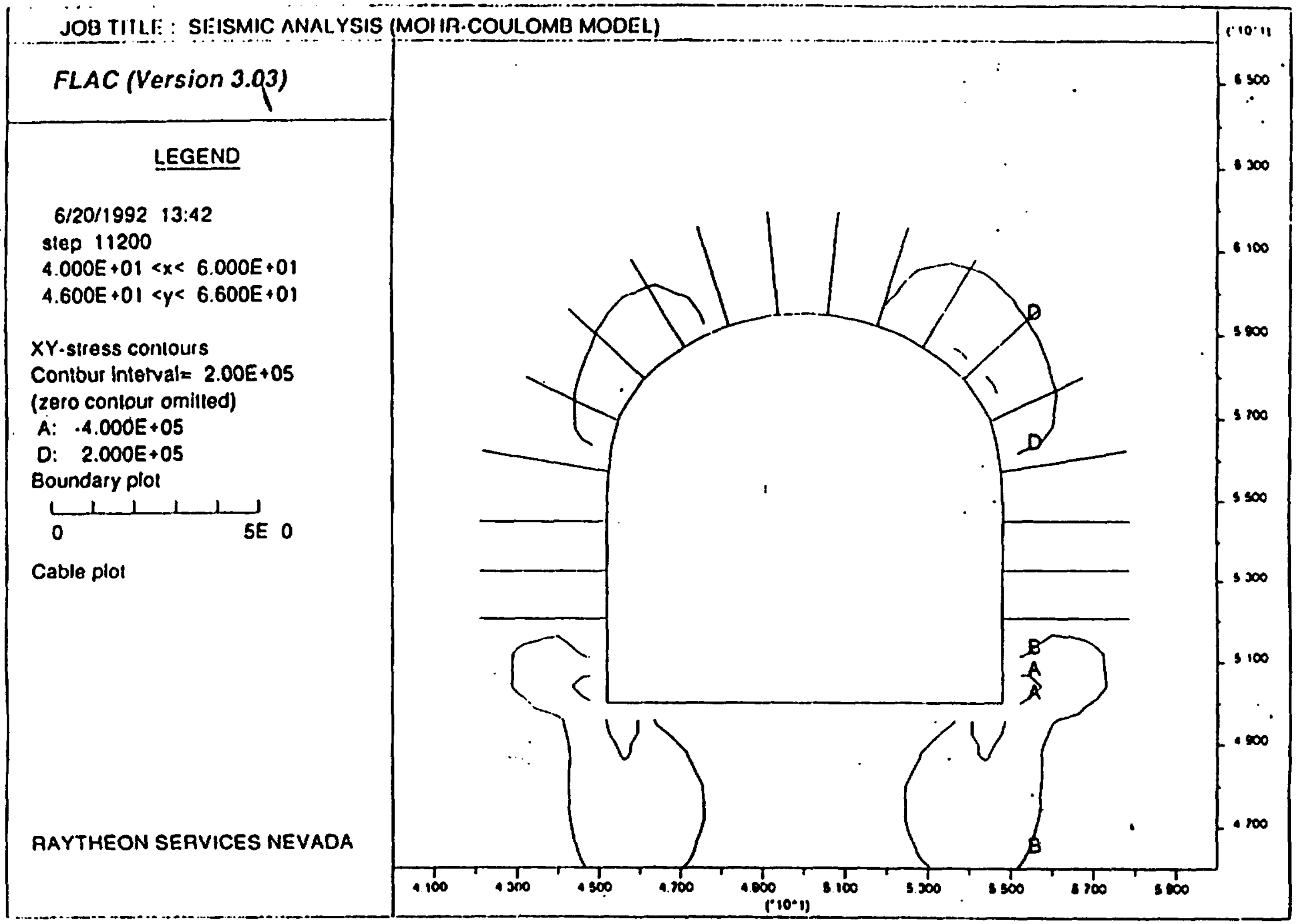

Fig. 7 Shear Stress Contours around the Tunnel Opening at Seismic Event with Horizontal and Vertical Components of Acceleration of 0.5g, Mohr-Coulomb Model (Case 1). Compression is Negative. Stresses are in Pascal.

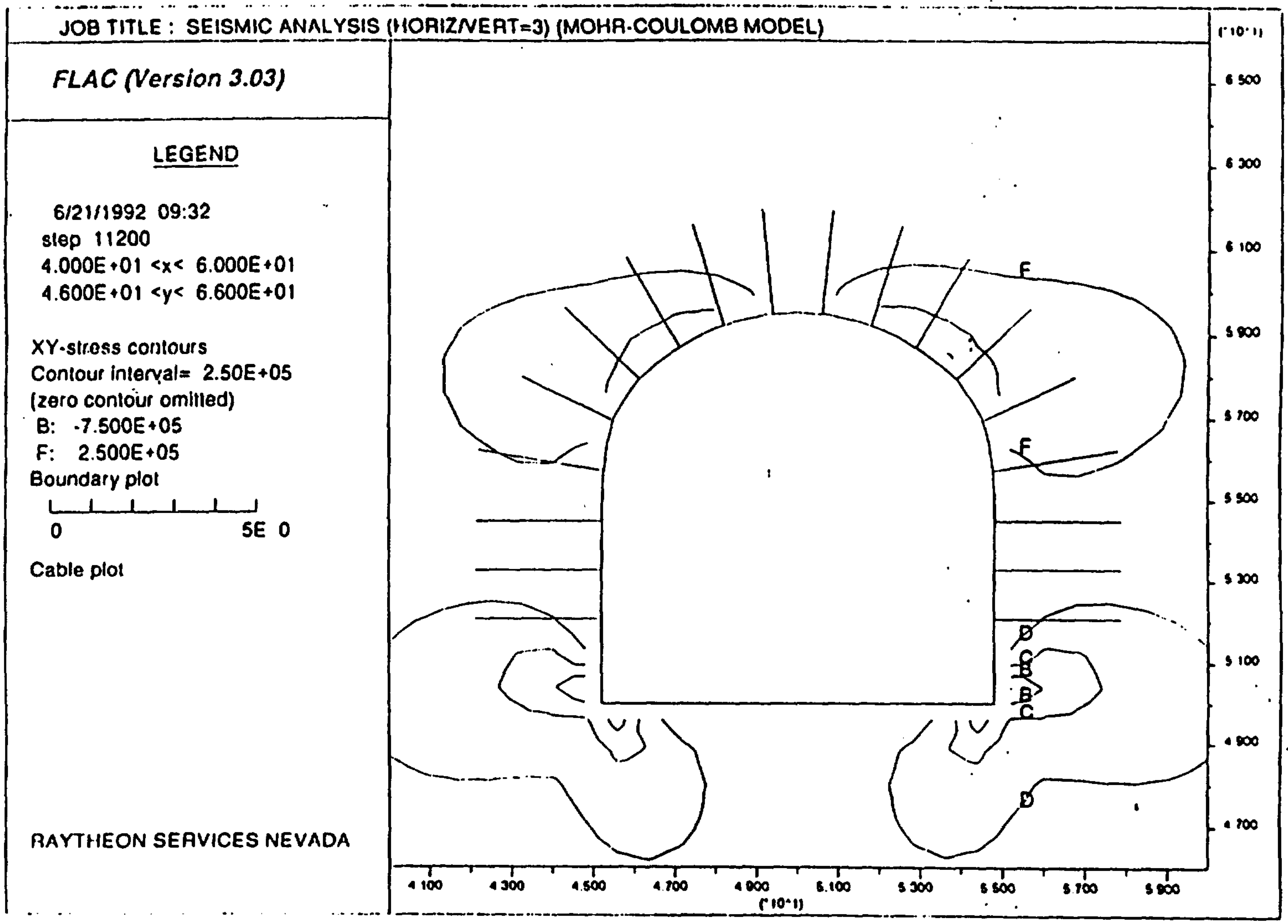

Fig. 8 Shear Stress Contours around the Tunnel Opening at Seismic Event with Horizontal and Vertical Components of Acceleration of 0.5g, Mohr-Coulomb Model (Case 2). Compression is Negative. Stresses are in Pascal.

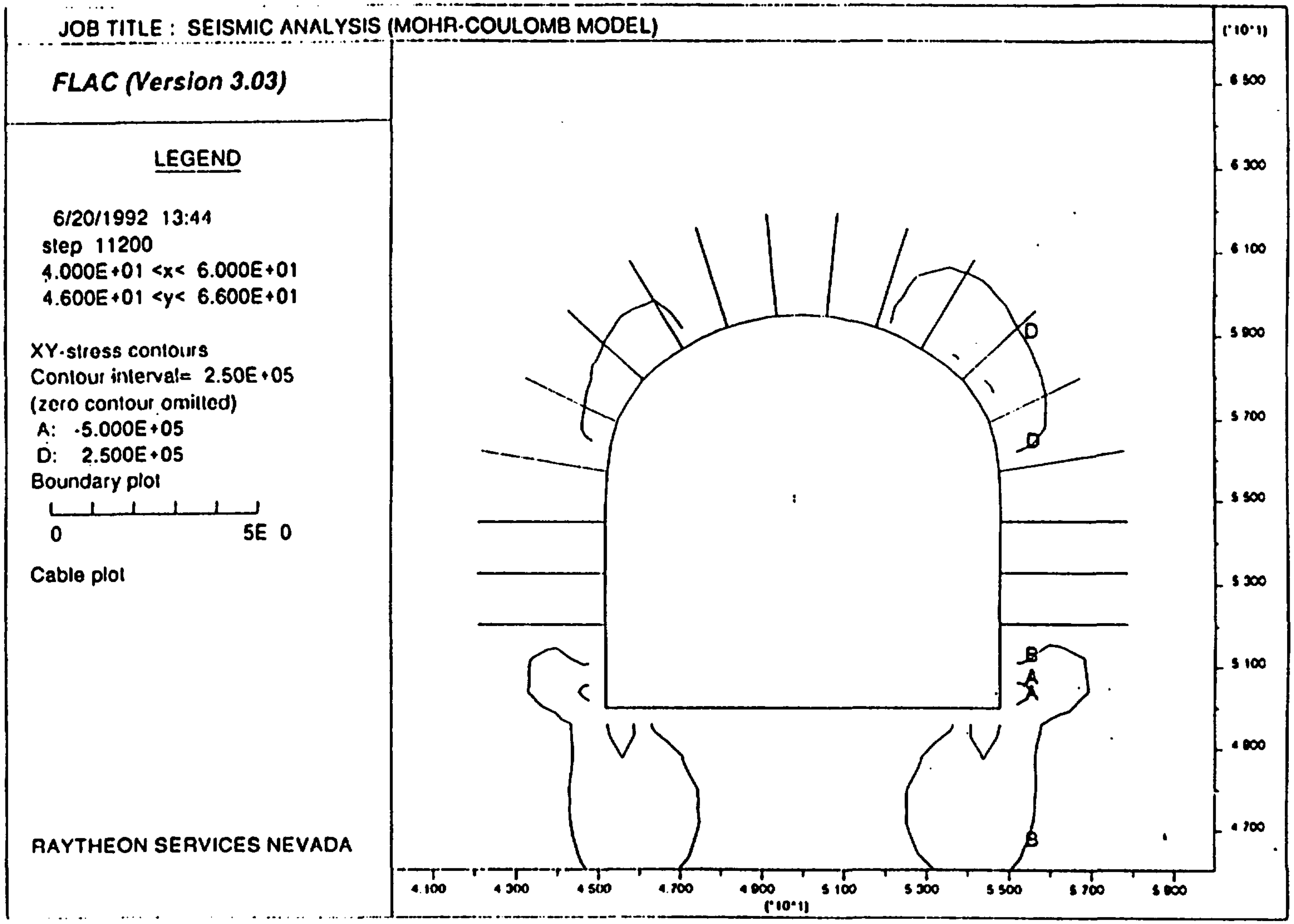

Fig. 9 Shear Stress Contours around the Tunnel Opening at Seismic Event with Horizontal and Vertical Components of Acceleration of 0.75g, Mohr-Coulomb Model (Case 1). Compression is Negative. Stresses are in Pascal.

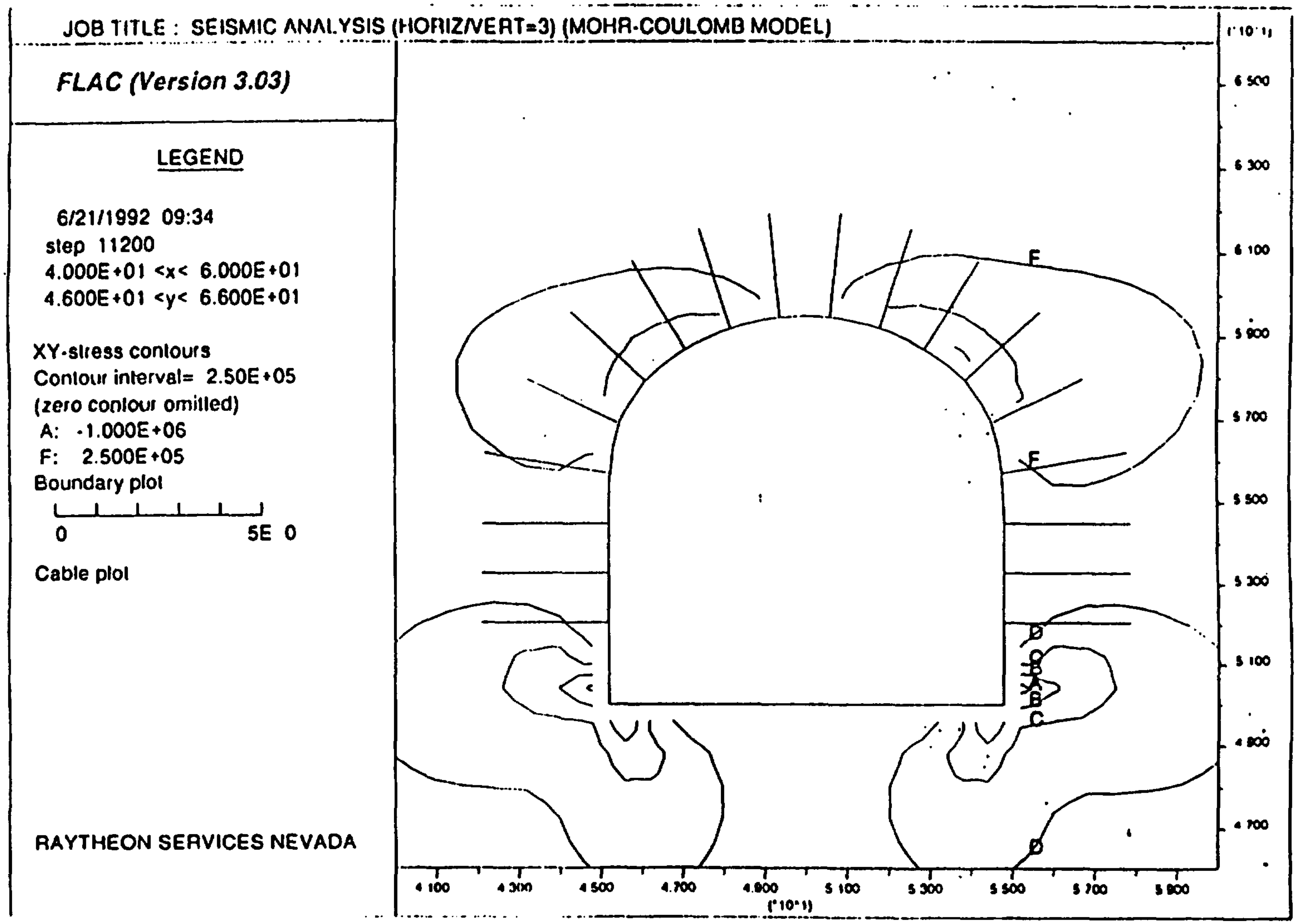

Fig. 10 Shear Stress Contours around the Tunnel Opening at Seismic Event with Horizontal and Vertical Components of Acceleration of 0.75g, Mohr-Coulomb Model (Case 2). Compression is Negative. Stresses are in Pascal.

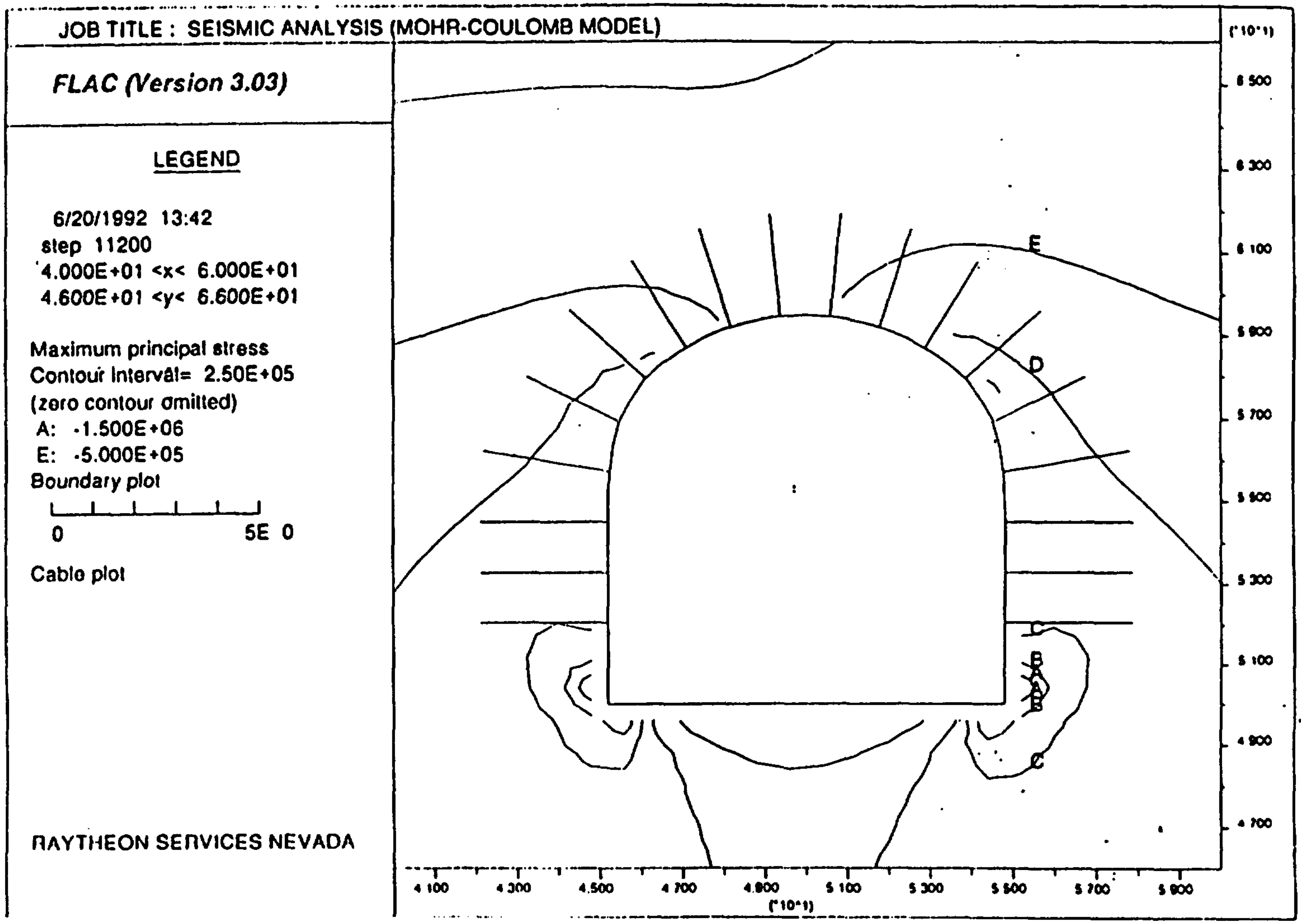

Fig. 11 Maximum Principal Stress Contours around the Tunnel Opening at Seismic Event with Horizontal and Vertical Components of Acceleration of 0.5g, Mohr-Coulomb Model (Case 1). Compression is Negative. Stresses are in Pascal.

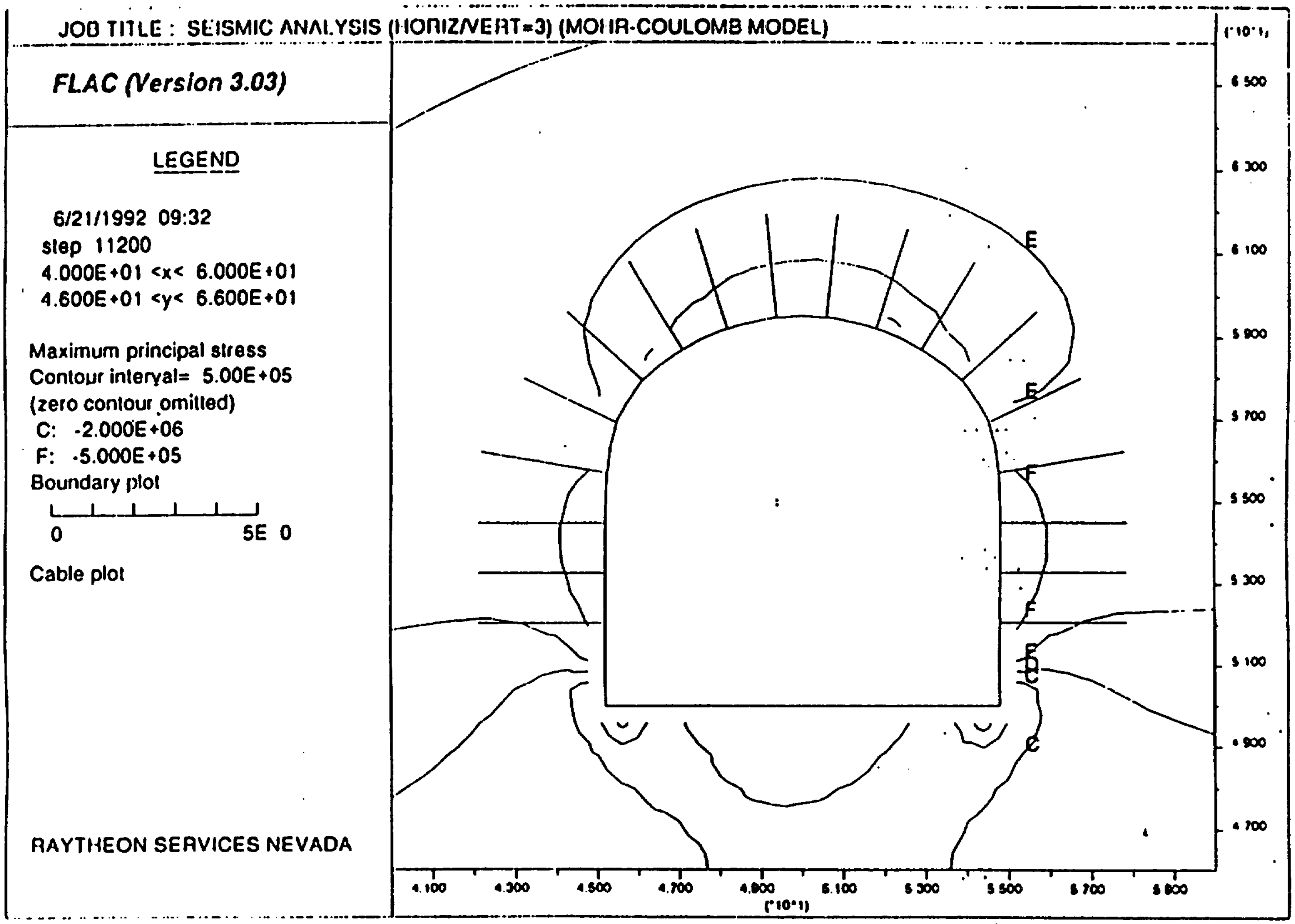

Fig. 12 Maximum Principal Stress Contours around the Tunnel Opening at Seismic Event with Horizontal and Vertical Components of Acceleration of 0.5g, Mohr-Coulomb Model (Case 2). Compression is Negative. Stresses are in Pascal.

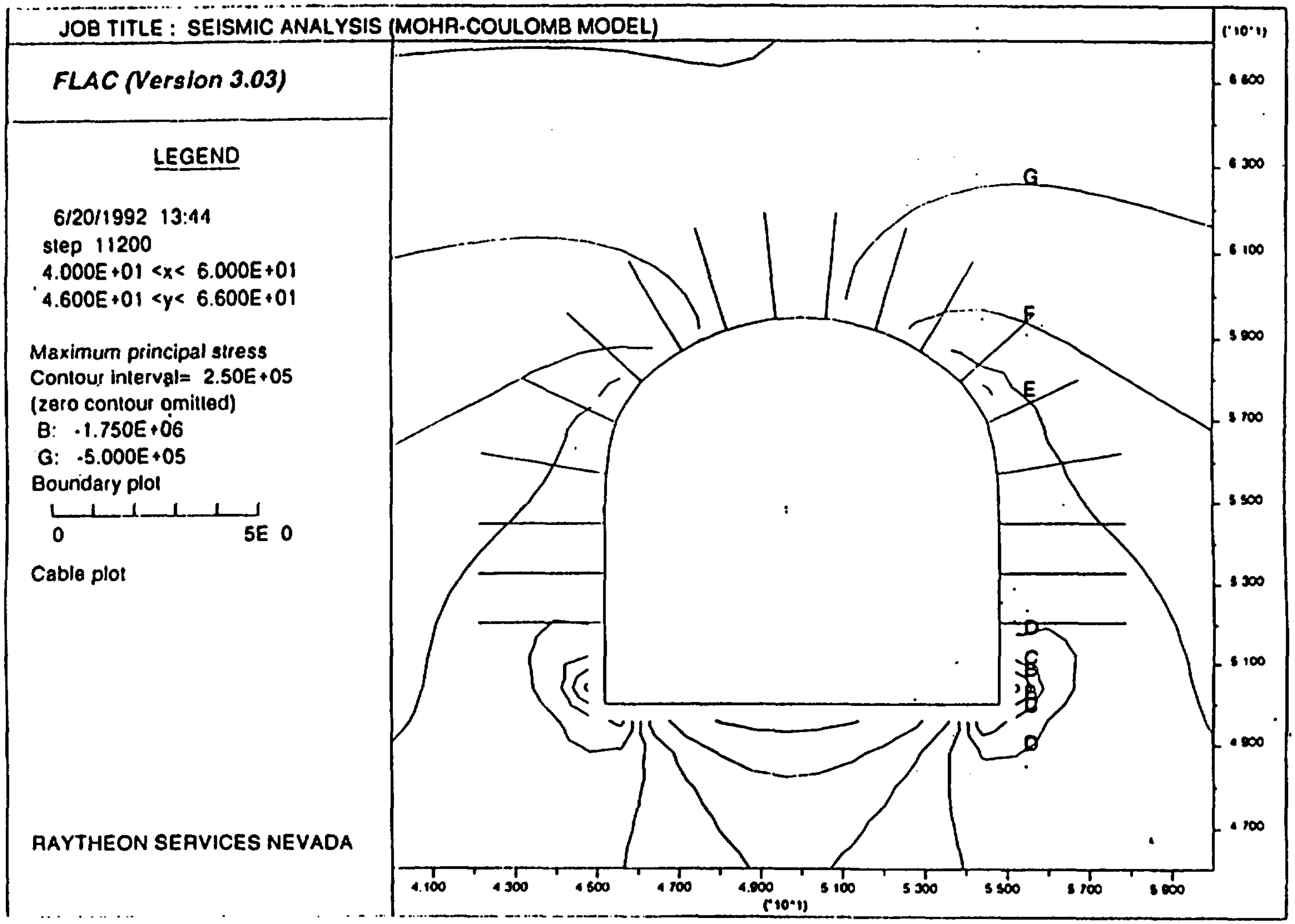

Fig. 13 Maximum Principal Stress Contours around the Tunnel Opening at Seismic Event with Horizontal and Vertical Components of Acceleration of 0.75g, Mohr-Coulomb Model (Case 1). Compression is Negative. Stresses are in Pascal.

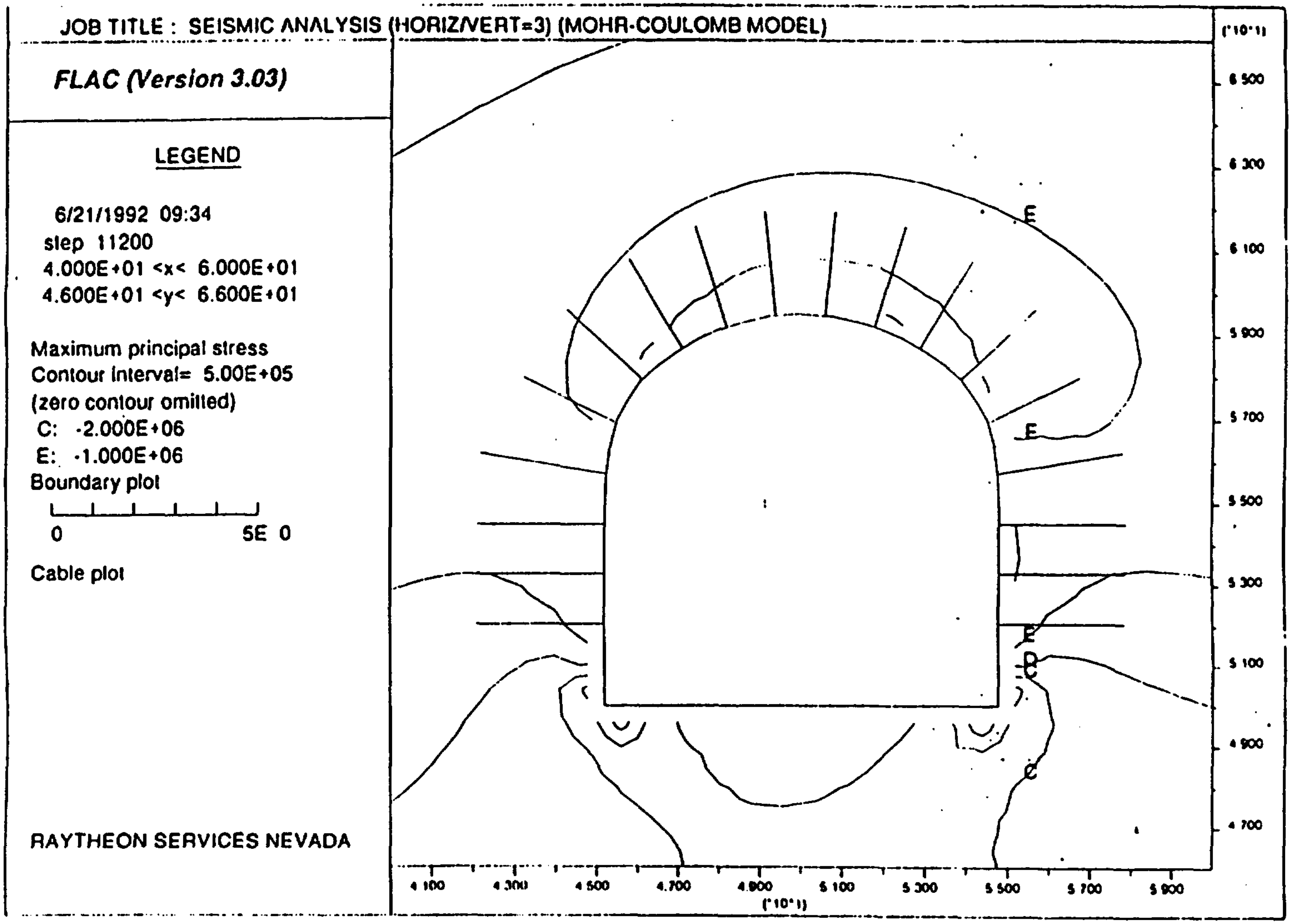

Fig. 14 Maximum Principal Stress Contours around the Tunnel Opening at Seismic Event with Horizontal and Vertical Components of Acceleration of 0.75g, Mohr-Coulomb Model (Case 2). Compression is Negative. Stresses are in Pascal.

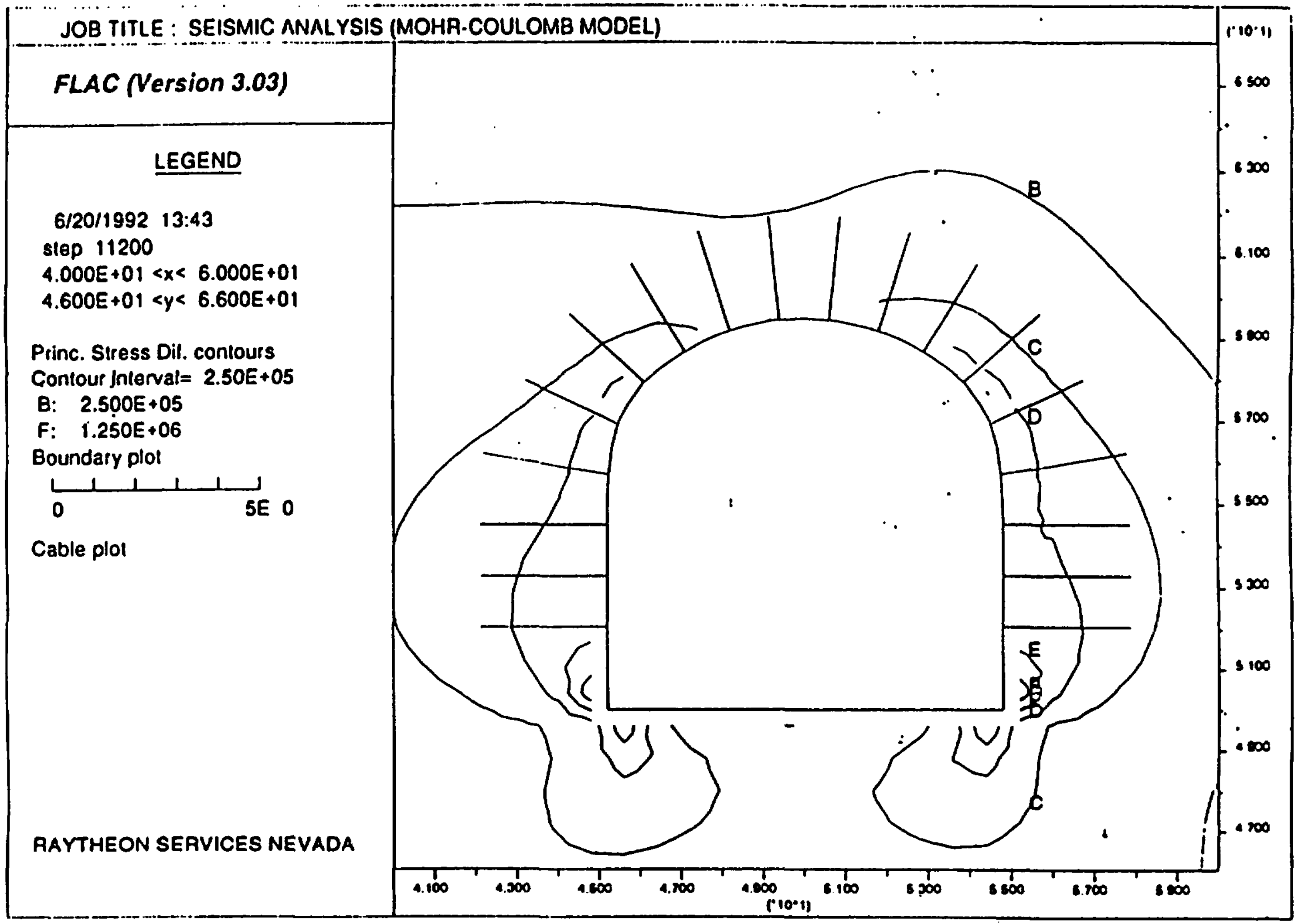

Fig. 15 Principal Stress Difference Contours around the Tunnel Opening at Seismic Event with Horizontal and Vertical Components of Acceleration of 0.5g, Mohr-Coulomb Model (Case 1). Compression is Negative. Stresses are in Pascal:

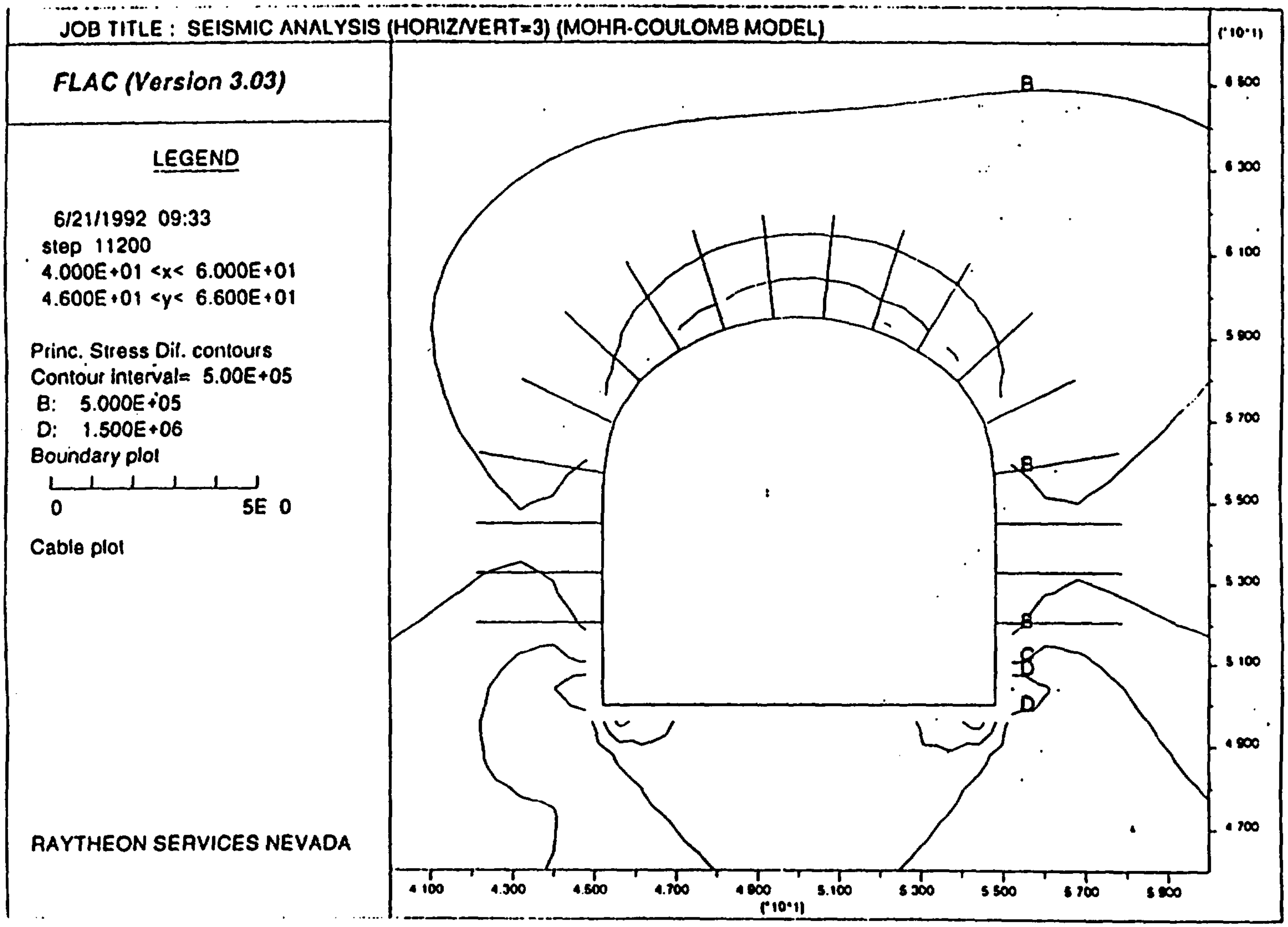

Fig. 16 Principal Stress Difference Contours around the Tunnel Opening at Seismic Event with Horizontal and Vertical Components of Acceleration of 0.5g, Mohr-Coulomb Model (Case 2). Compression is Negative. Stresses are in Pascal.

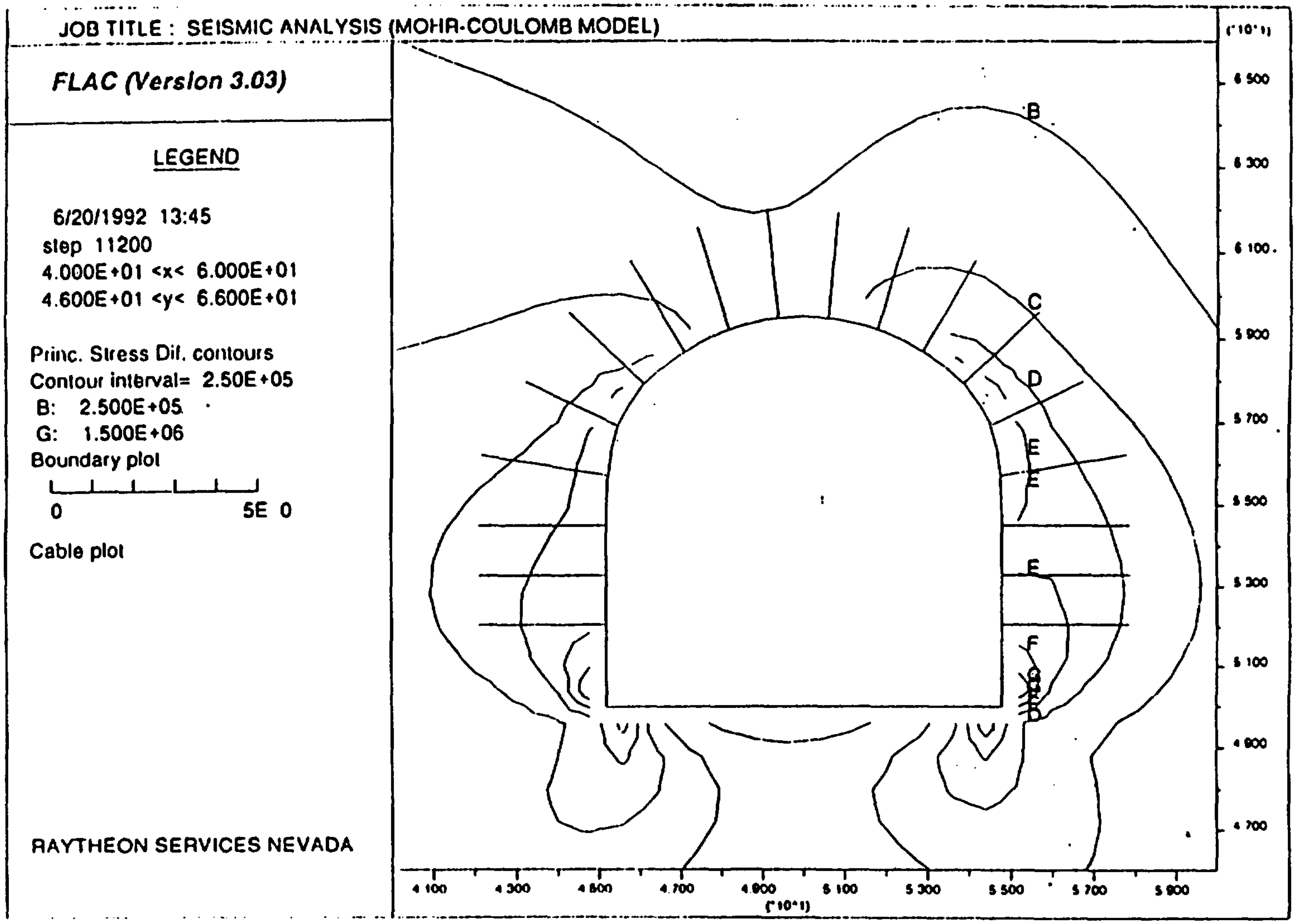

Fig. 17 Principal Stress Difference Contours around the Tunnel Opening at Seismic Event with Horizontal and Vertical Components of Acceleration of 0.75g, Mohr-Coulomb Model (Case 1). Compression is Negative. Stresses are in Pascal.

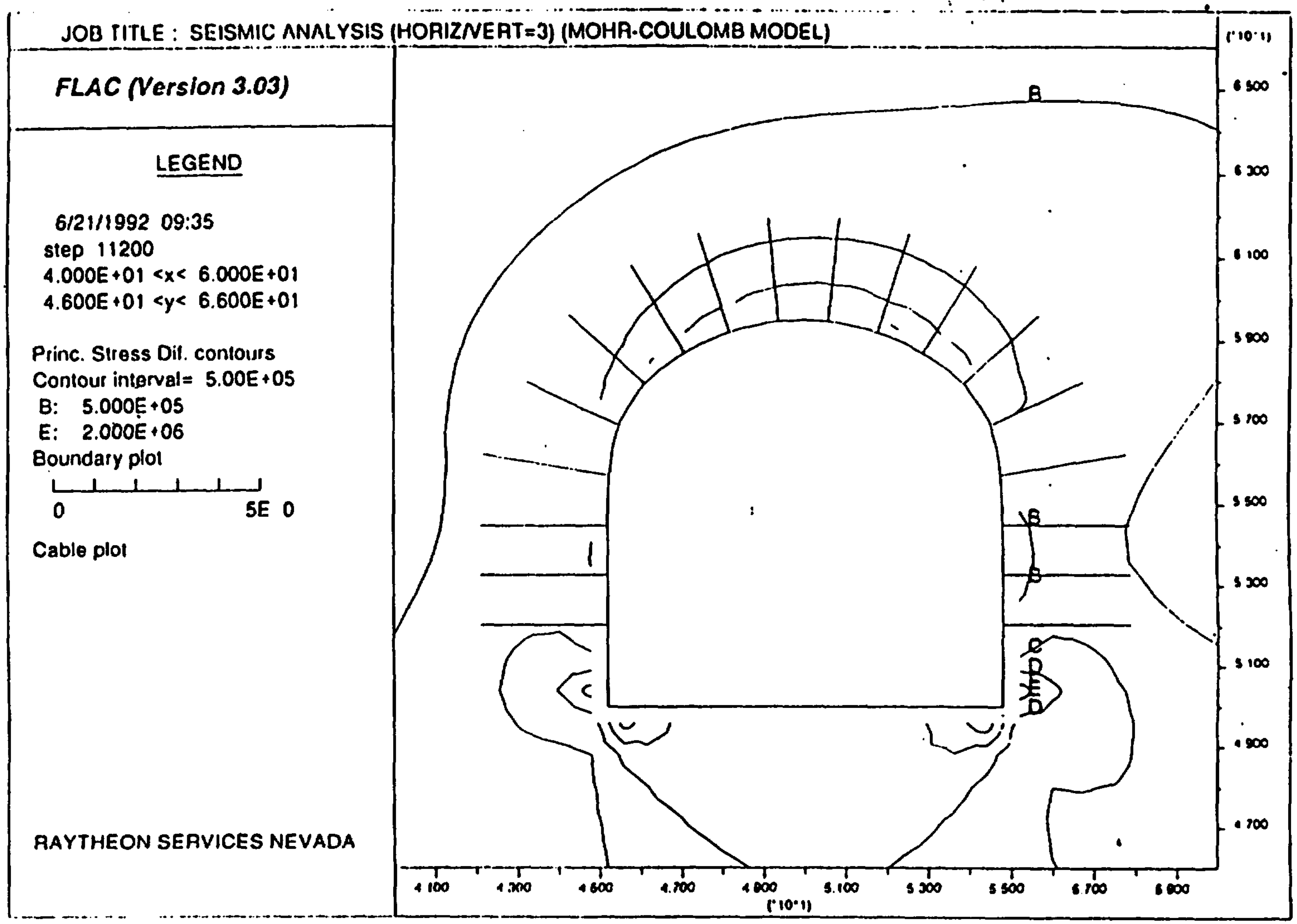

Fig. 18 Principal Stress Difference Contours around the Tunnel Opening at Seismic Event with Horizontal and Vertical Components of Acceleration of 0.75g, Mohr-Coulomb Model (Case 2). Compression is Negative. Stresses are in Pascal.

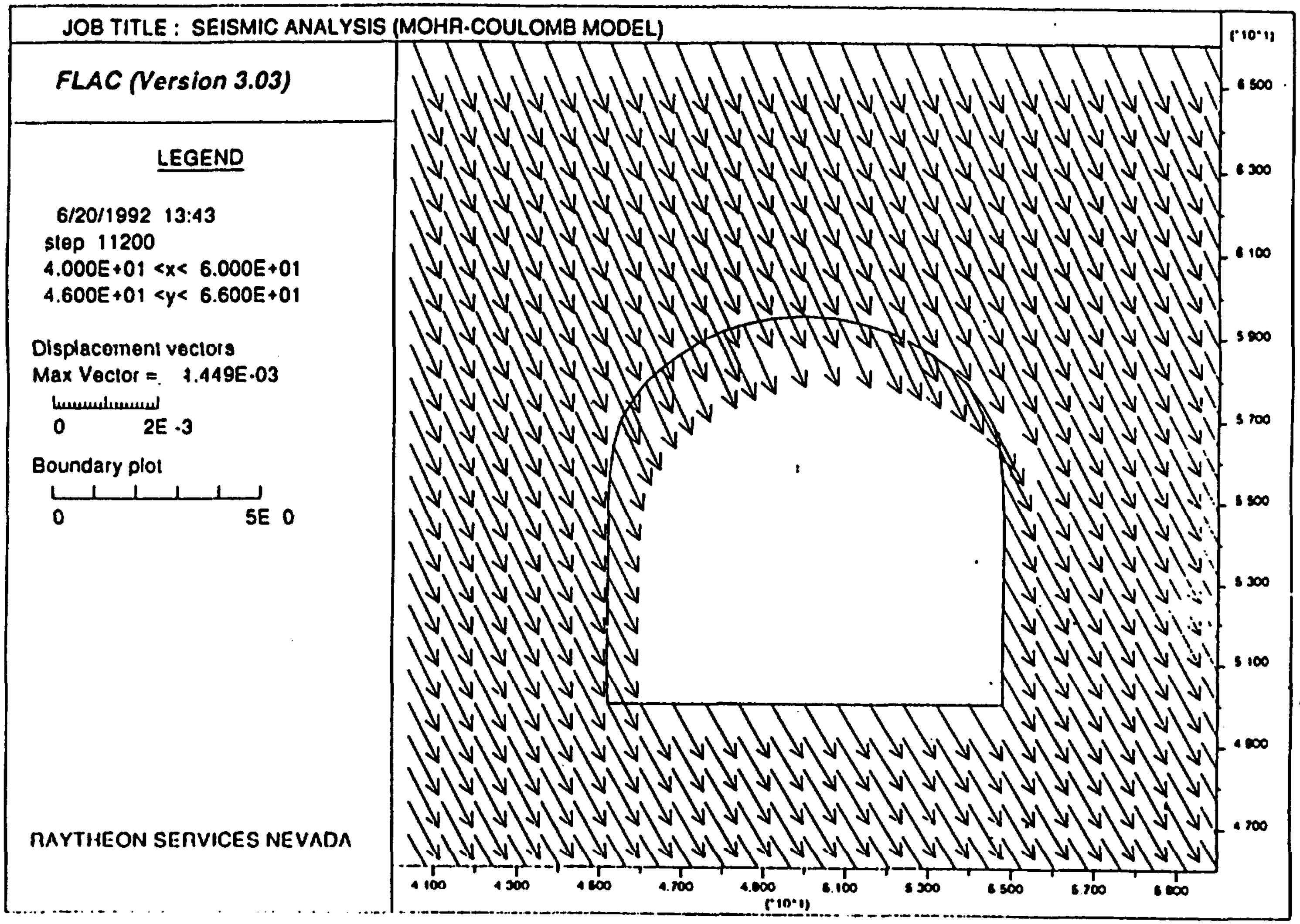

Fig. 19 Displacement Vectors around the Tunnel Opening at Seismic Event with Horizontal and Vertical Components of Acceleration of 0.5g, Mohr-Coulomb Model (Case 1). Compression is Negative. Stresses are in Pascal.

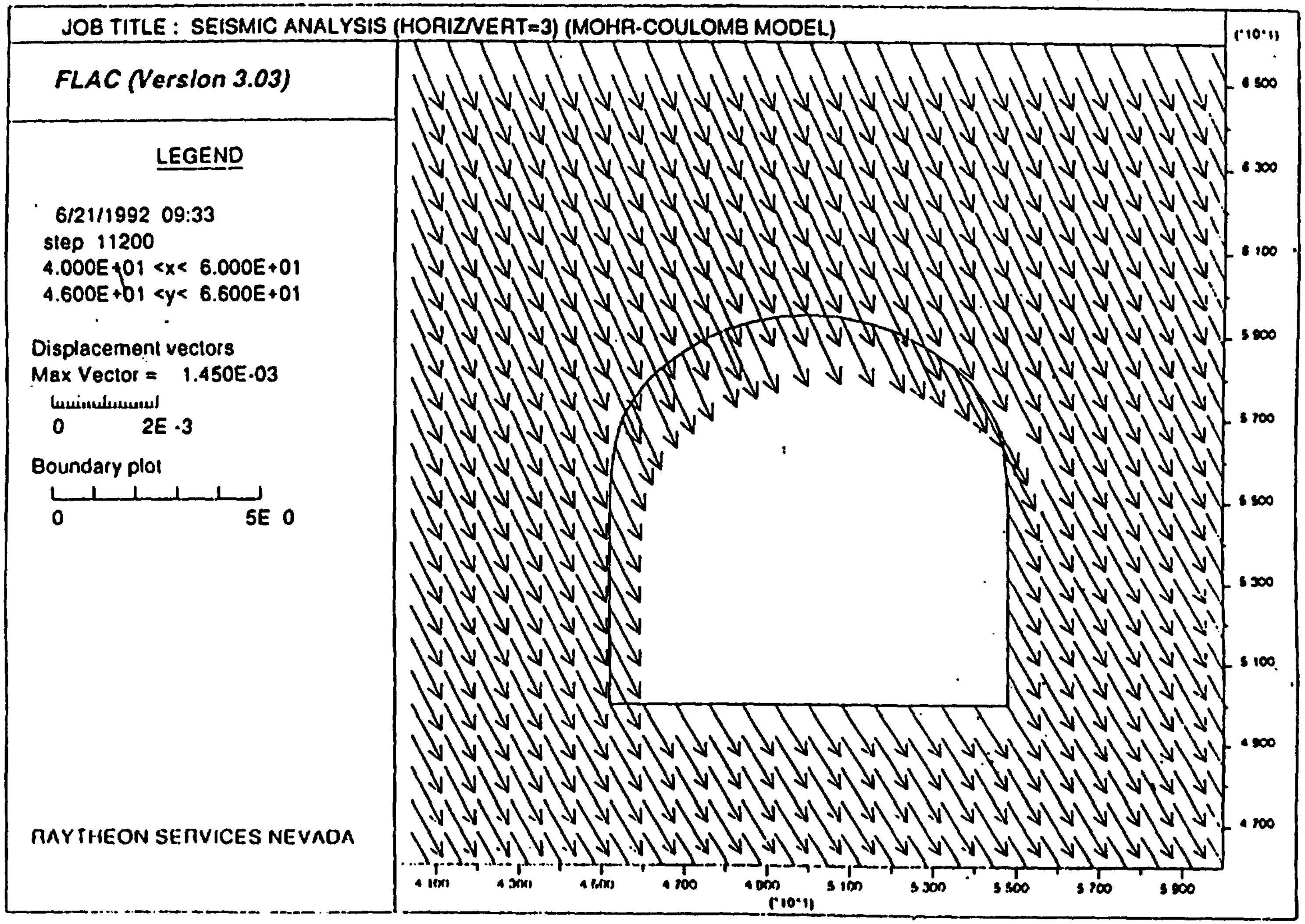

Fig. 20 Displacement Vectors around the Tunnel Opening at Seismic Event with Horizontal and Vertical Components of Acceleration of 0.5g, Mohr-Coulomb Model (Case 2). Compression is Negative. Stresses are in Pascal.

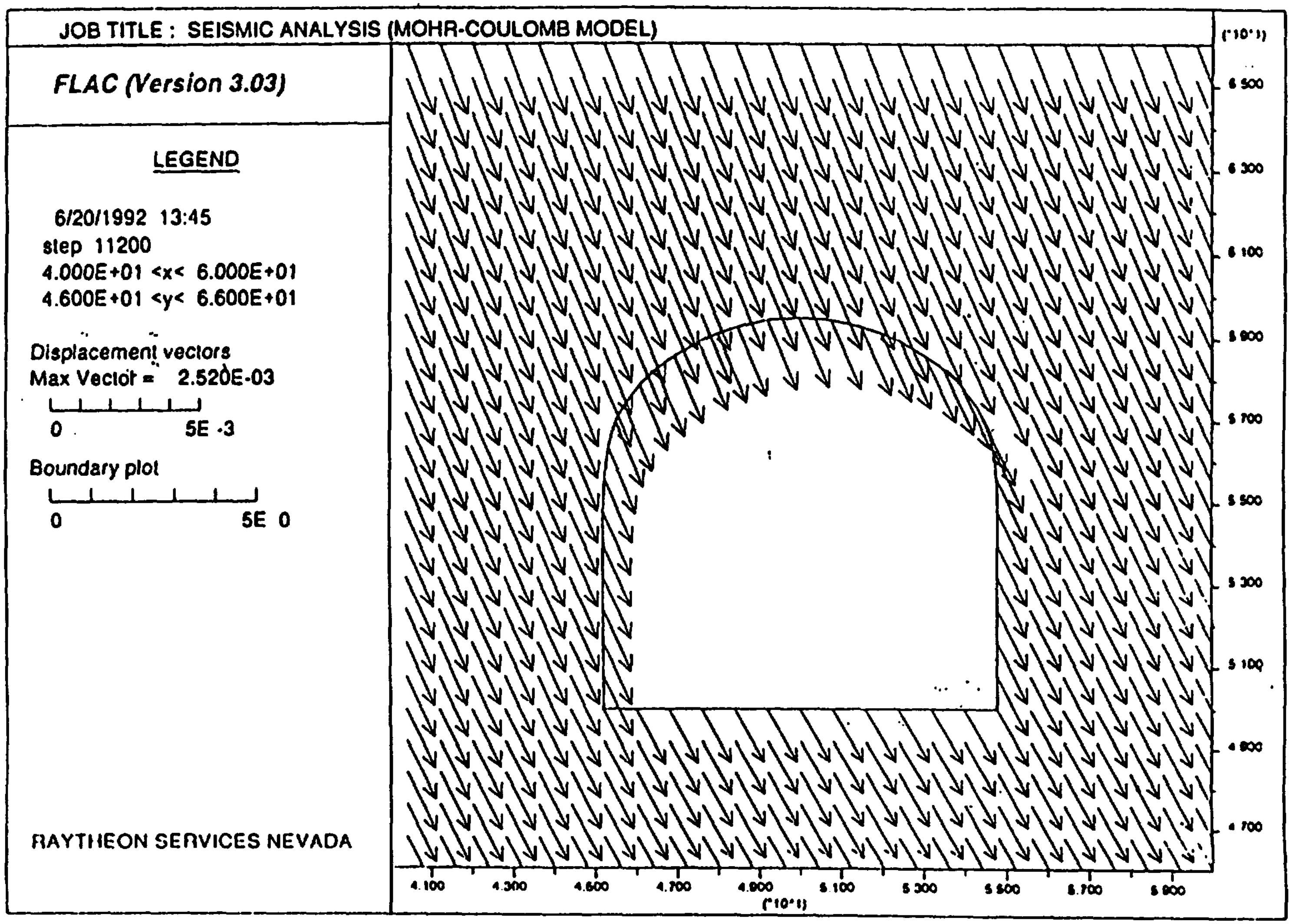

Fig. 21 Displacement Vectors around the Tunnel Opening at Seismic Event with Horizontal and Vertical Components of Acceleration of 0.75g, Mohr-Coulomb Model (Case 1). Compression is Negative. Stresses are in Pascal.

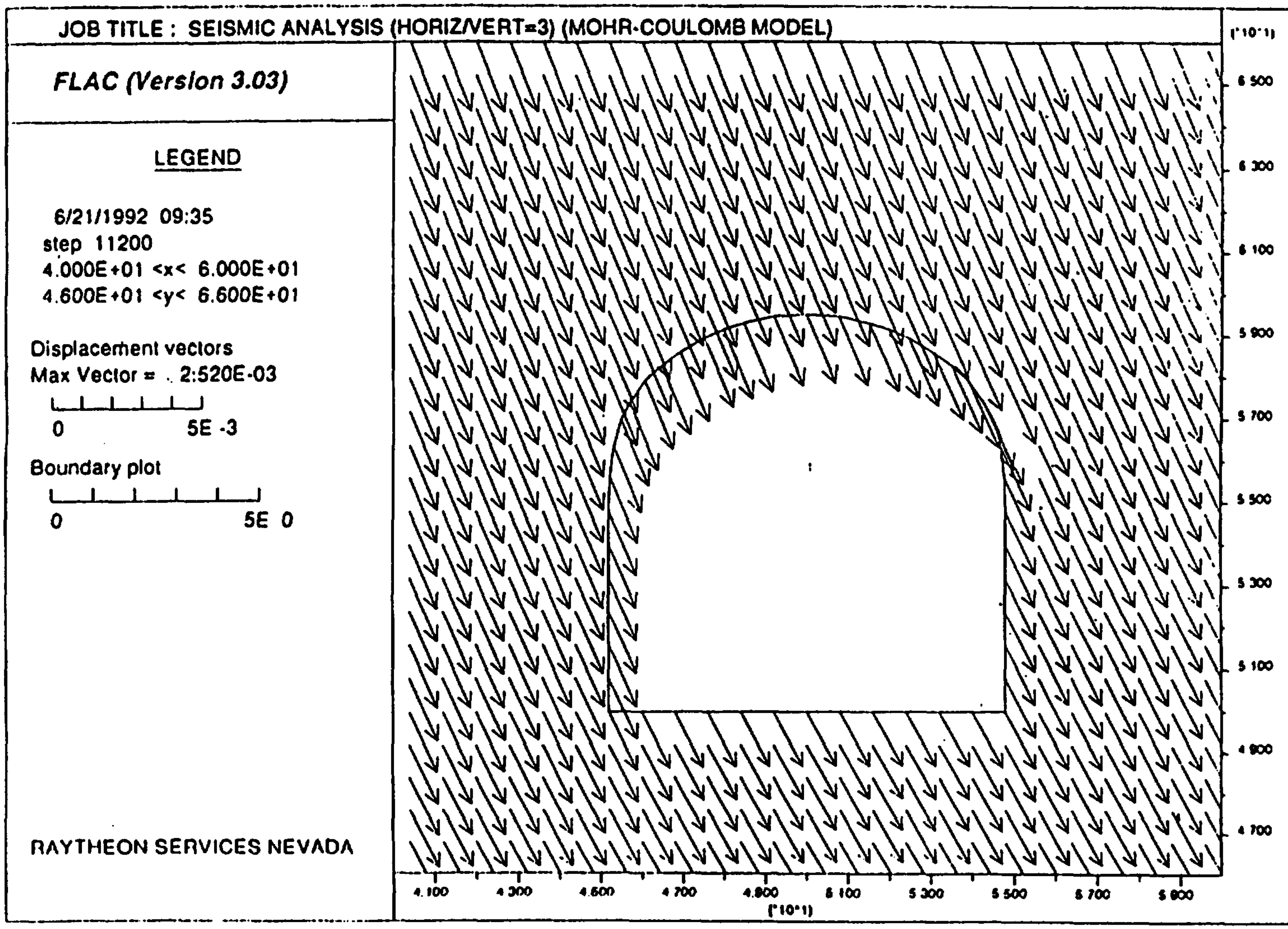

Fig. 22 Displacement Vectors around the Tunnel Opening at Seismic Event with Horizontal and Vertical Components of Acceleration of 0.75g, Mohr-Coulomb Model (Case 2). Compression is Negative. Stresses are in Pascal.

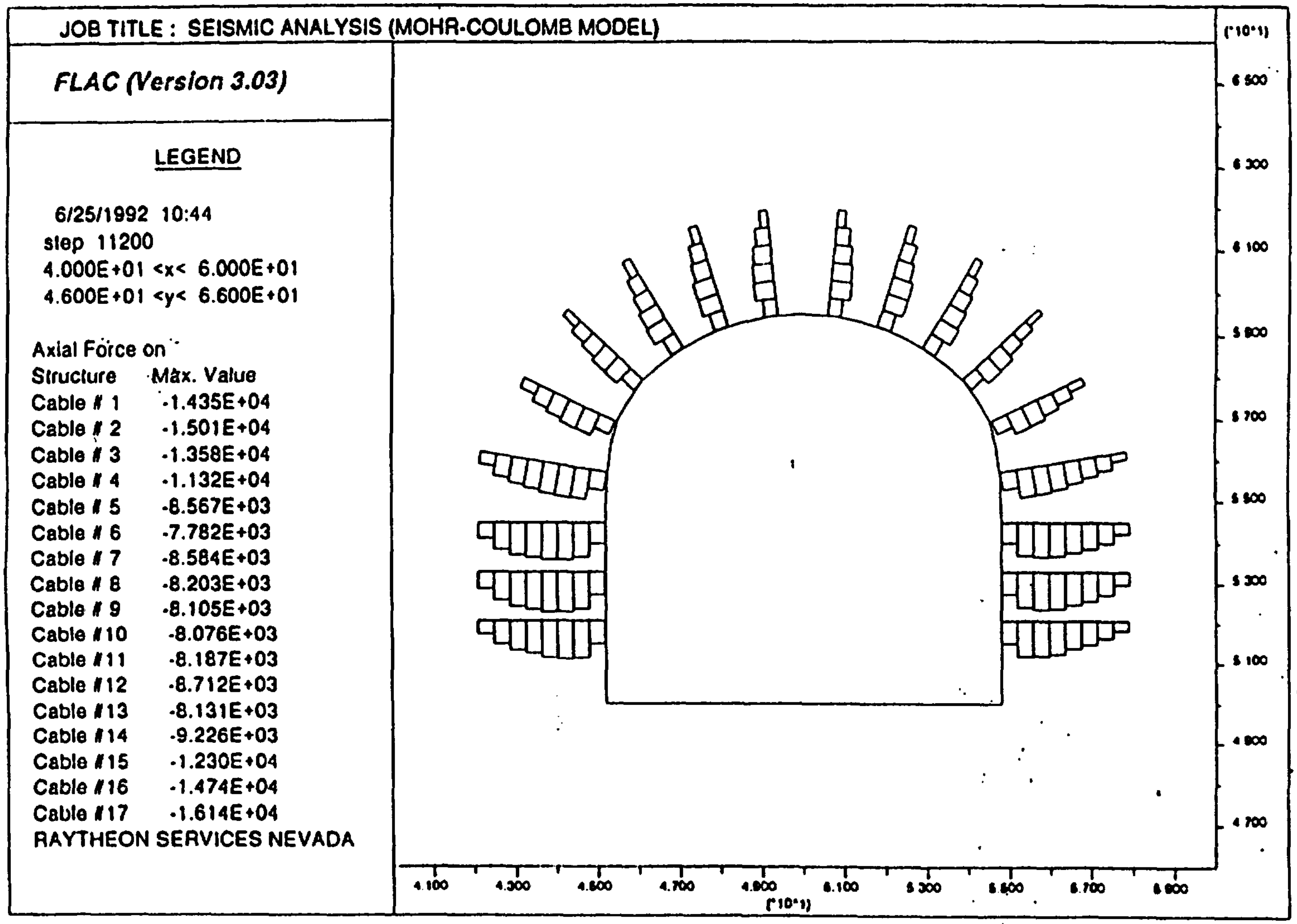

Fig. 23 Axial Force in Bolts at Seismic Event with Horizontal and Vertical Components of Acceleration of 0.5g, Mohr-Coulomb Model (Case 1). Forces are in Newton. Bolts are Numbered in CCW Direction.

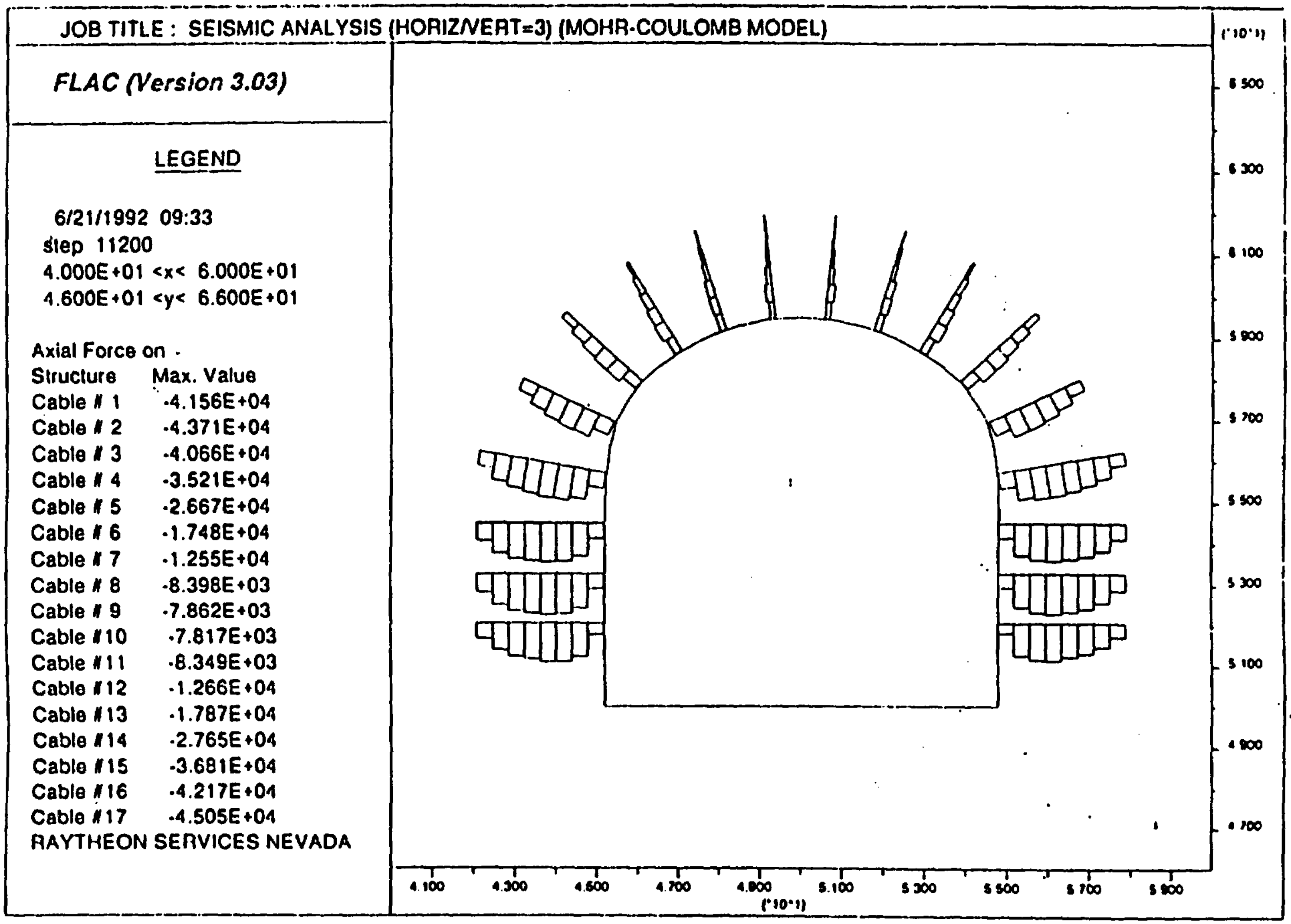

Fig. 24 Axial Force in Bolts at Seismic Event with Horizontal and Vertical Components of Acceleration of 0.5g, Mohr-Coulomb Model (Case 2). Forces are in Newton. Bolts are Numbered in CCW Direction.

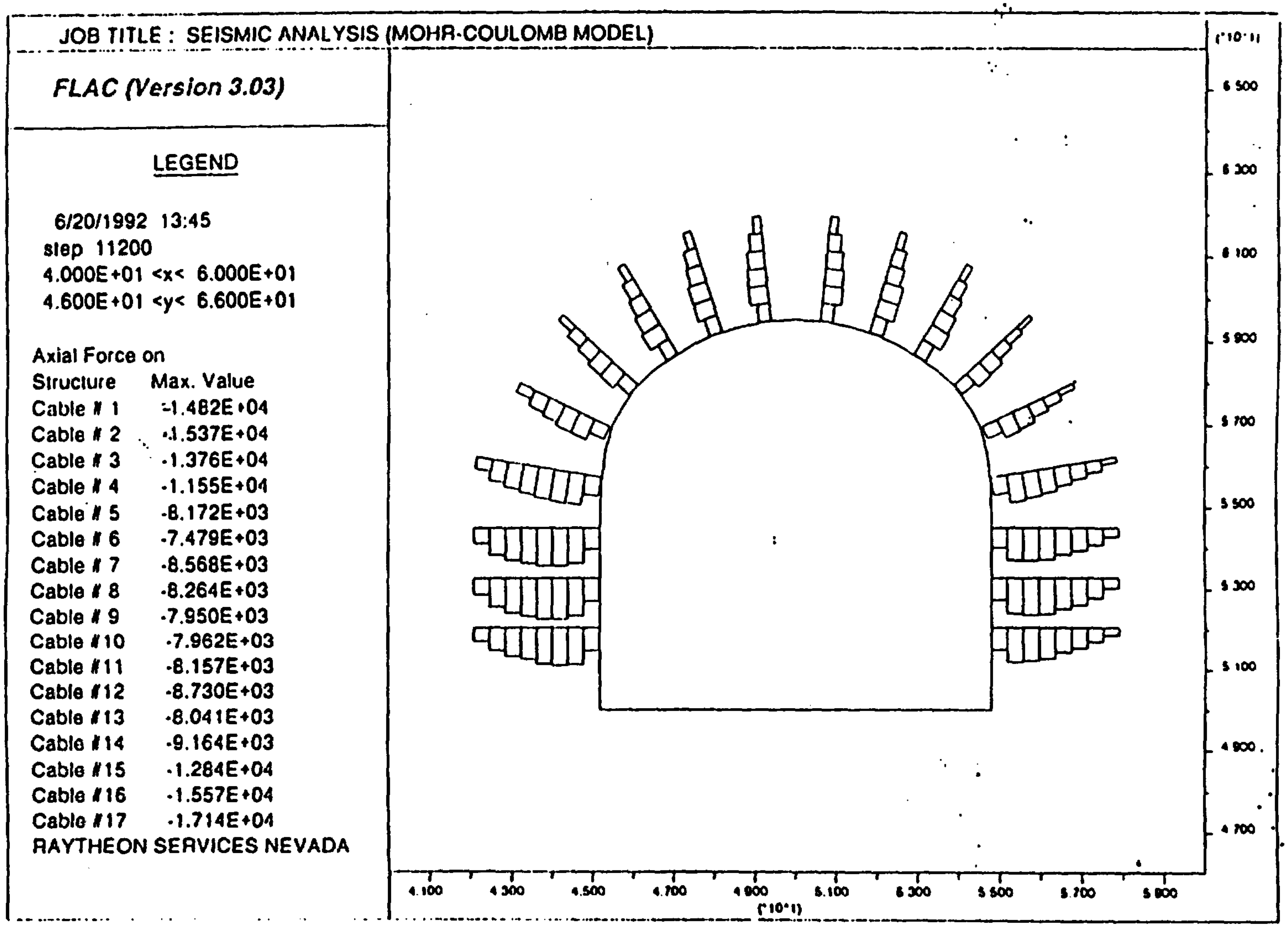

Fig. 25 Axial Force in Bolts at Seismic Event with Horizontal and Vertical Components of Acceleration of 0.75g, Mohr-Coulomb Model (Case 1). Forces are in Newton. Bolts are Numbered in CCW Direction.

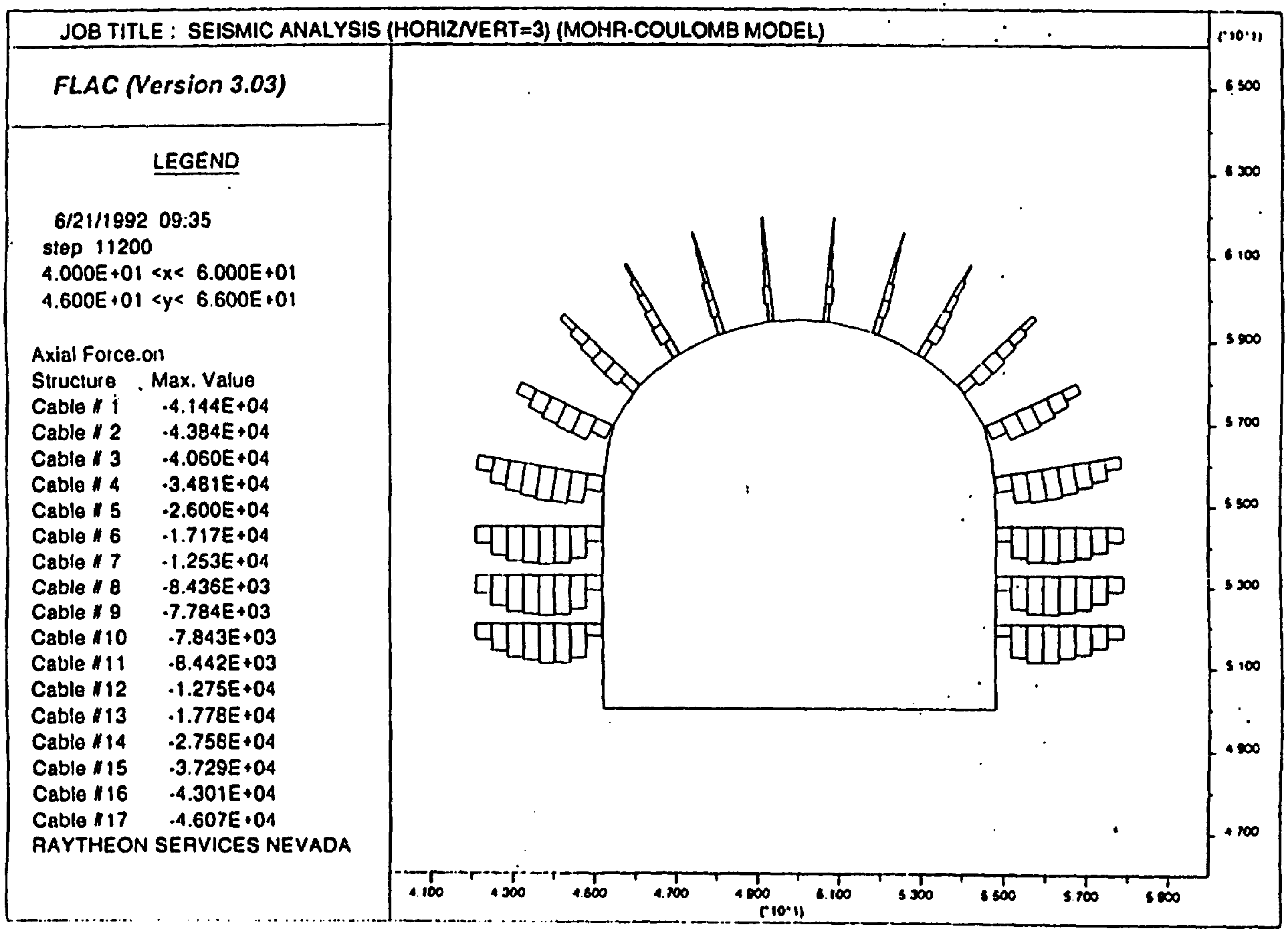

Fig. 26 Axial Force in Bolts at Seismic Event with Horizontal and Vertical Components of Acceleration of 0.75g, Mohr-Coulomb Model (Case 2). Forces are in Newton. Bolts are Numbered in CCW Direction.

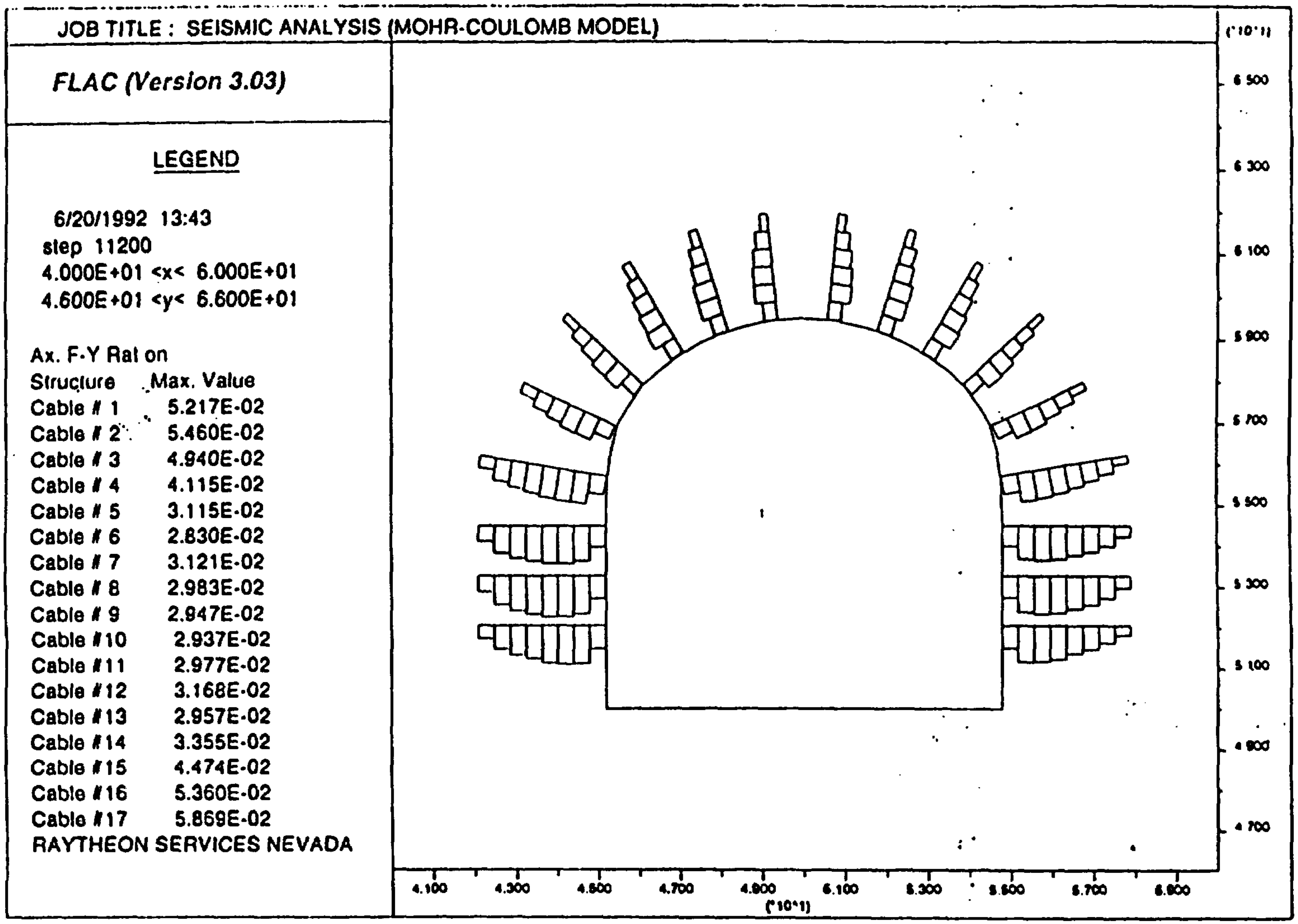

Fig. 27 Ratio of Axial Load to Yield Strength of Bolts at Seismic Event with Horizontal and Vertical Components of Acceleration of 0.5g, Mohr-Coulomb Model (Case 1). Bolts are Numbered in CCW Direction.

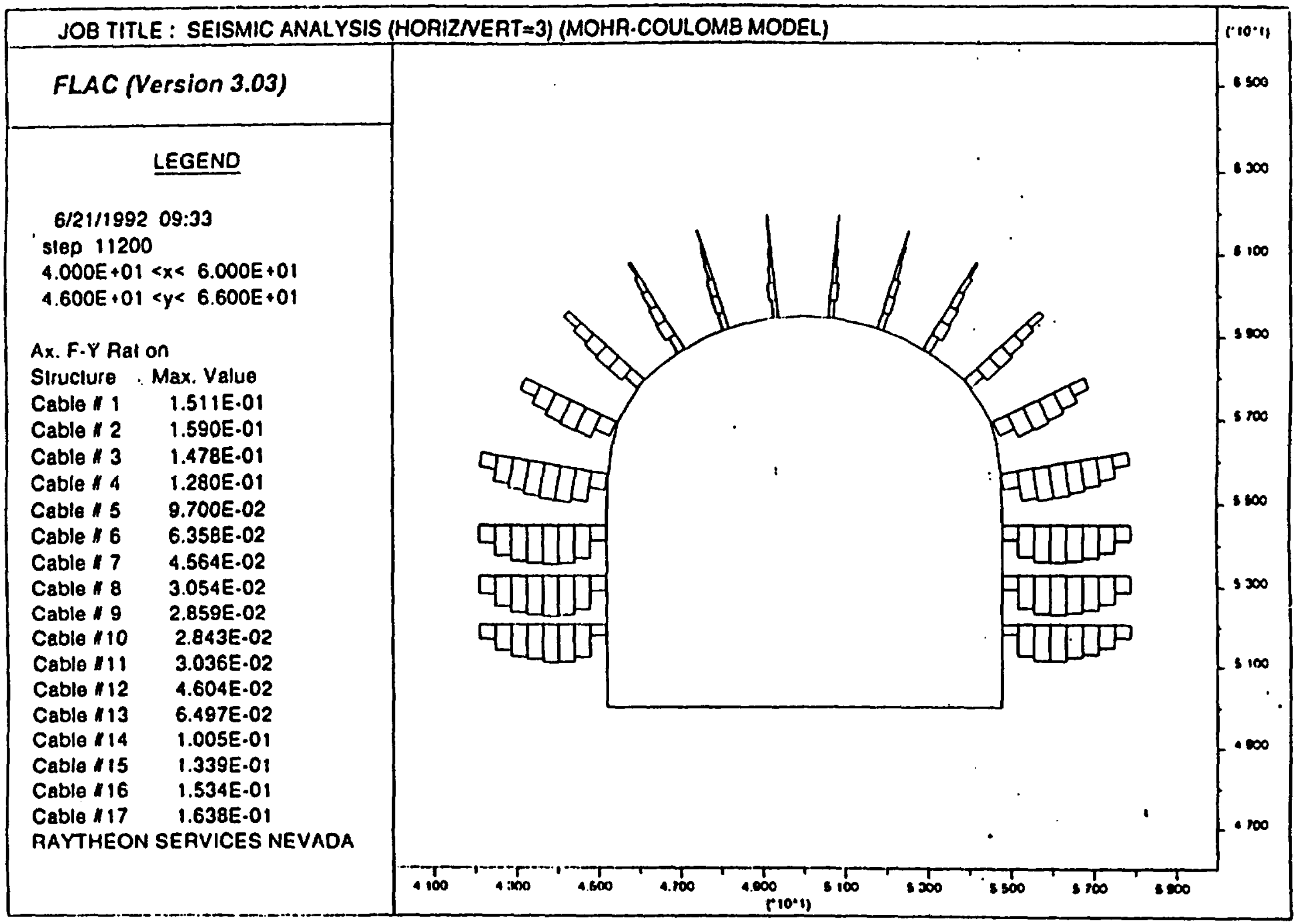

Fig. 28 Ratio of Axial Load to Yield Strength of Bolts at Seismic Event with Horizontal and Vertical Components of Acceleration of 0.5g, Mohr-Coulomb Model (Case 2). Bolts are Numbered in CCW Direction.

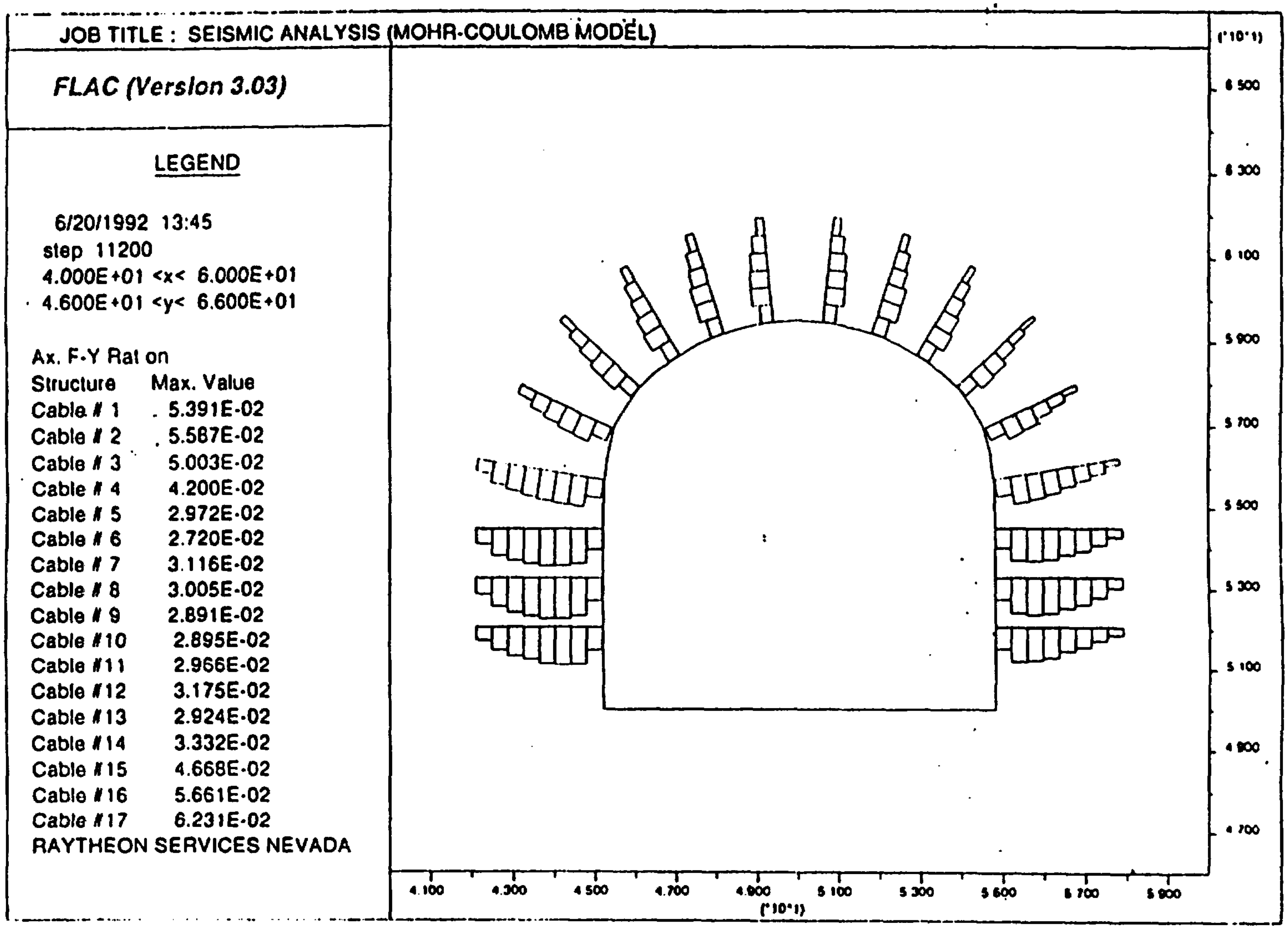

Fig. 29 Ratio of Axial Load to Yield Strength of Bolts at Seismic Event with Horizontal and Vertical Components of Acceleration of 0.75g, Mohr-Coulomb Model (Case 1). Bolts are Numbered in CCW Direction.

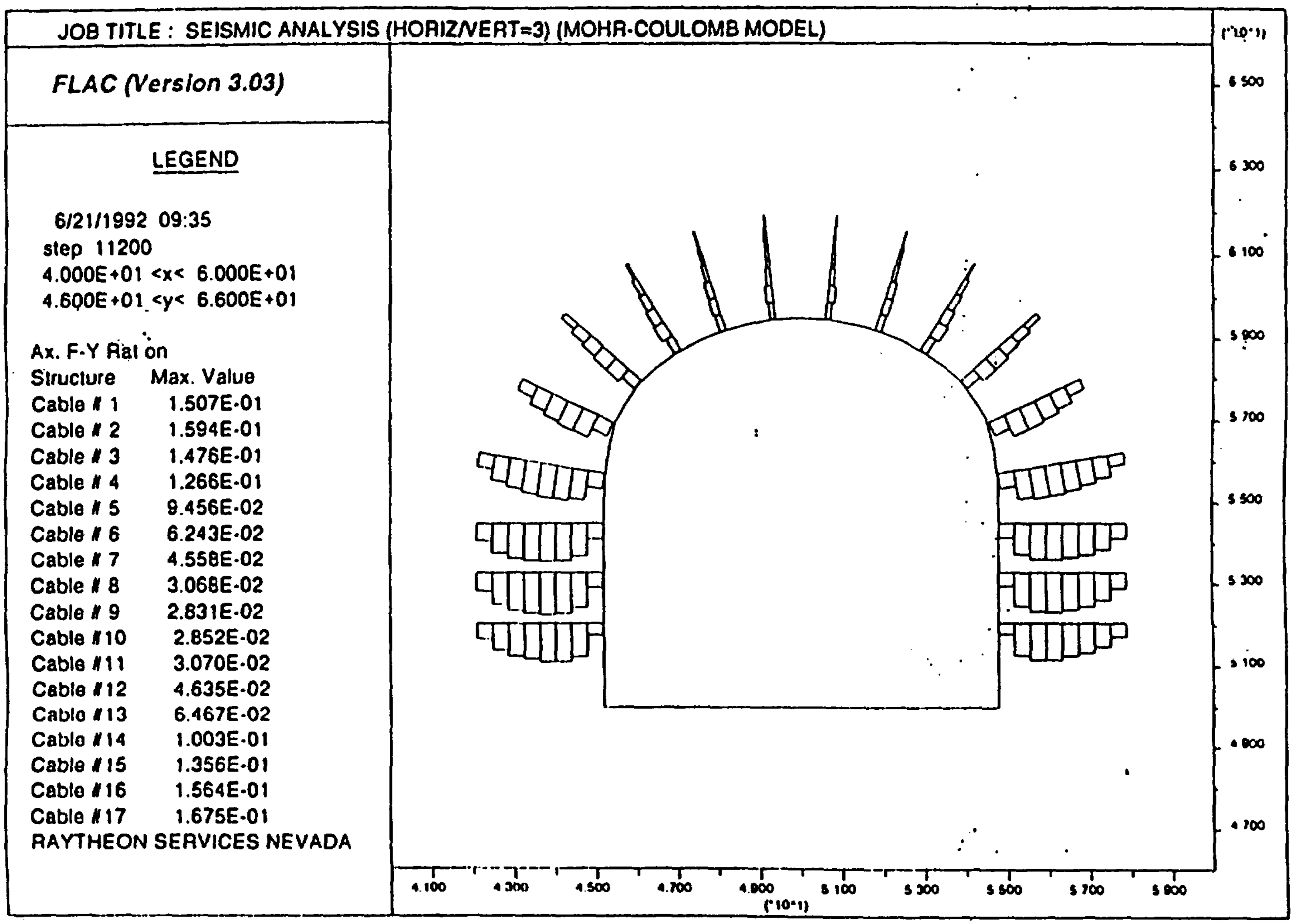

Fig. 30 Ratio of Axial Load to Yield Strength of Bolts at Seismic Event with Horizontal and Vertical Components of Acceleration of 0.75g, Mohr-Coulomb Model (Case 2). Bolts are Numbered in CCW Direction.

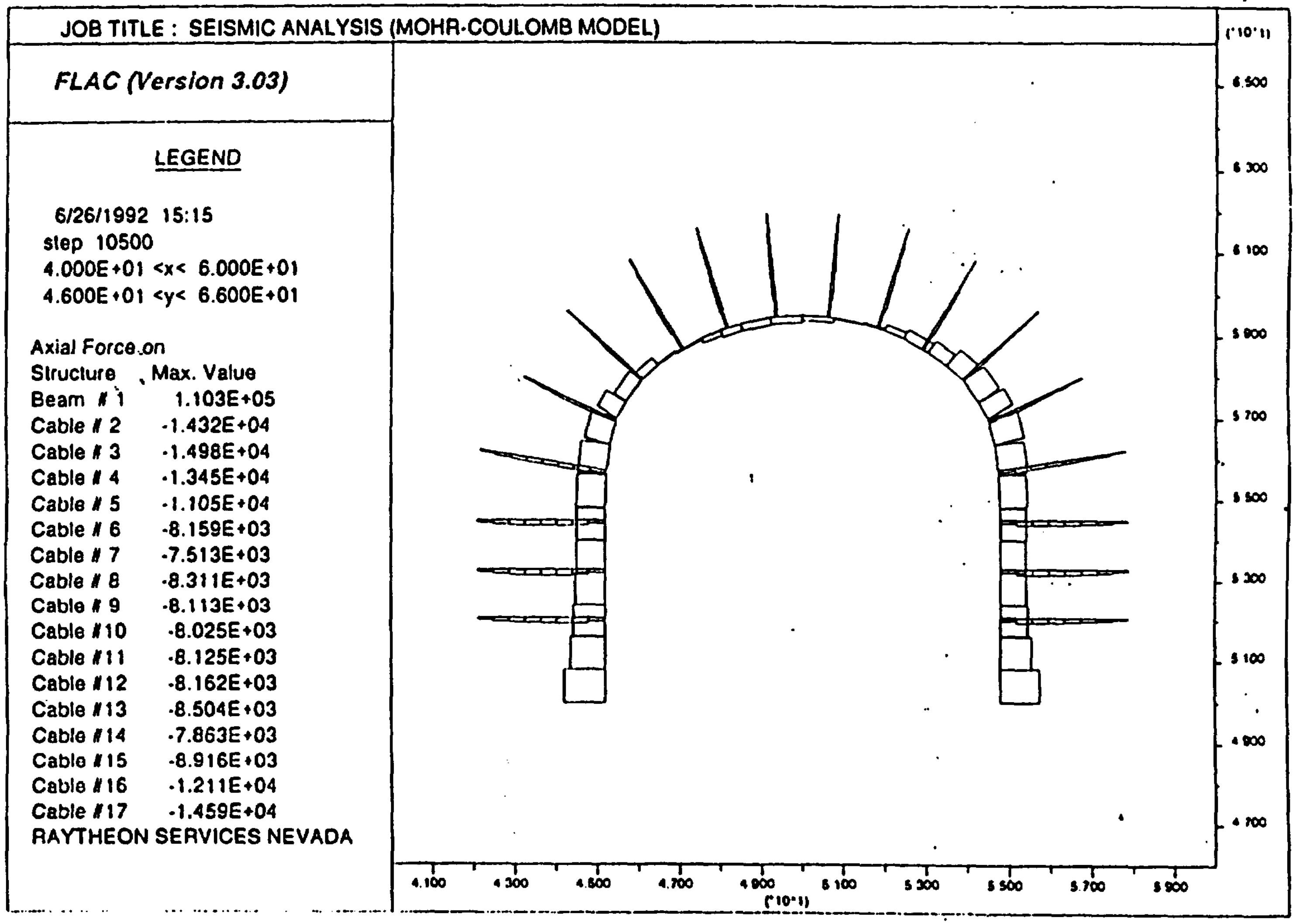

Fig. 31 Axial Force in 61 cm Starter Tunnel Liner and Bolts at Seismic Event with Horizontal and Vertical Components of Acceleration of 0.5g, Mohr-Coulomb Model (Case 1). Forces are in Newton. Bolts are Numbered in CCW Direction.

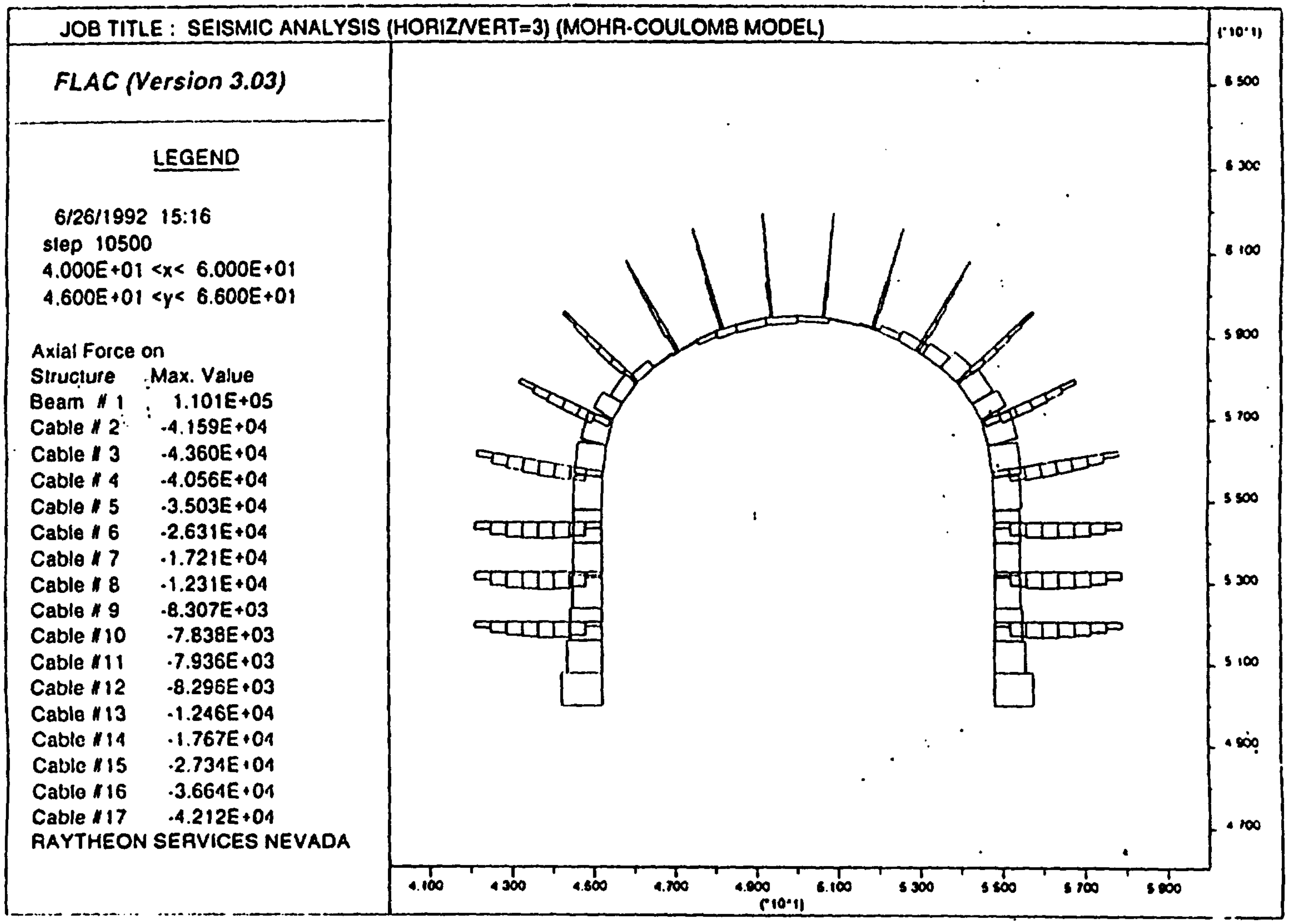

Fig. 32 Axial Force in 61 cm Starter Tunnel Liner and Bolts at Seismic Event with Horizontal and Vertical Components of Acceleration of 0.5g, Mohr-Coulomb Model (Case 2). Forces are in Newton. Bolts are Numbered in CCW Direction.

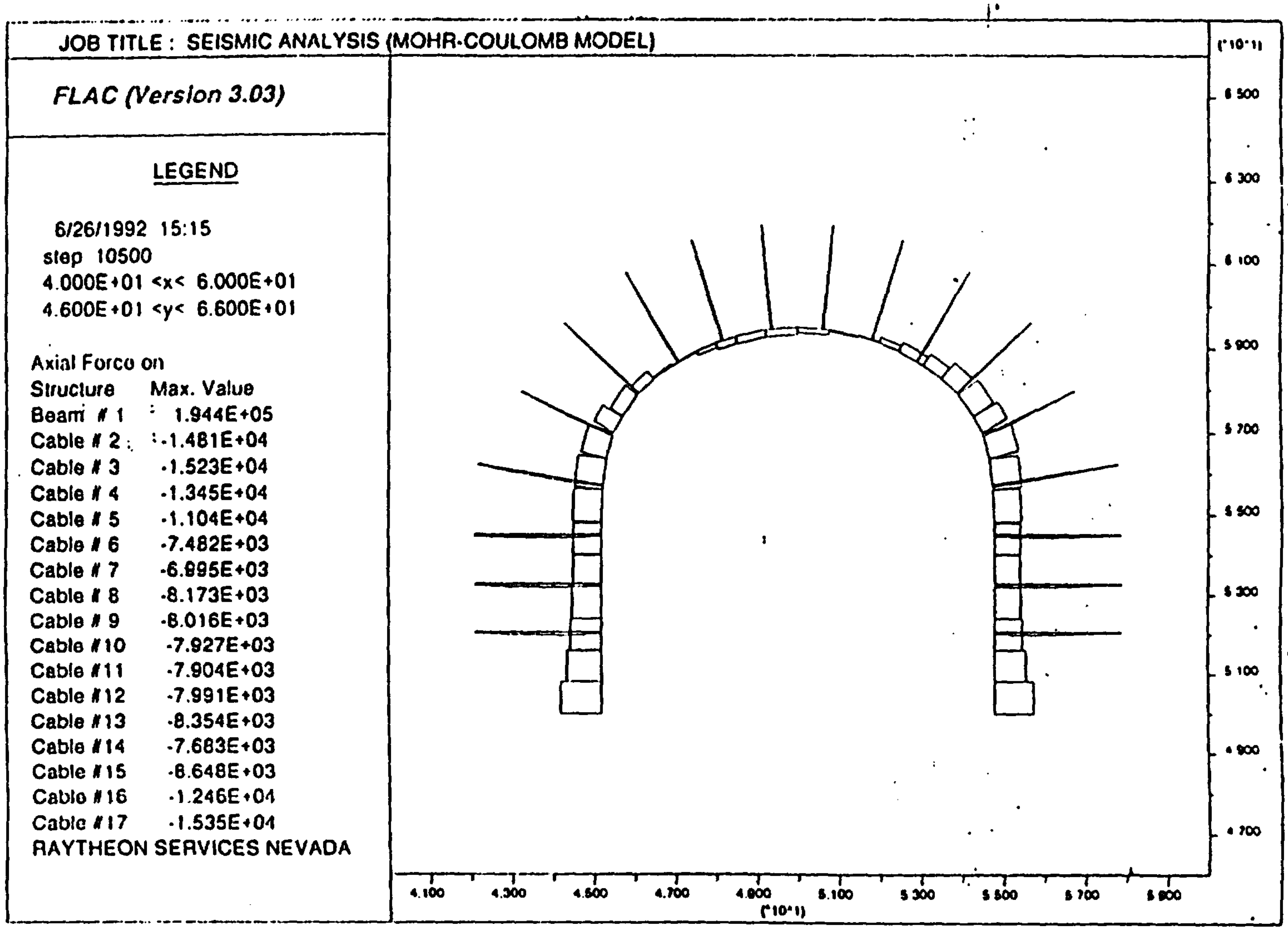

Fig. 33 Axial Force in 61 cm Starter Tunnel Liner and Bolts at Seismic Event with Horizontal and Vertical Components of Acceleration of 0.75g, Mohr-Coulomb Model (Case 1). Forces are in Newton. Bolts are Numbered in CCW Direction.

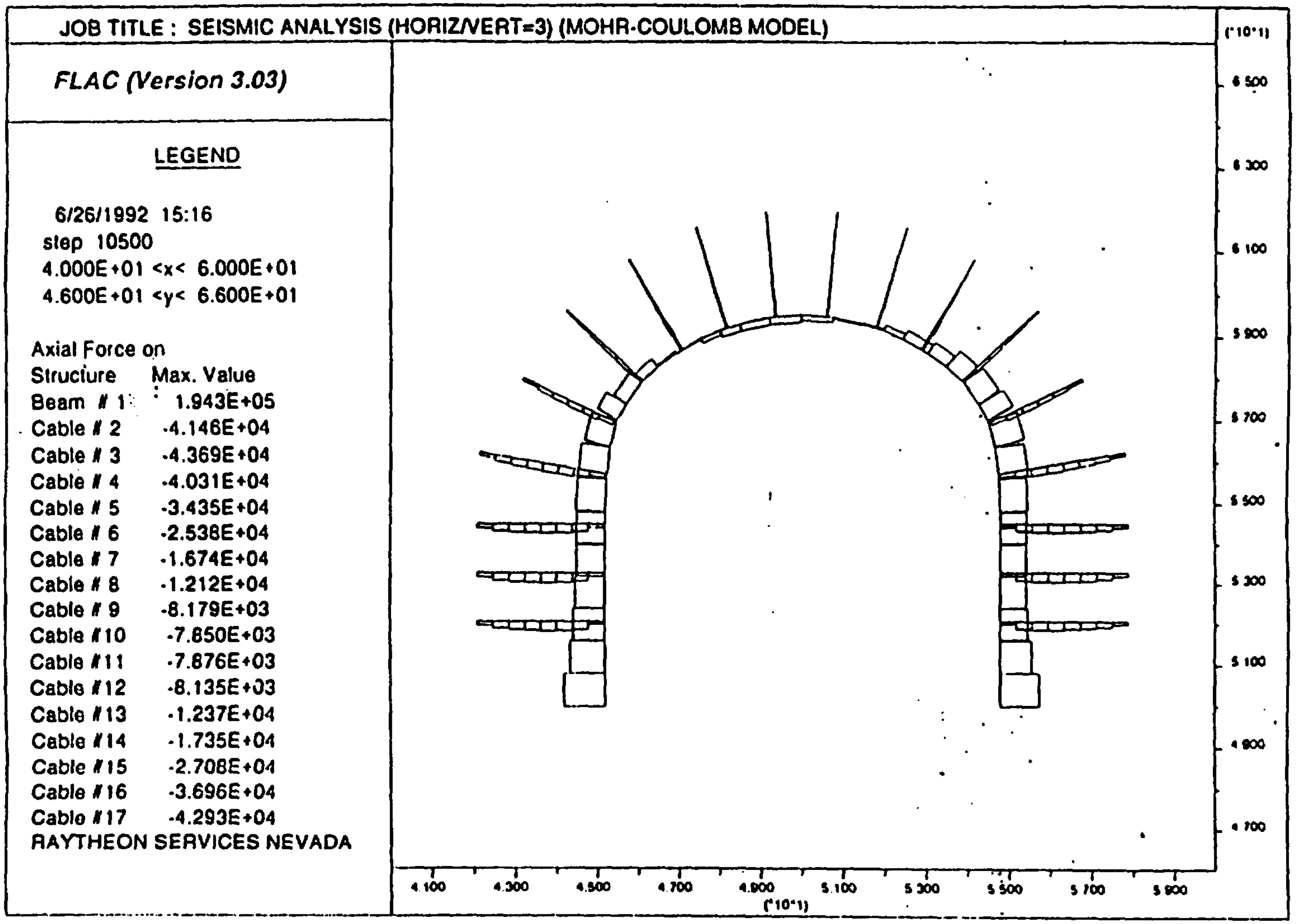

Fig. 34 Axial Force in 61 cm Starter Tunnel Liner and Bolts at Seismic Event with Horizontal and Vertical Components of Acceleration of 0.75g, Mohr-Coulomb Model (Case 2). Forces are in Newton. Bolts are Numbered in CCW Direction.

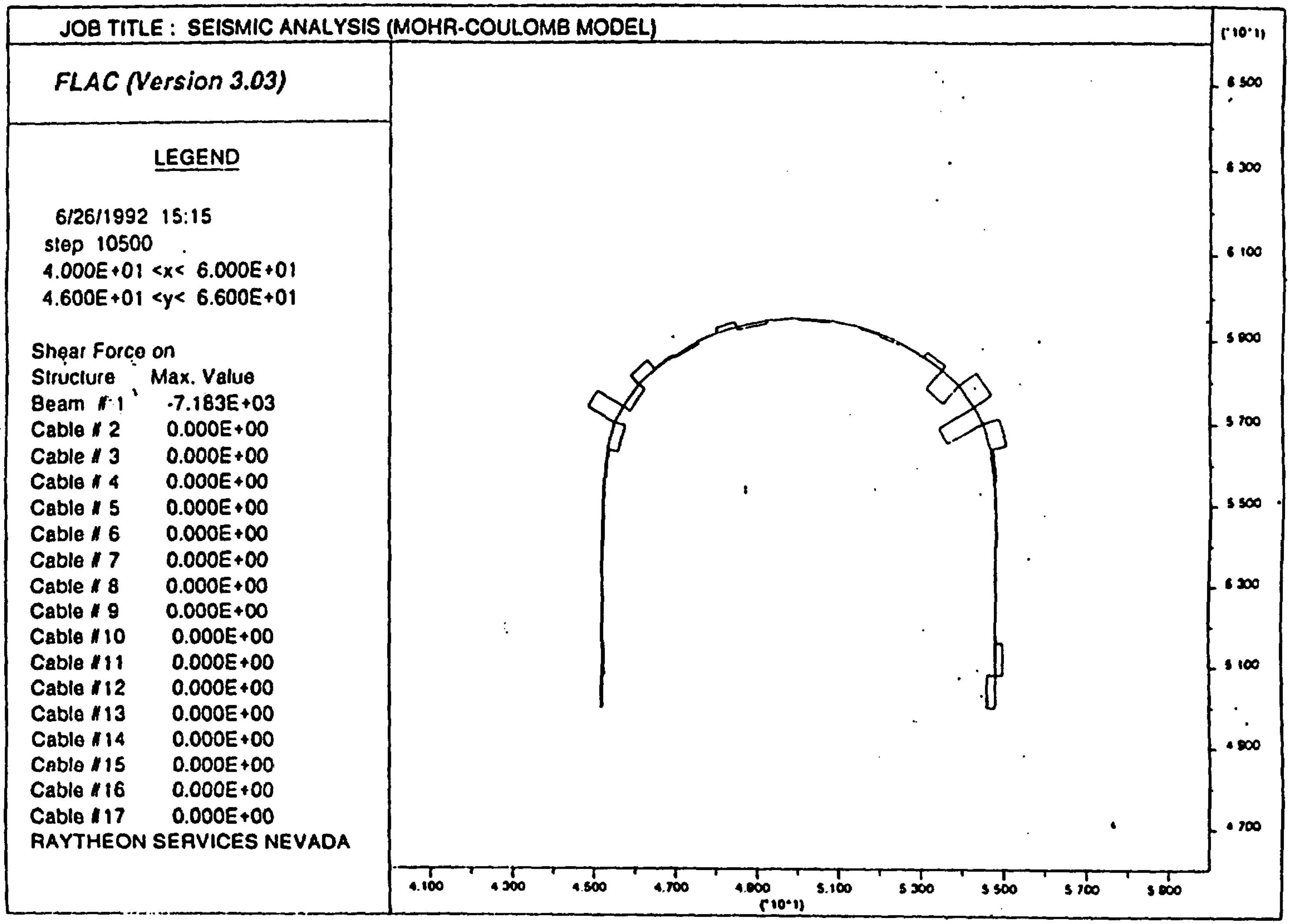

Fig. 35 Shear Force in 61 cm Starter Tunnel Liner at Seismic Event with Horizontal and Vertical Components of Acceleration of 0.5g, Mohr-Coulomb Model (Case 1). Forces are in Newton.

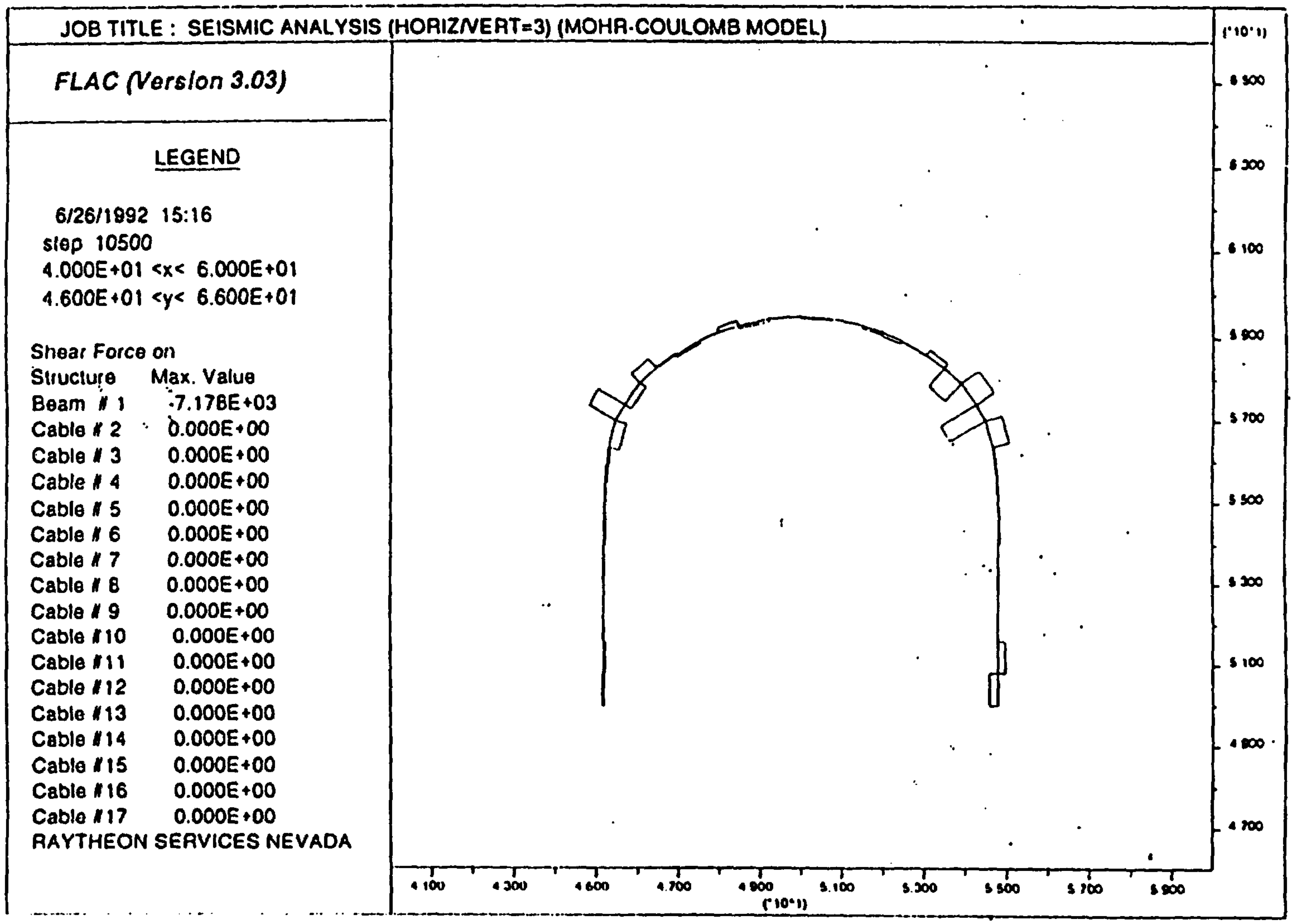

Fig. 36 Shear Force in 61 cm Starter Tunnel Liner at Seismic Event with Horizontal and Vertical Components of Acceleration of 0.5g, Mohr-Coulomb Model (Case 2). Forces are in Newton.

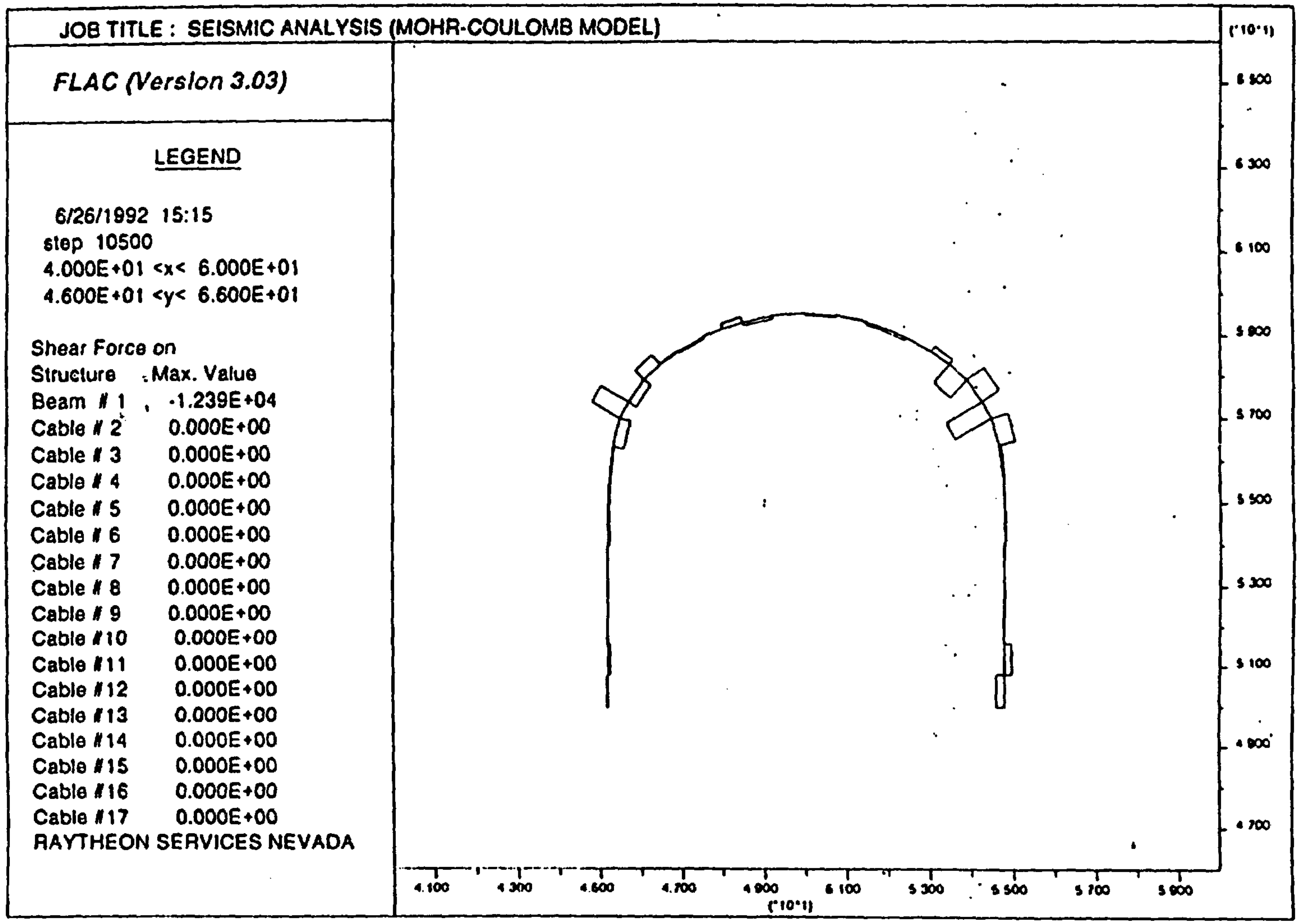

Fig. 37 Shear Force in 61 cm Starter Tunnel Liner at Seismic Event with Horizontal and Vertical Components of Acceleration of 0.75g, Mohr-Coulomb Model (Case 1). Forces are in Newton.

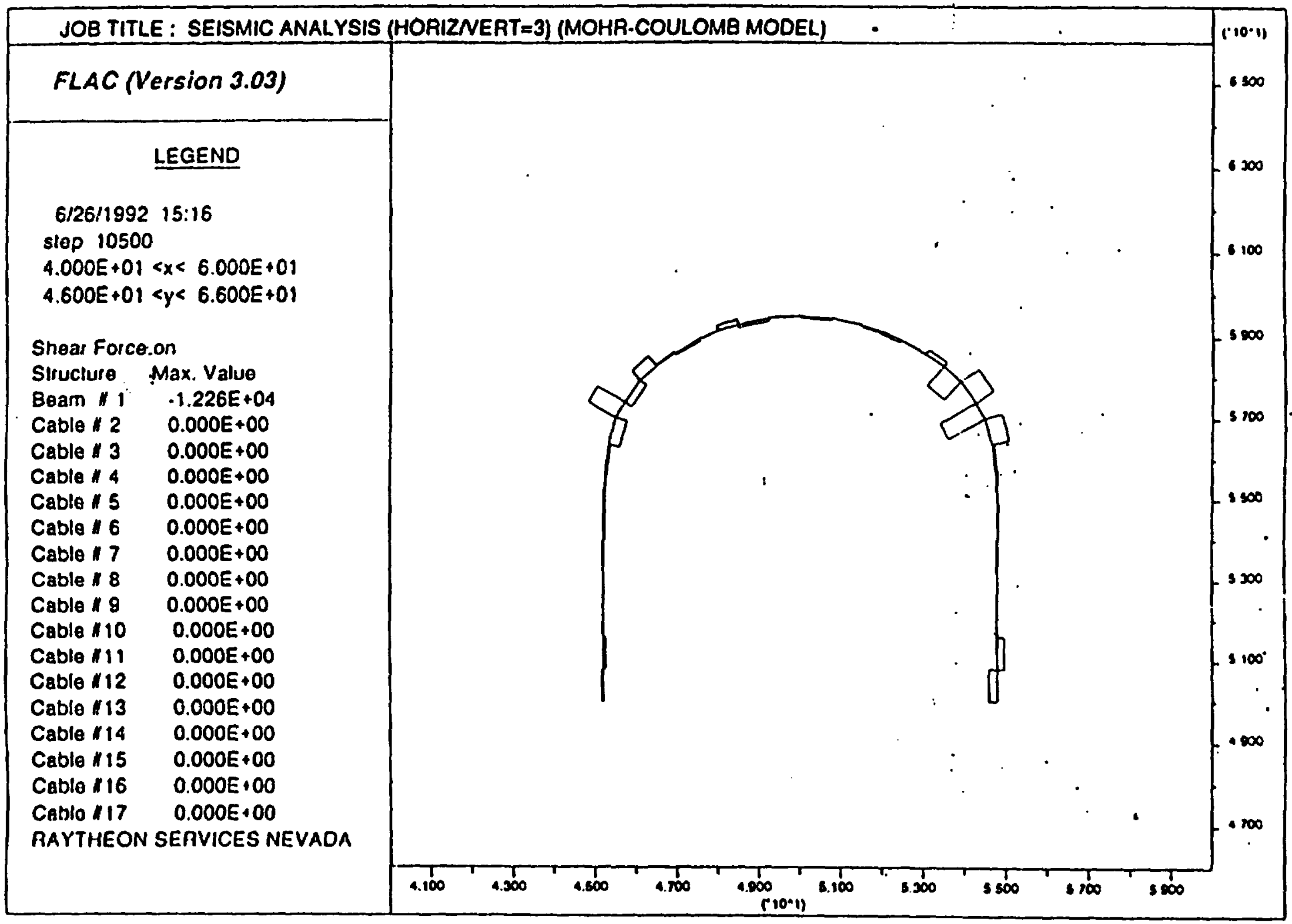

Fig. 38 Shear Force in 61 cm Starter Tunnel Liner Bolts at Seismic Event with Horizontal and Vertical Components of Acceleration of 0.75g, Mohr-Coulomb Model (Case 2). Forces are in Newton.

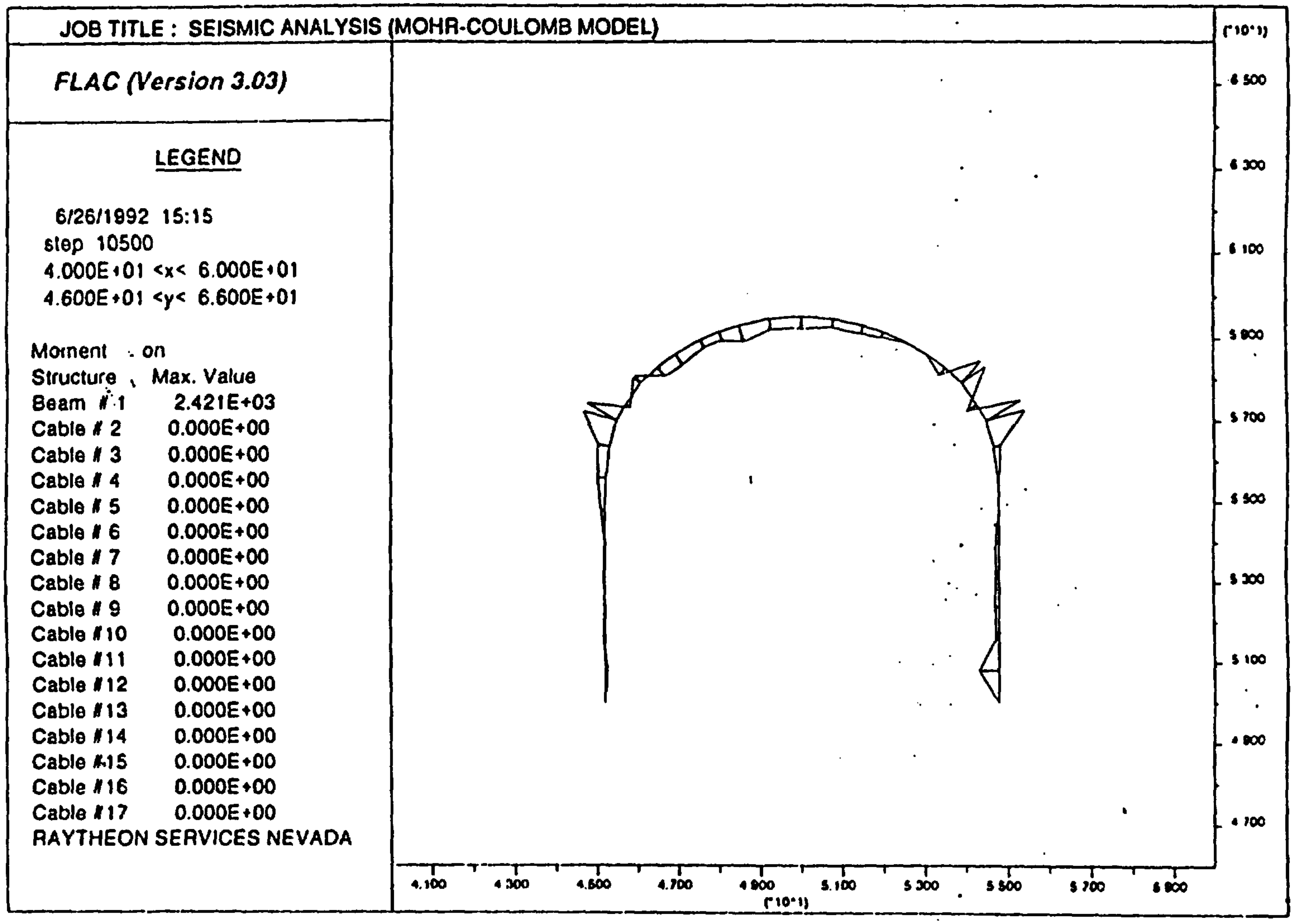

Fig. 39 Moment in 61 cm Starter Tunnel Liner at Seismic Event with Horizontal and Vertical Components of Acceleration of 0.5g, Mohr-Coulomb Model (Case 1). Moment is in Newton-Meters.

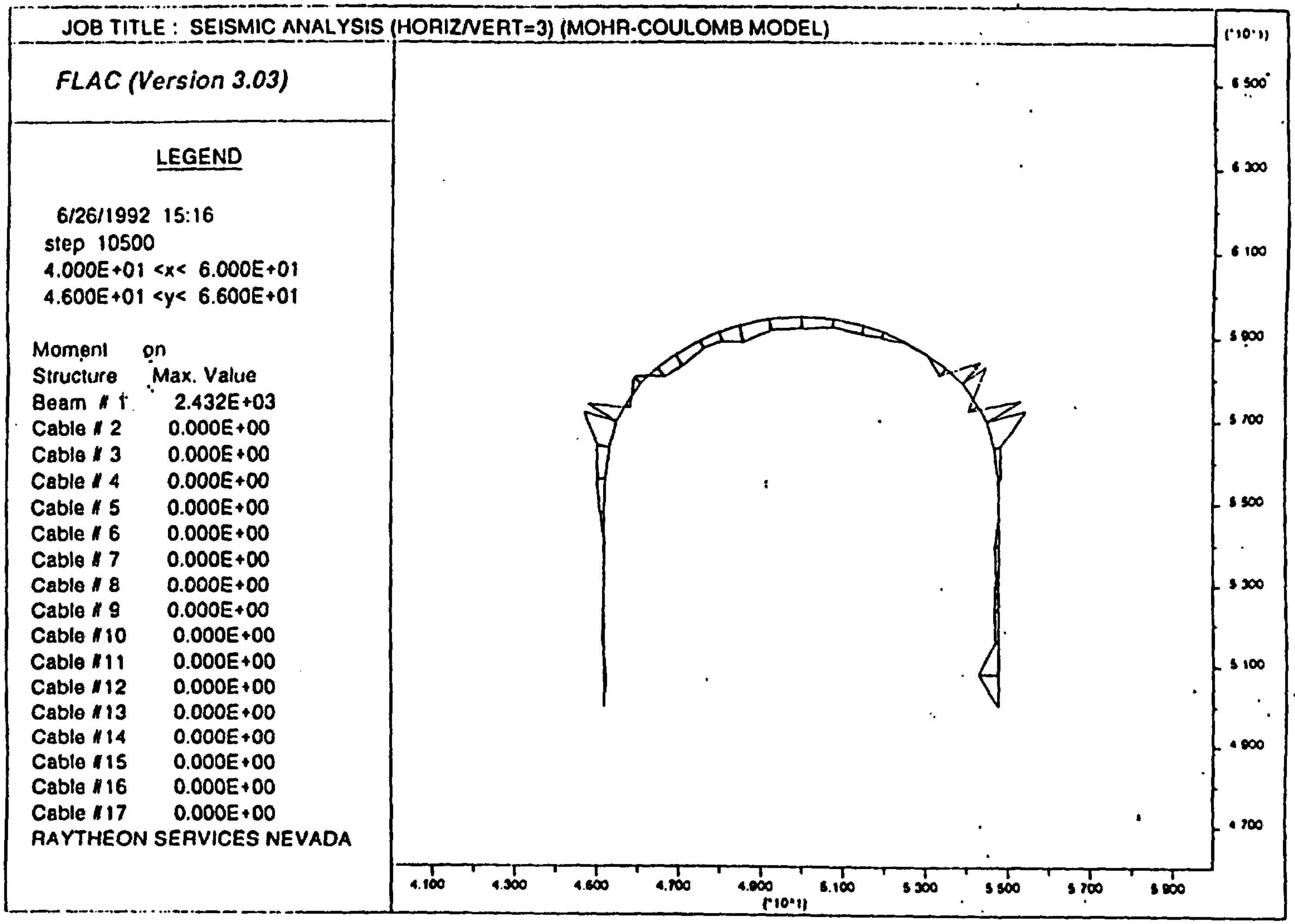

Fig. 40 Moment in 61 cm Starter Tunnel Liner at Seismic Event with Horizontal and Vertical Components of Acceleration of 0.5g, Mohr-Coulomb Model (Case 2). Moment is in Newton-Meters.

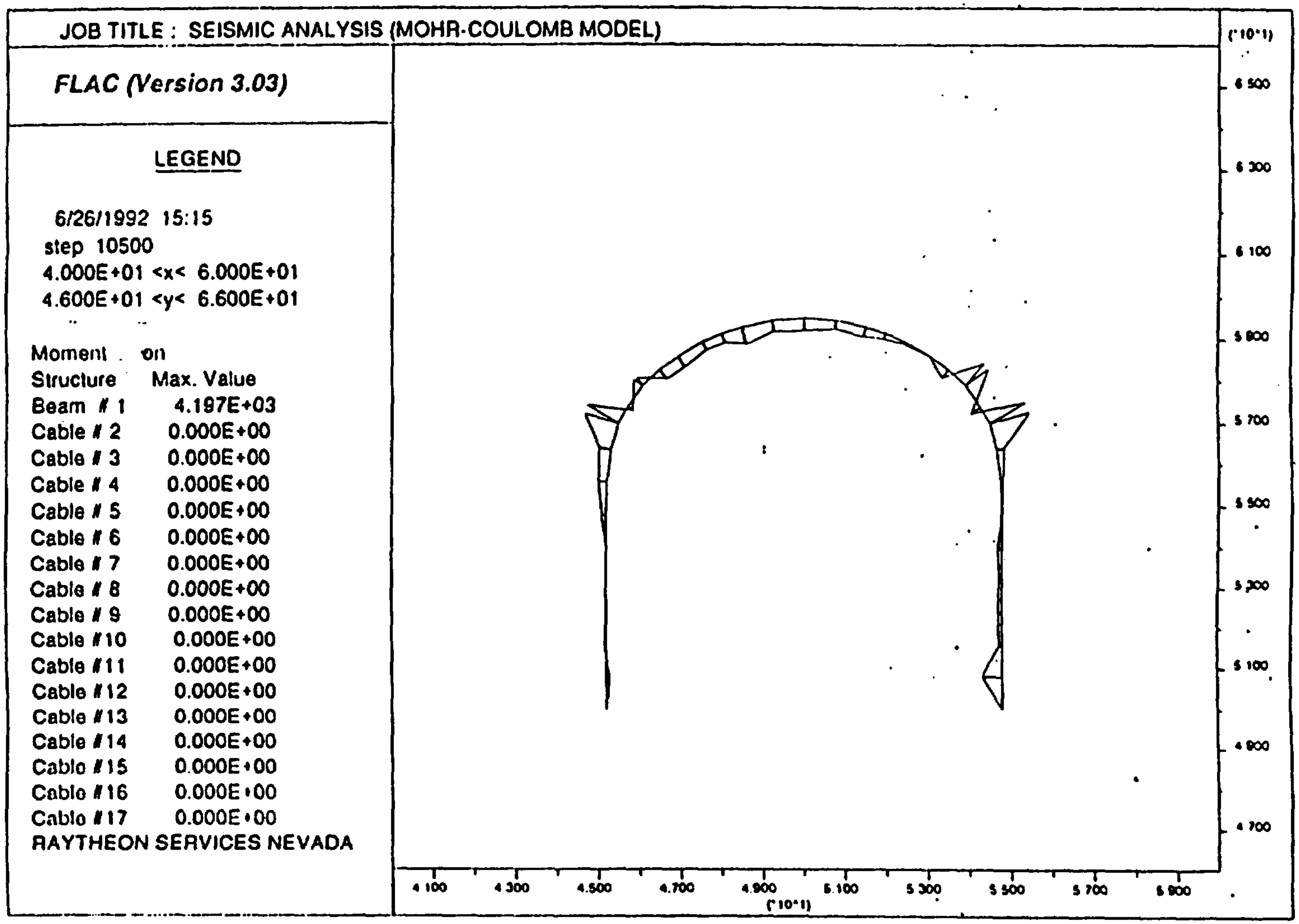

Fig. 41 Moment in 61 cm Starter Tunnel Liner at Seismic Event with Horizontal and Vertical Components of Acceleration of 0.75g, Mohr-Coulomb Model (Case 1). Moment is in Newton-Meters.

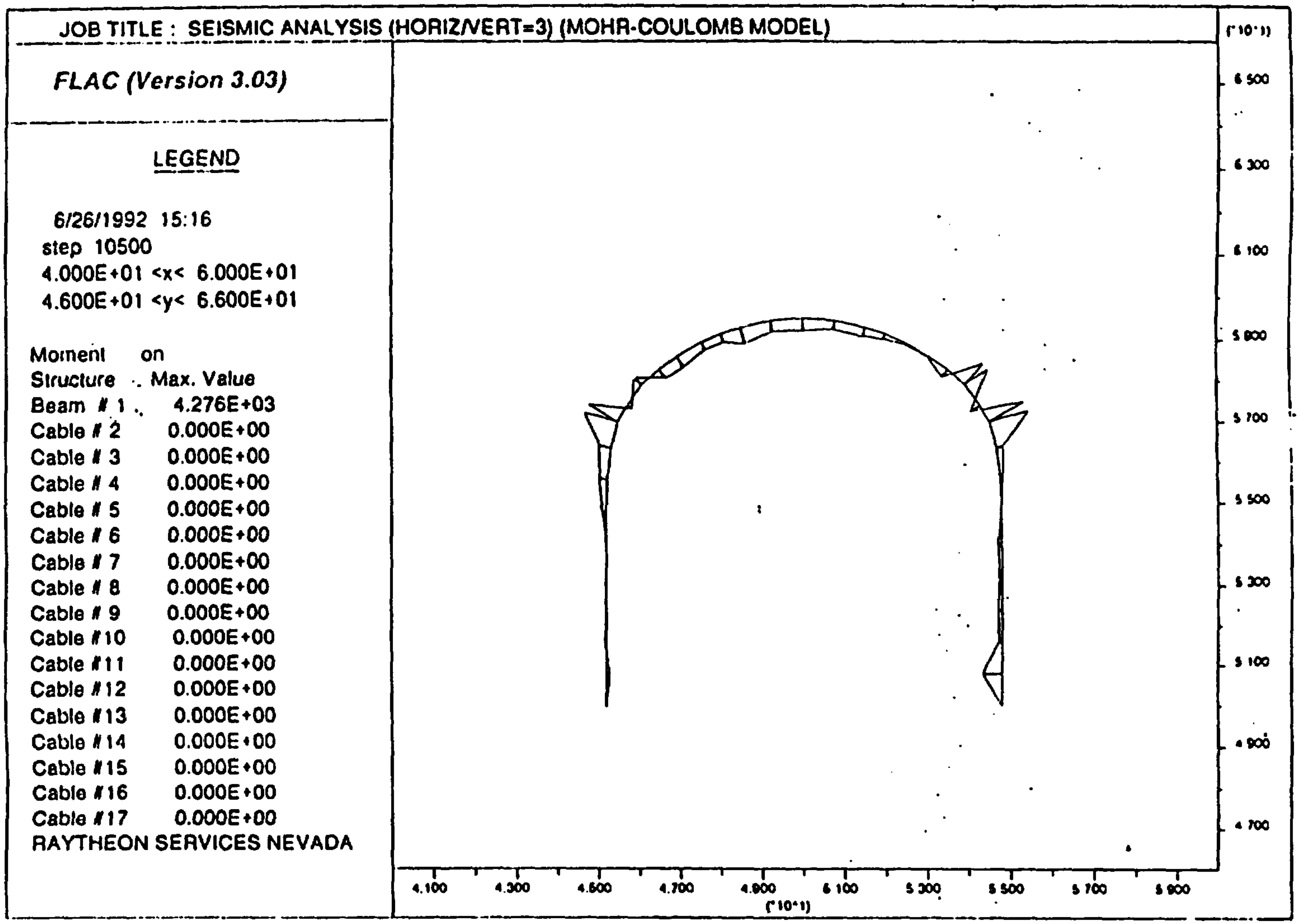

Fig. 42 Moment in 61 cm Starter Tunnel Liner Bolts at Seismic Event with Horizontal and Vertical Components of Acceleration of 0.75g, Mohr-Coulomb Model (Case 2). Moment is in Newton-Meters.

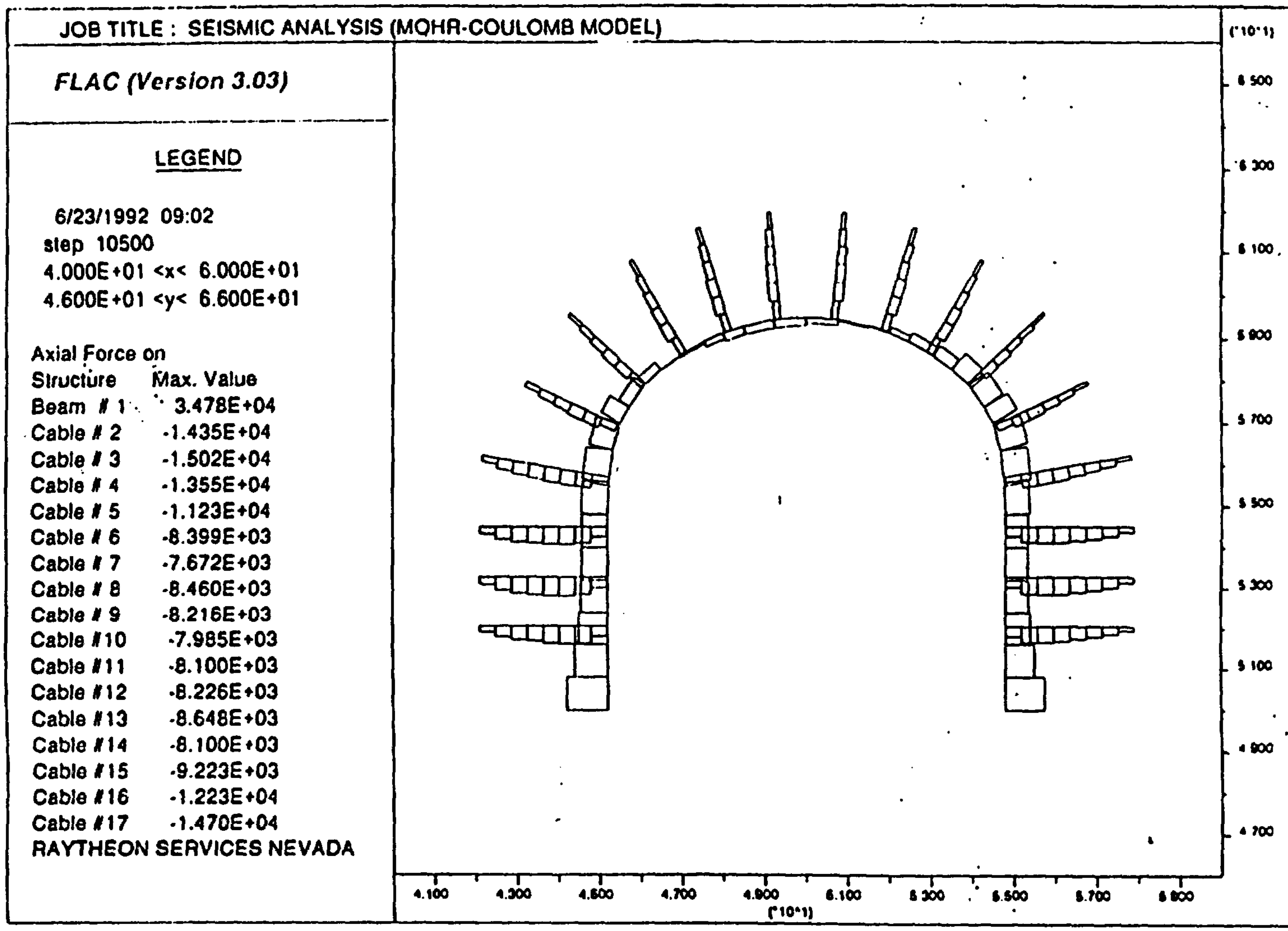

Fig. 43 Axial Force in 15 cm Shotcrete and Bolts at Seismic Event with Horizontal and Vertical Components of Acceleration of 0.5g, Mohr-Coulomb Model (Case 1). Forces are in Newton..

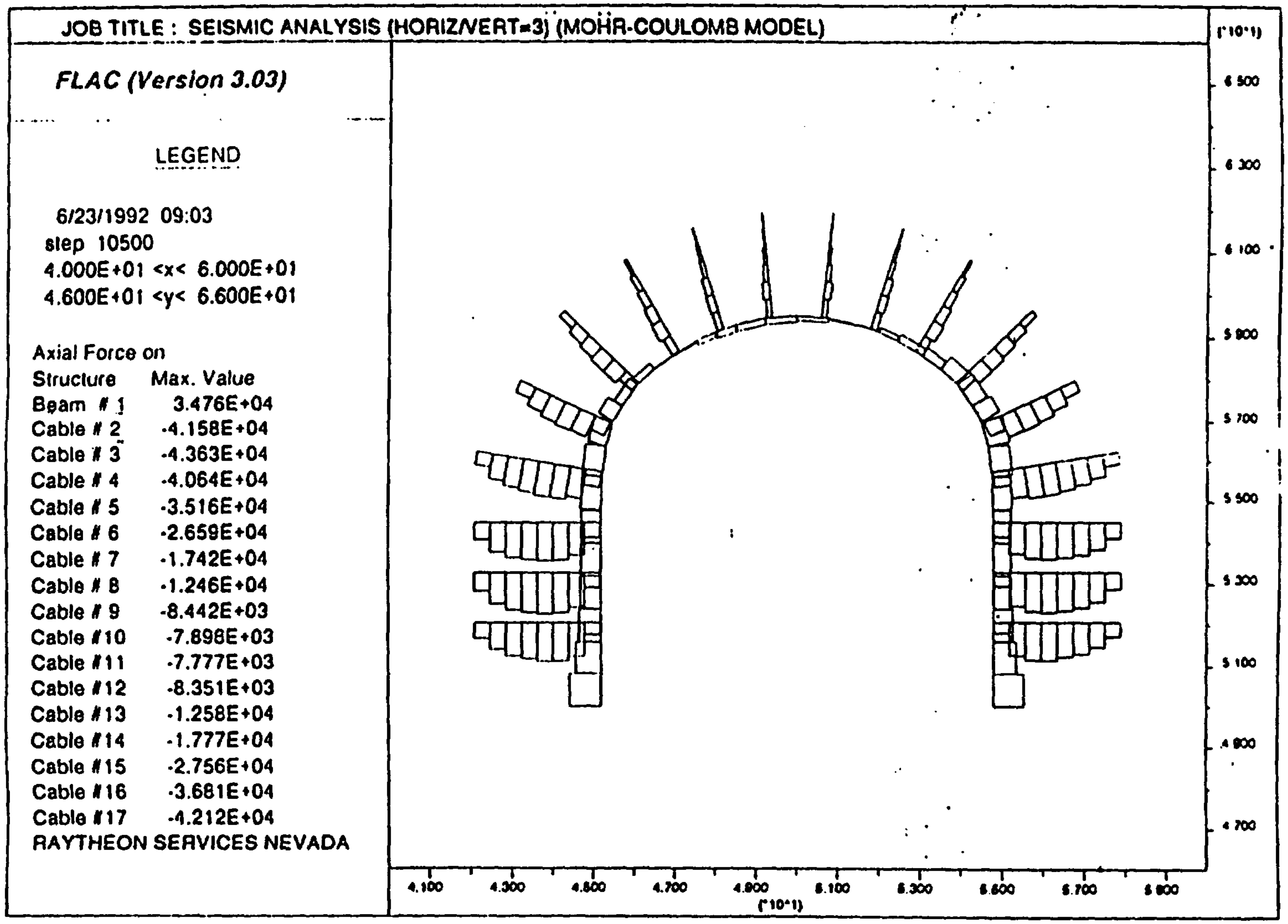

Fig. 44 Axial Force in 15 cm Shotcrete and Bolts at Seismic Event with Horizontal and Vertical Components of Acceleration of 0.5g, Mohr-Coulomb Model (Case 2). Forces are in Newton.

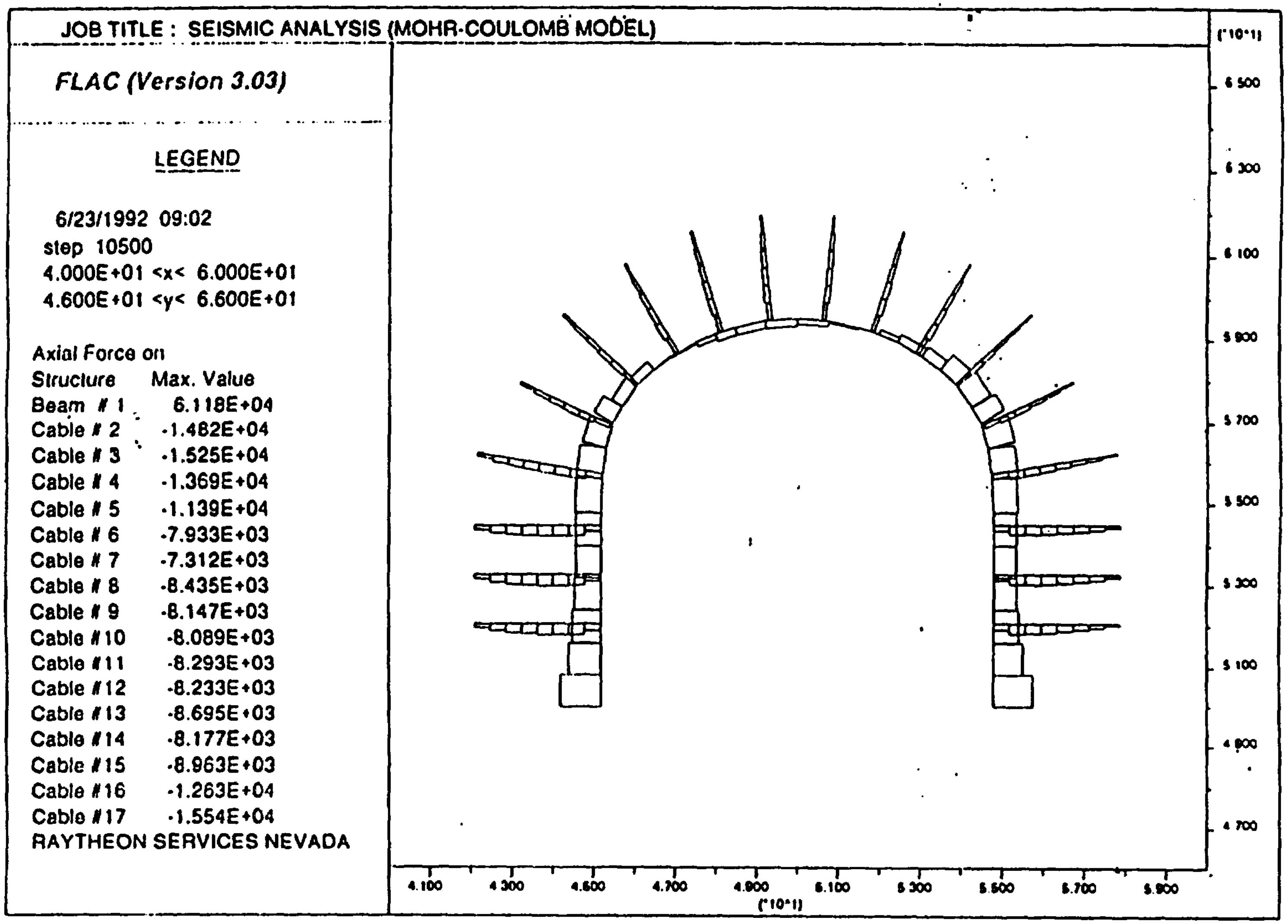

Fig. 45 Axial Force in 15 cm Shotcrete and Bolts at Seismic Event with Horizontal and Vertical Components of Acceleration of 0.75g, Mohr-Coulomb Model (Case 1). Forces are in Newton.

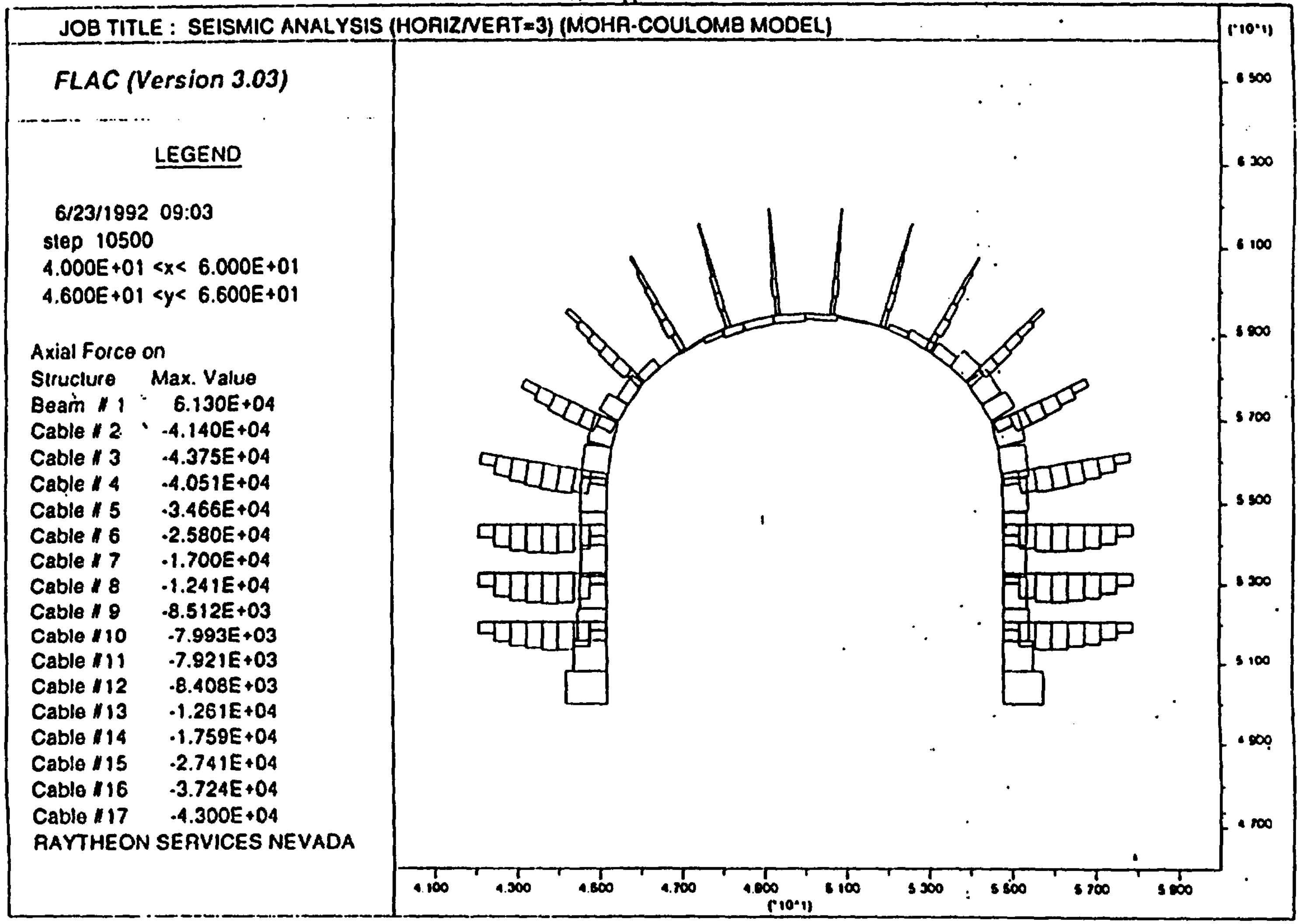

Fig. 46 Axial Force in 15 cm Shotcrete and Bolts at Seismic Event with Horizontal and Vertical Components of Acceleration of 0.75g, Mohr-Coulomb Model (Case 2). Forces are in Newton.

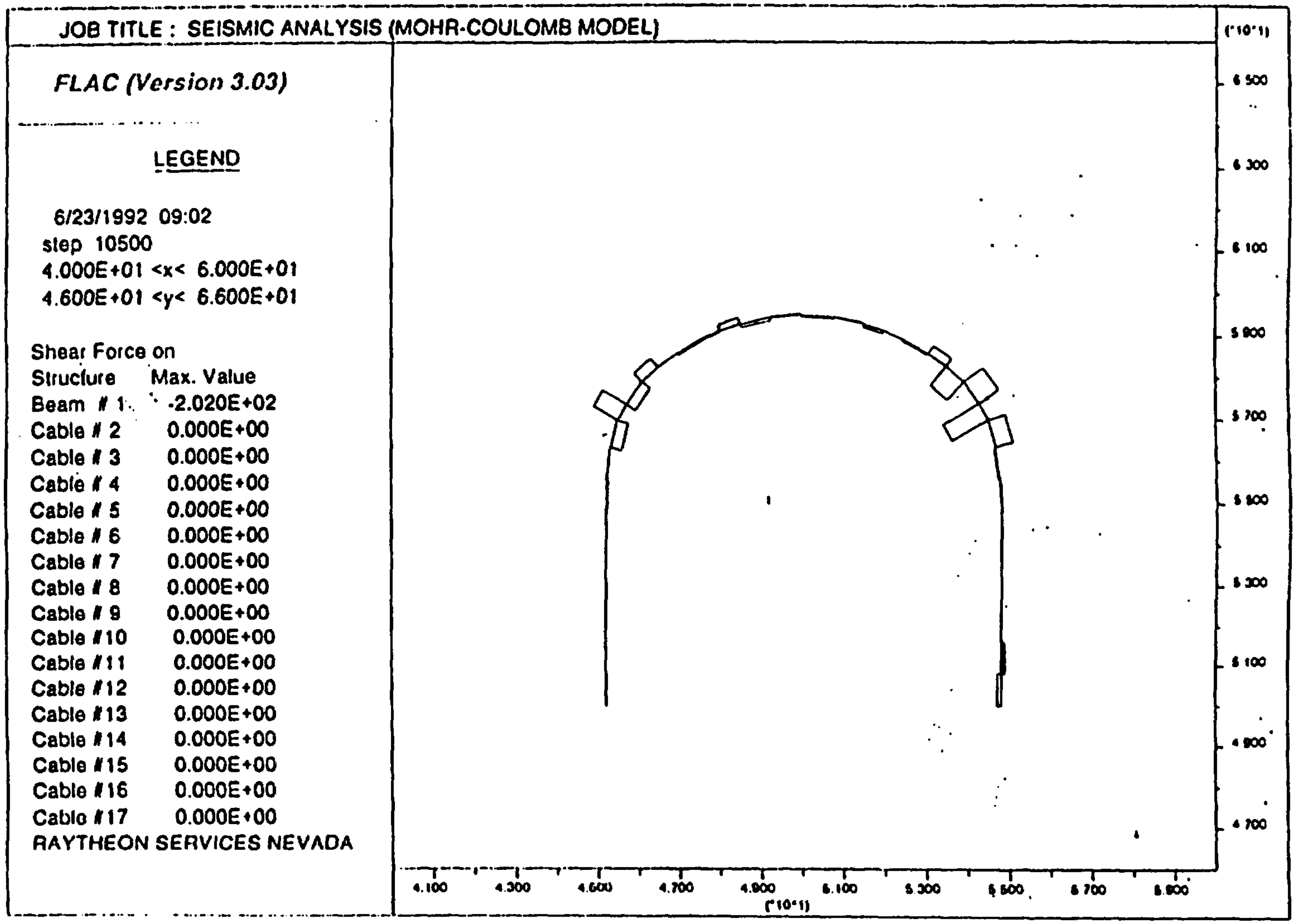

Fig. 47 Shear Force in 15 cm Shotcrete at Seismic Event with Horizontal and Vertical Components of Acceleration of 0.5g, Mohr-Coulomb Model (Case 1). Forces are in Newton.

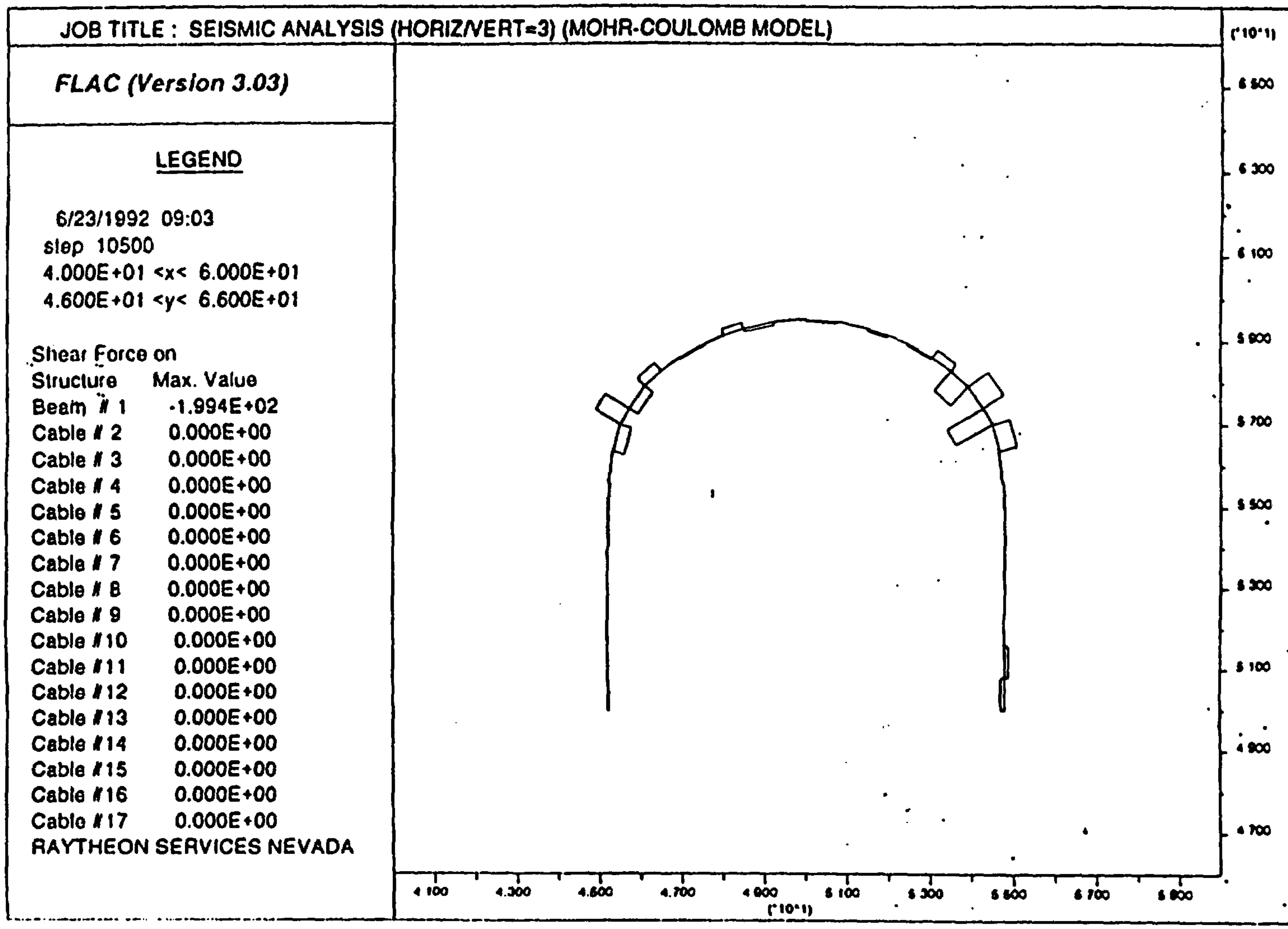

Fig. 48 Shear Force in 15 cm Shotcrete at Seismic Event with Horizontal and Vertical Components of Acceleration of 0.5g, Mohr-Coulomb Model (Case 2). Forces are in Newton.

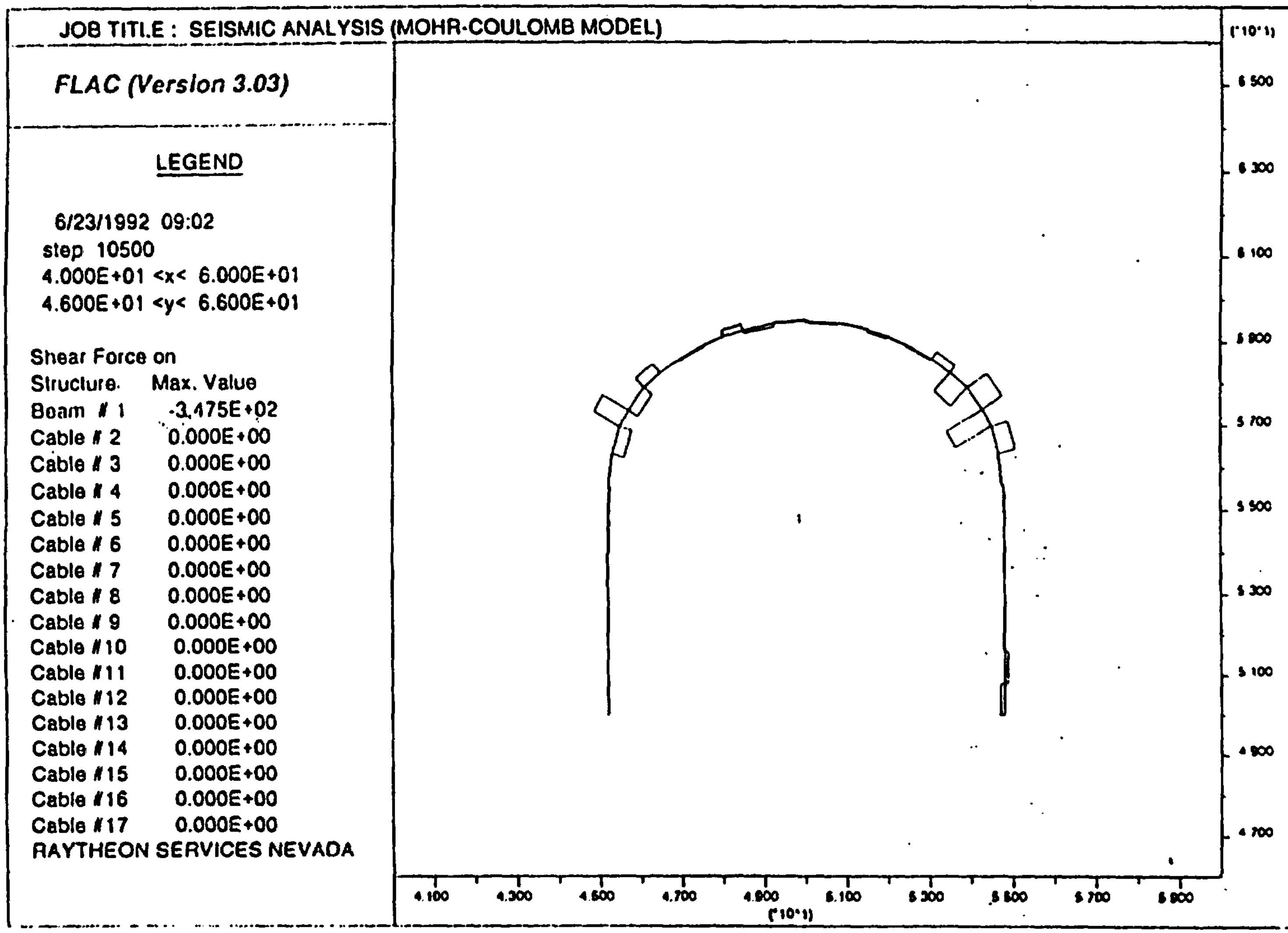

Fig. 49 Shear Force in 15 cm Shotcrete at Seismic Event with Horizontal and Vertical Components of Acceleration of 0.75g, Mohr-Coulomb Model (Case 1). Forces are in Newton.

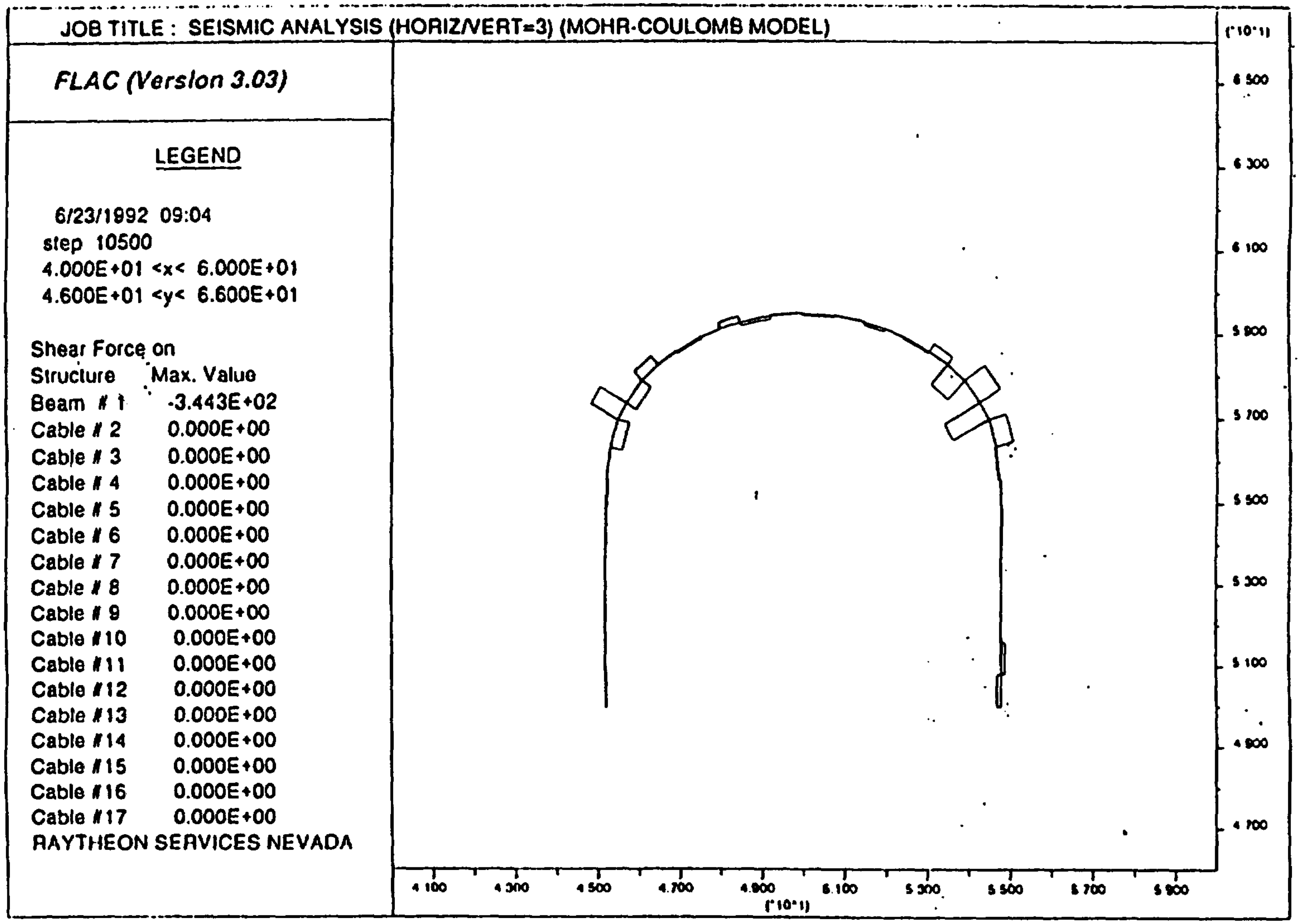

Fig. 50 Shear Force in 15 cm Shotcrete at Seismic Event with Horizontal and Vertical Components of Acceleration of 0.75g, Mohr-Coulomb Model (Case 2). Forces are in Newton.

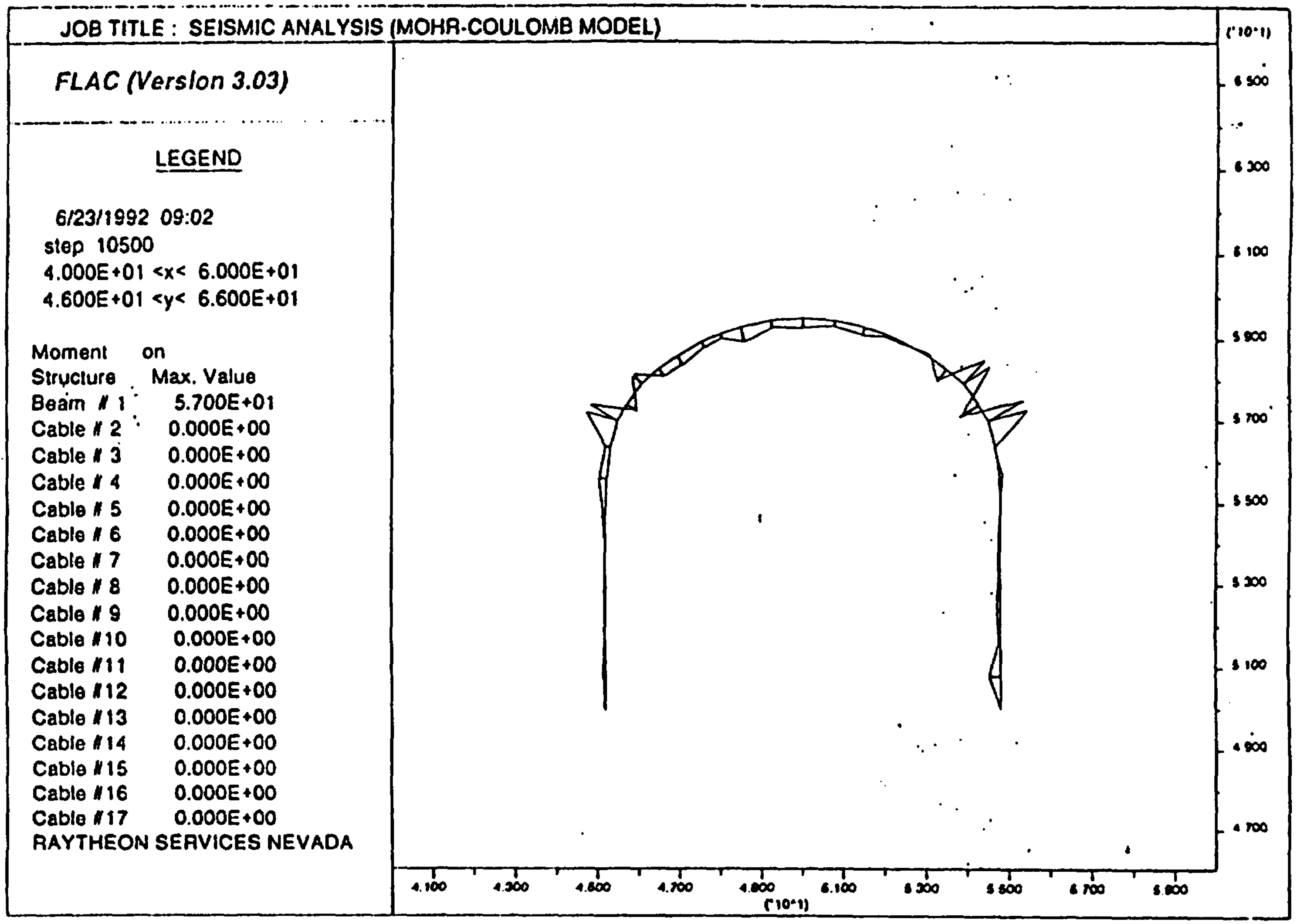

Fig. 51 Moment in 15 cm Shotcrete at Seismic Event with Horizontal and Vertical Components of Acceleration of 0.5g, Mohr-Coulomb Model (Case 1). Moment is in Newton-Meters.

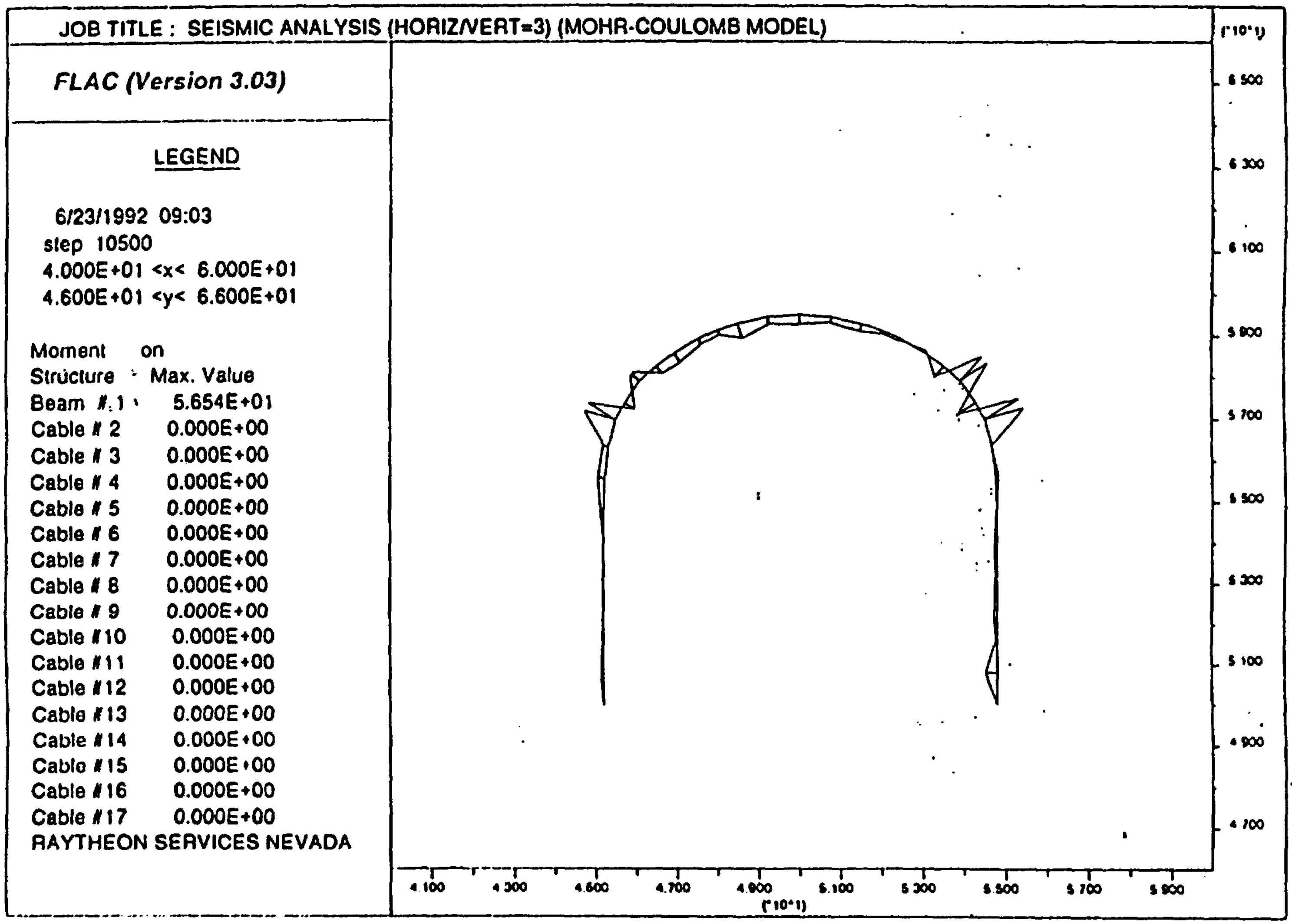

Fig. 52 Moment in 15 cm Shotcrete at Seismic Event with Horizontal and Vertical Components of Acceleration of 0.5g, Mohr-Coulomb Model (Case 2). Moment is in Newton-Meters.

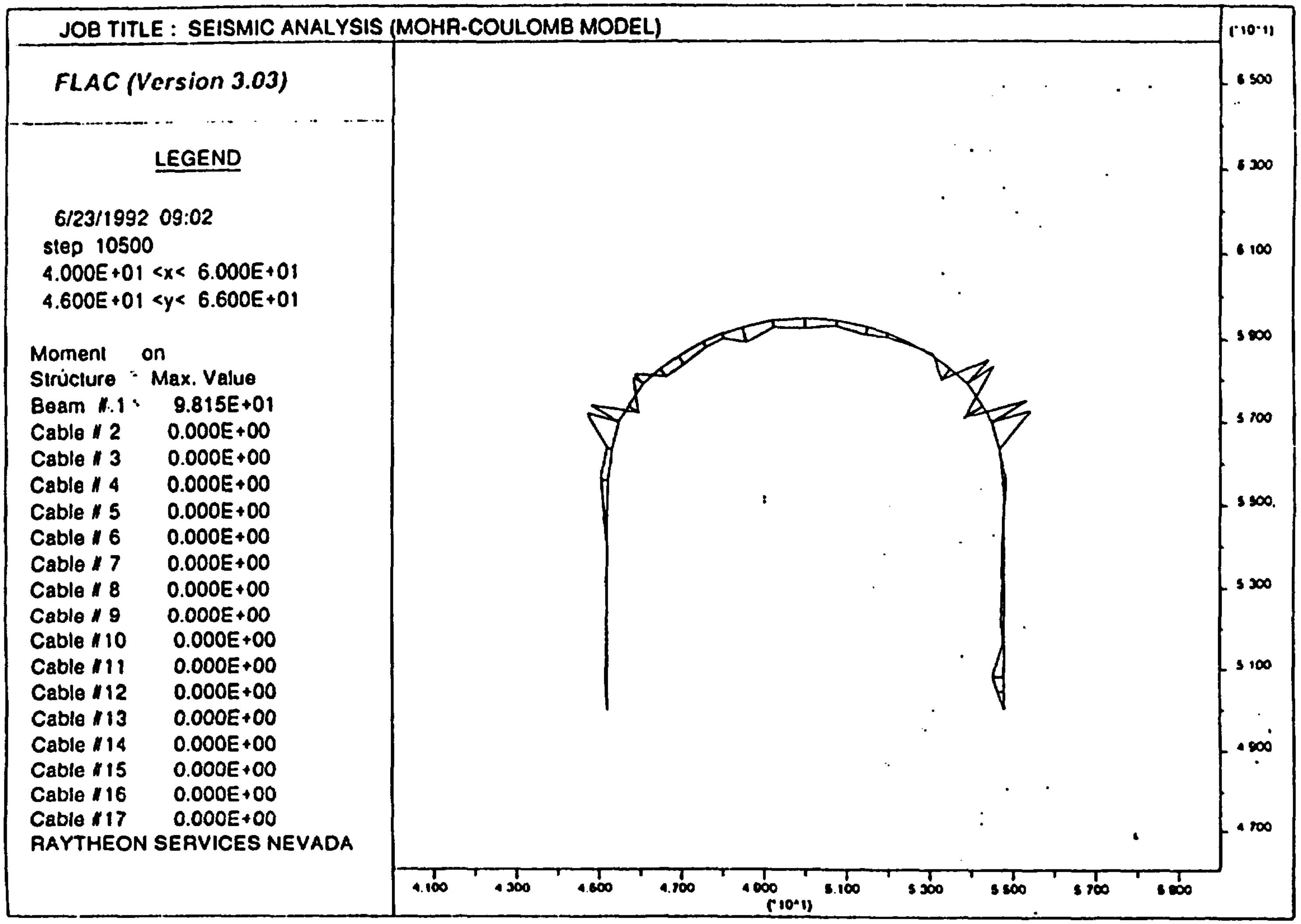

Fig. 53 Moment in 15 cm Shotcrete at Seismic Event with Horizontal and Vertical Components of Acceleration of 0.75g, Mohr-Coulomb Model (Case 1). Moment is in Newton-Meters.

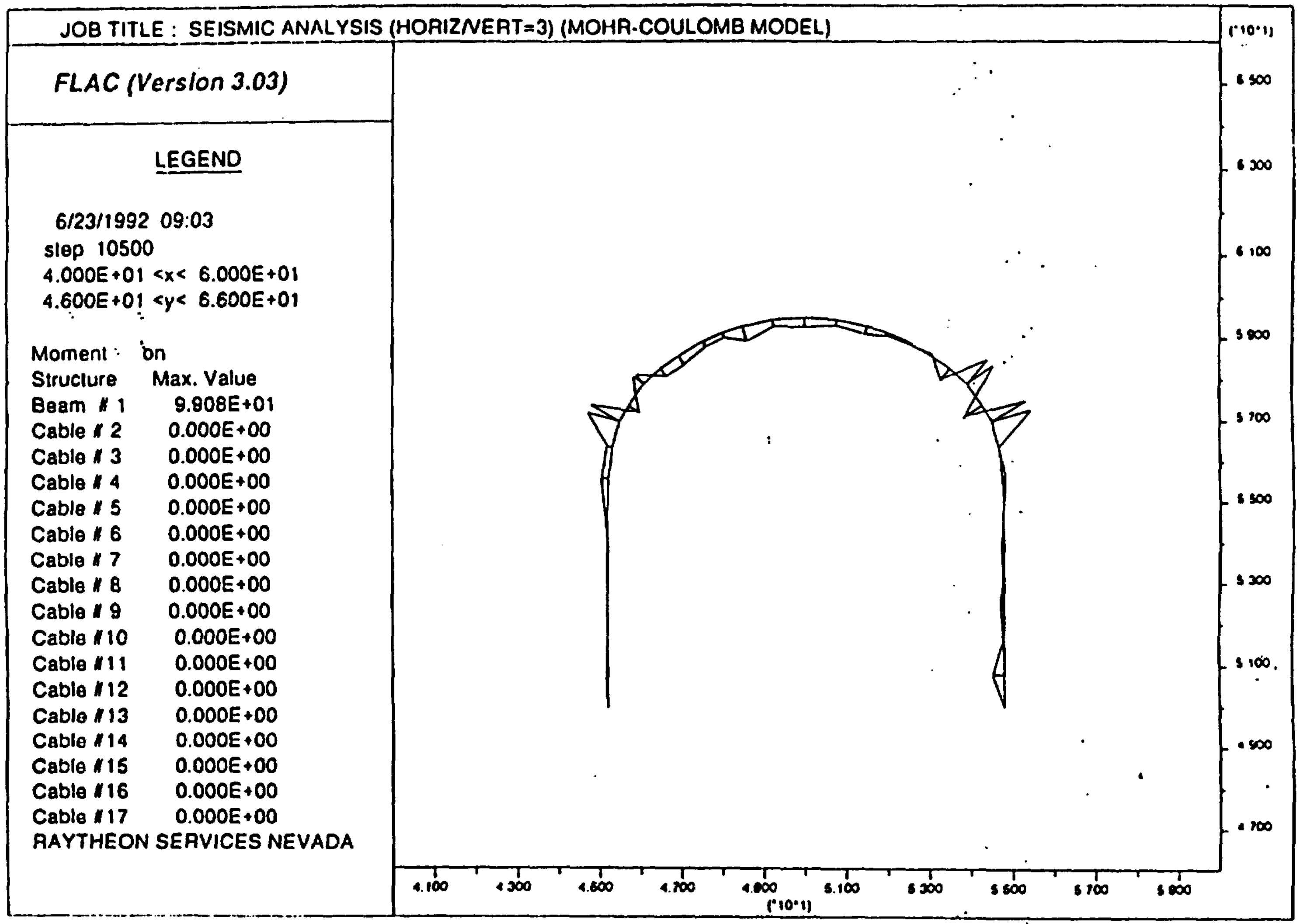

Fig. 54 Moment in 15 cm Shotcrete at Seismic Event with Horizontal and Vertical Components of Acceleration of 0.75g, Mohr-Coulomb Model (Case 2). Moment is in Newton-Meters.

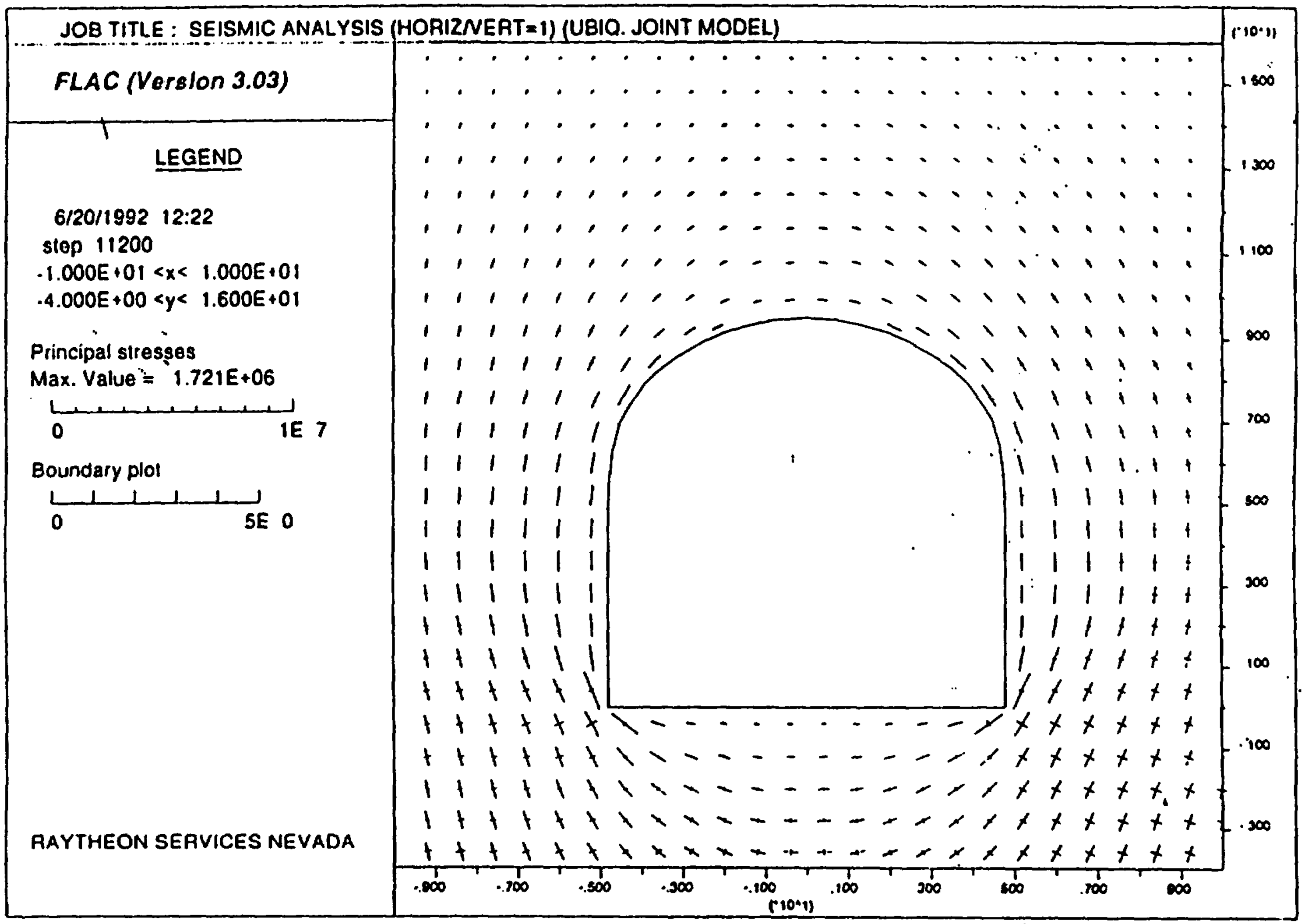

Fig. 55 Principal Stress Vectors around the Tunnel Opening at Seismic Event with Horizontal and Vertical Components of Acceleration of 0.5g, Ubiquitous Joint Model (Case 1). Compression is Negative. Stresses are in Pascal.

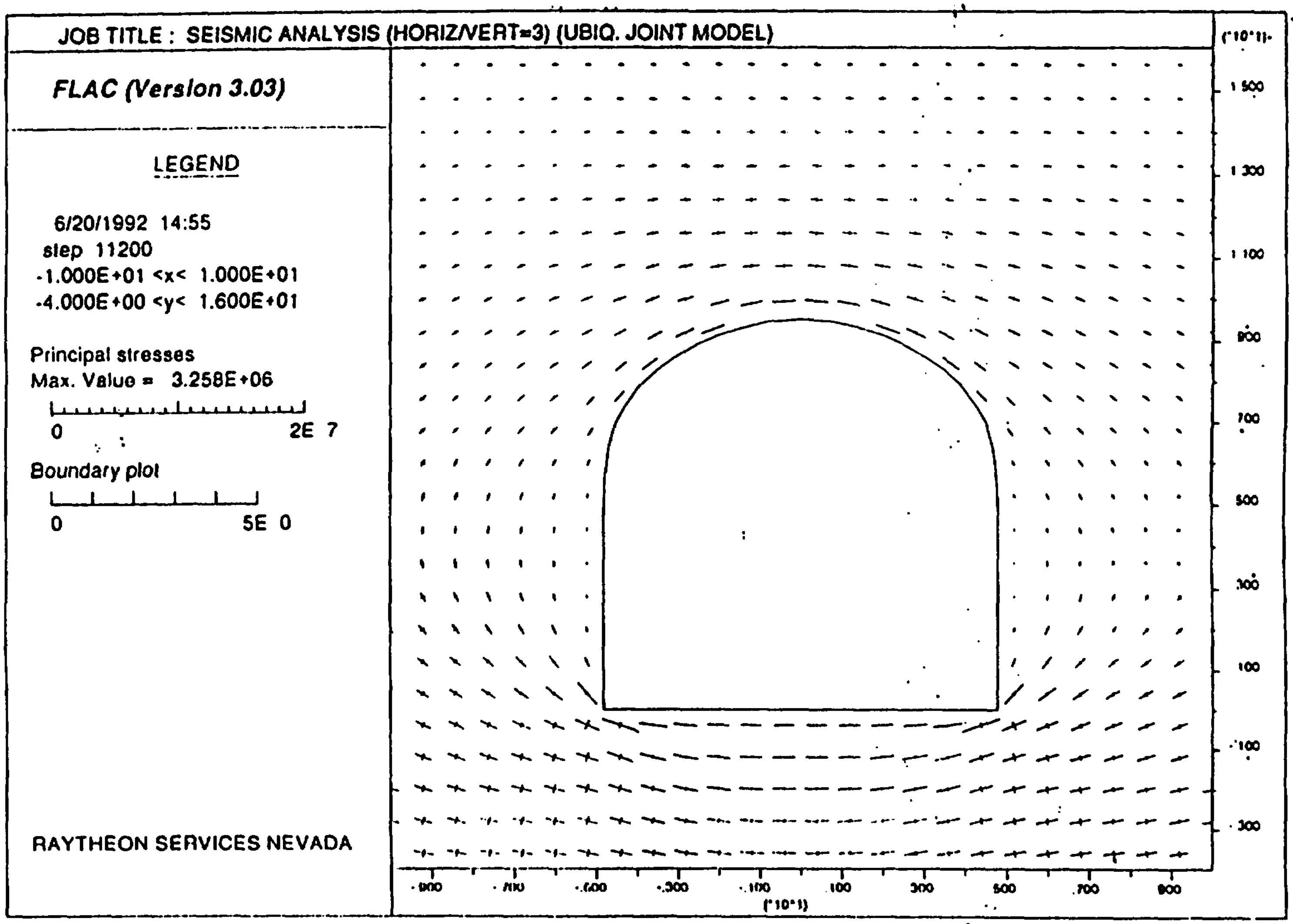

Fig. 56 Principal Stress Vectors around the Tunnel Opening at Seismic Event with Horizontal and Vertical Components of Acceleration of 0.5g, Ubiquitous Joint Model (Case 2). Compression is Negative. Stresses are in Pascal.

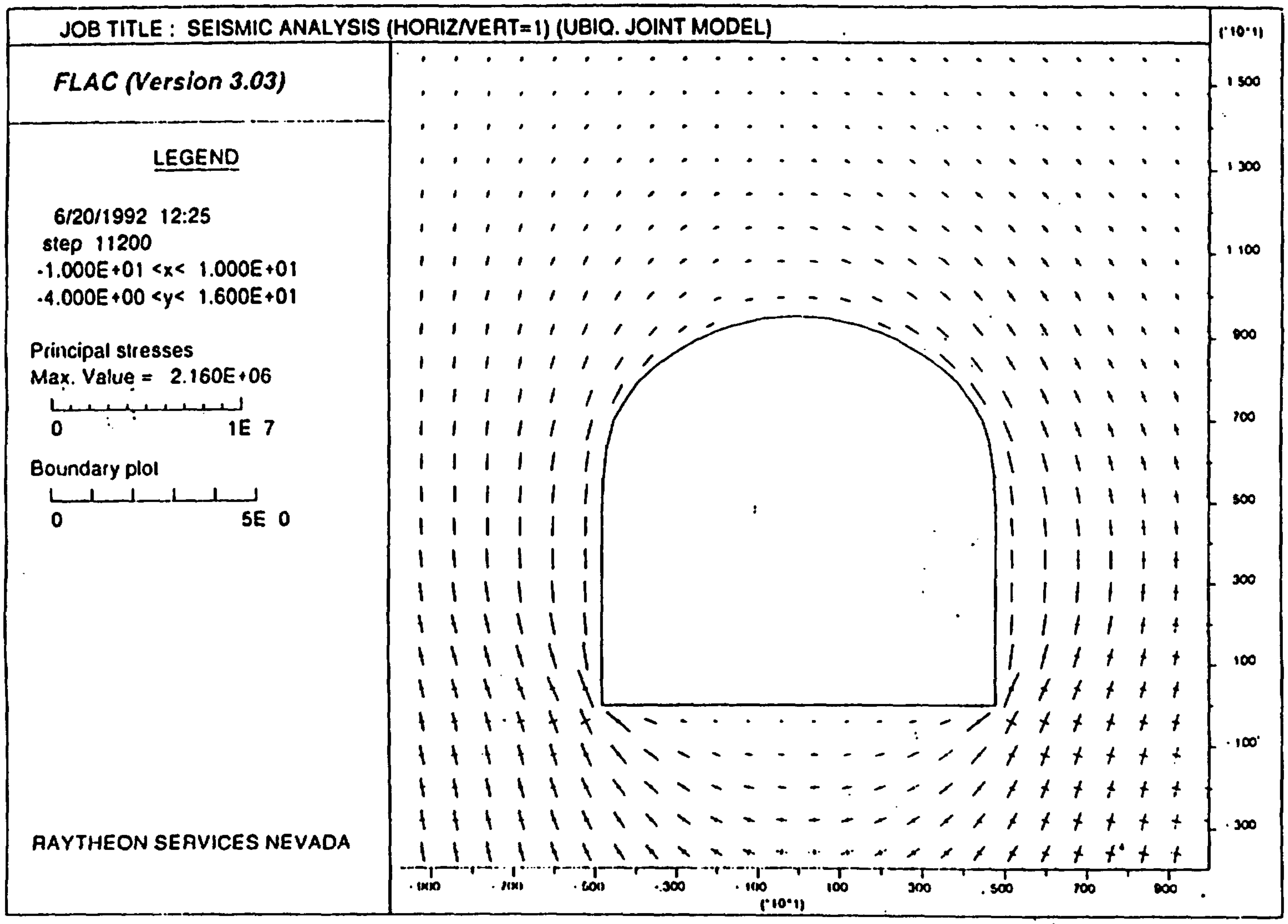

Fig. 57 Principal Stress Vectors around the Tunnel Opening at Seismic Event with Horizontal and Vertical Components of Acceleration of 0.75g, Ubiquitous Joint Model (Case 1). Compression is Negative. Stresses are in Pascal.

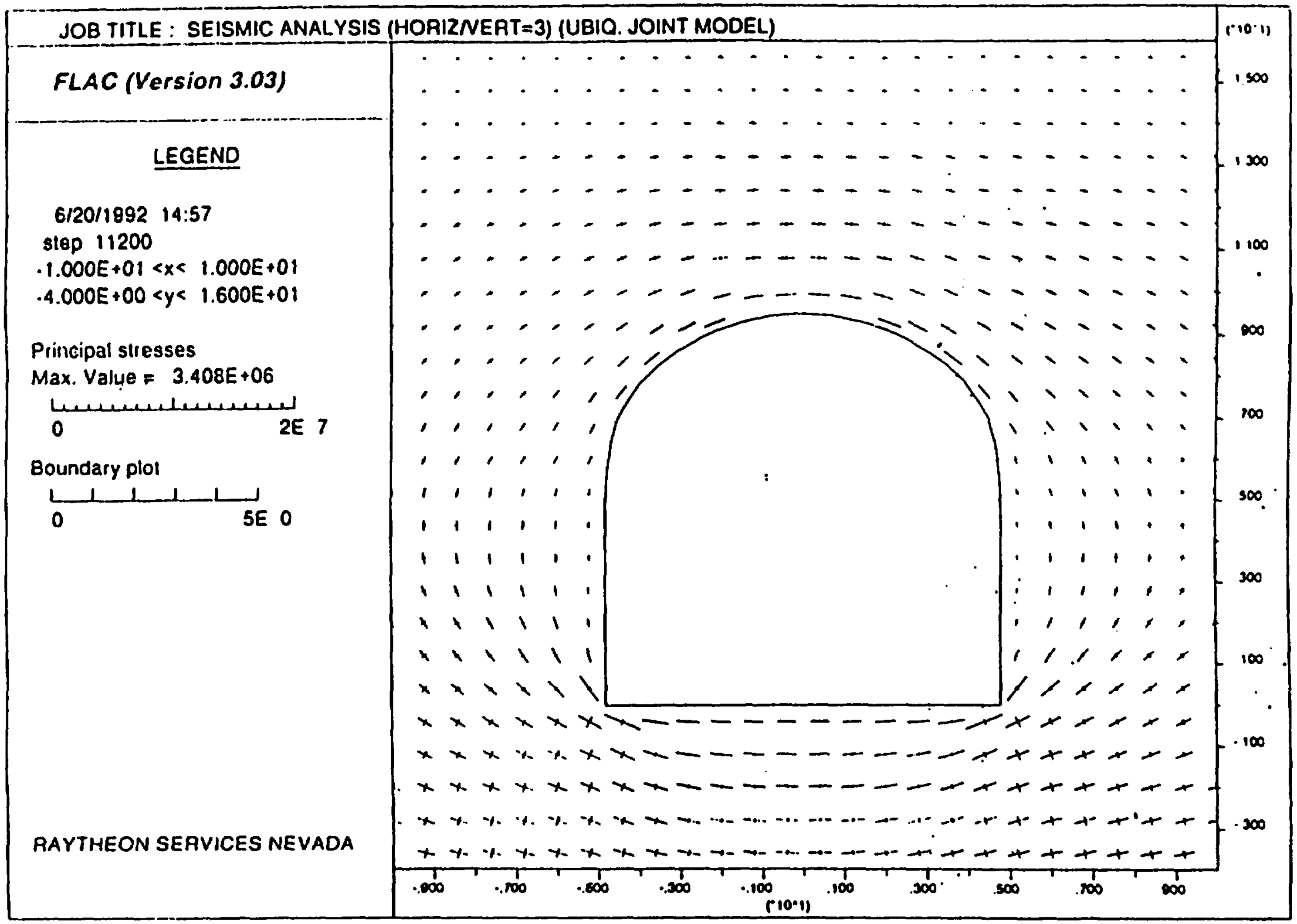

Fig. 58 Principal Stress Vectors around the Tunnel Opening at Seismic Event with Horizontal and Vertical Components of Acceleration of 0.75g, Ubiquitous Joint Model (Case 2). Compression is Negative. Stresses are in Pascal.

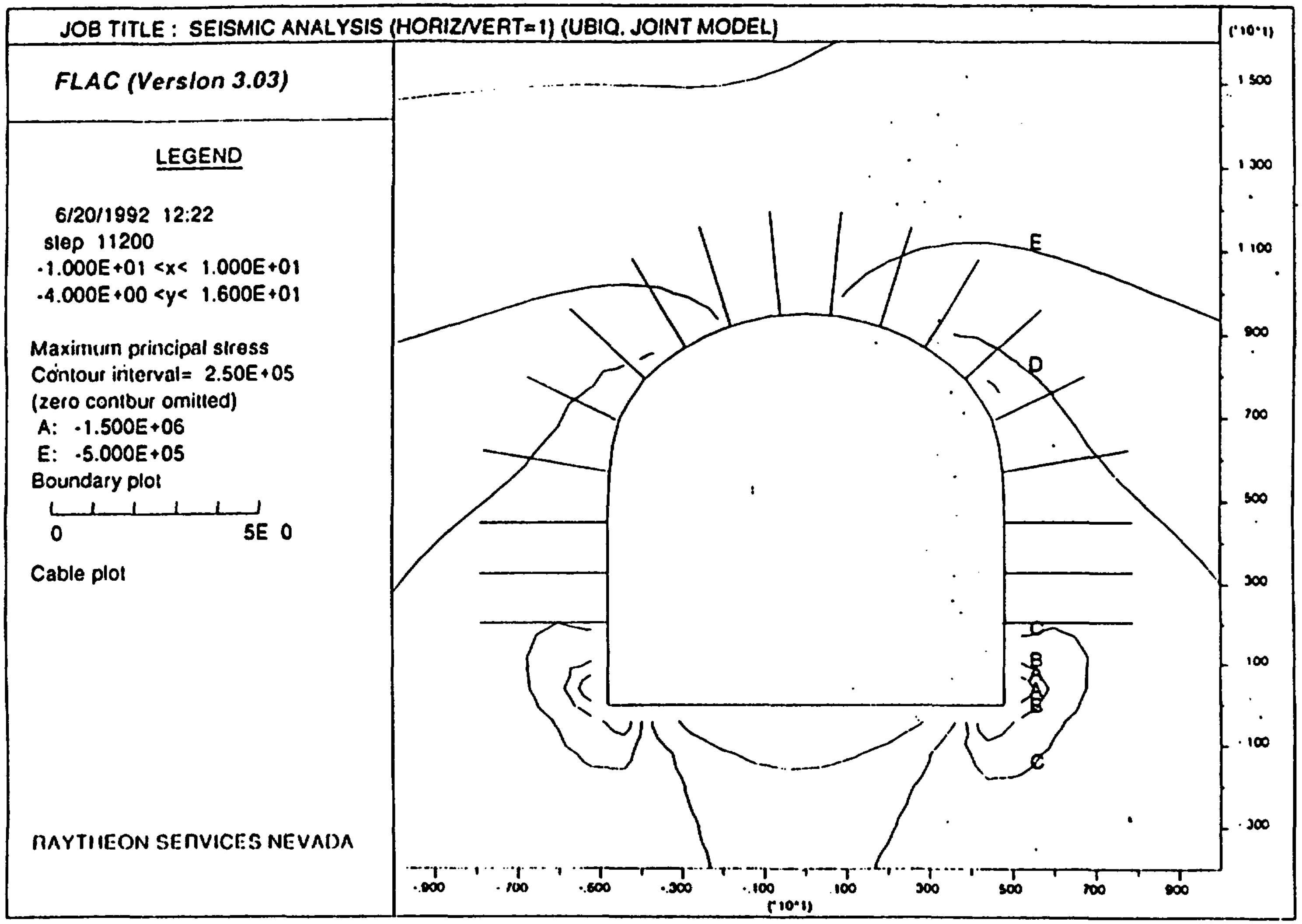

Fig. 59 Maximum Principal Stress Contours around the Tunnel Opening at Seismic Event with Horizontal and Vertical Components of Acceleration of 0.5g, Ubiquitous Joint Model (Case 1). Compression is Negative. Stresses are in Pascal.

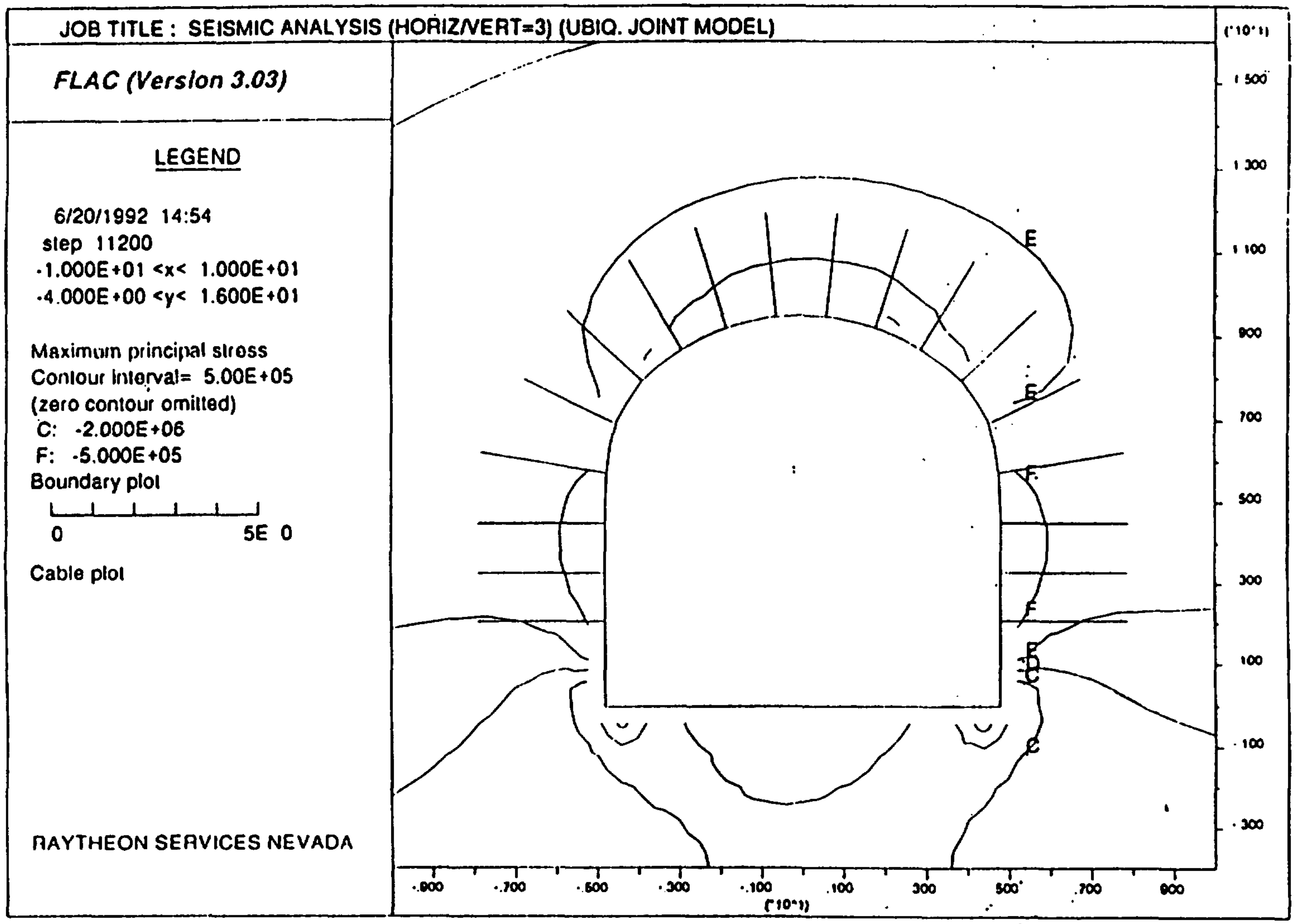

Fig. 60 Maximum Principal Stress Contours around the Tunnel Opening at Seismic Event with Horizontal and Vertical Components of Acceleration of 0.5g, Ubiquitous Joint Model (Case 2). Compression is Negative. Stresses are in Pascal.

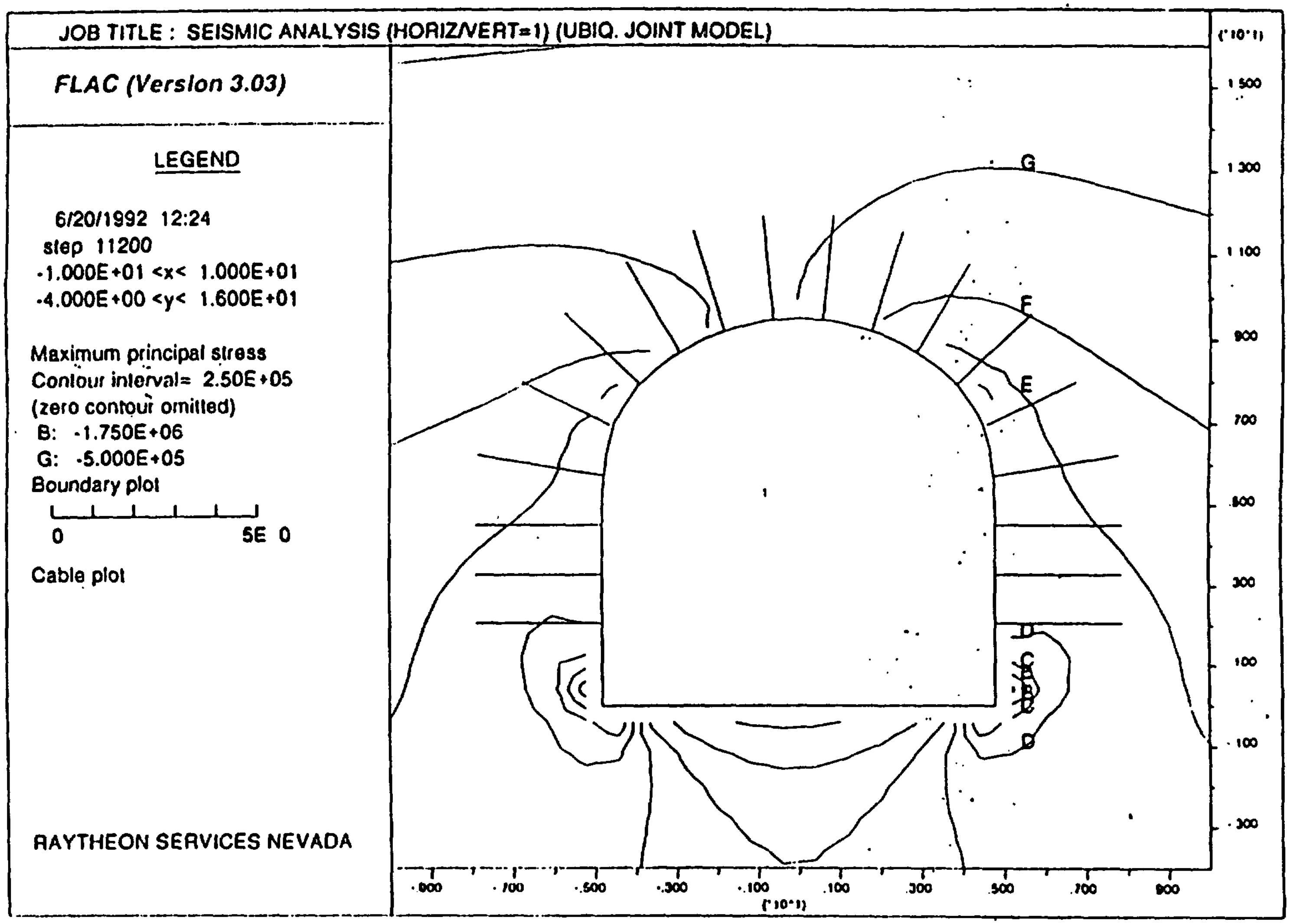

Fig. 61 Maximum Principal Stress Contours around the Tunnel Opening at Seismic Event with Horizontal and Vertical Components of Acceleration of 0.75g, Ubiquitous Joint Model (Case 1). Compression is Negative. Stresses are in Pascal.

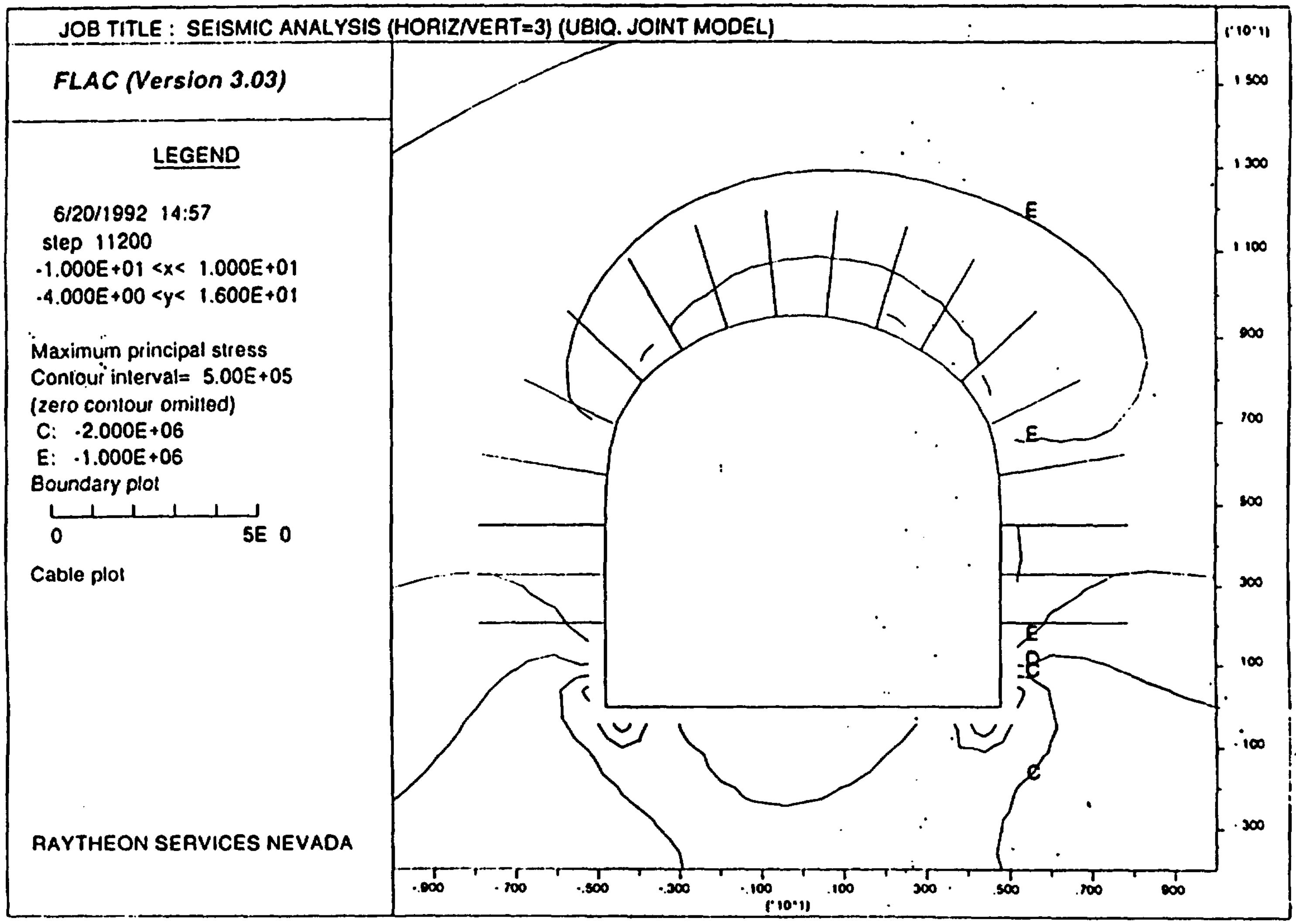

Fig. 62 Maximum Principal Stress Contours around the Tunnel Opening at Seismic Event with Horizontal and Vertical Components of Acceleration of 0.75g, Ubiquitous Joint Model (Case 2). Compression is Negative. Stresses are in Pascal.

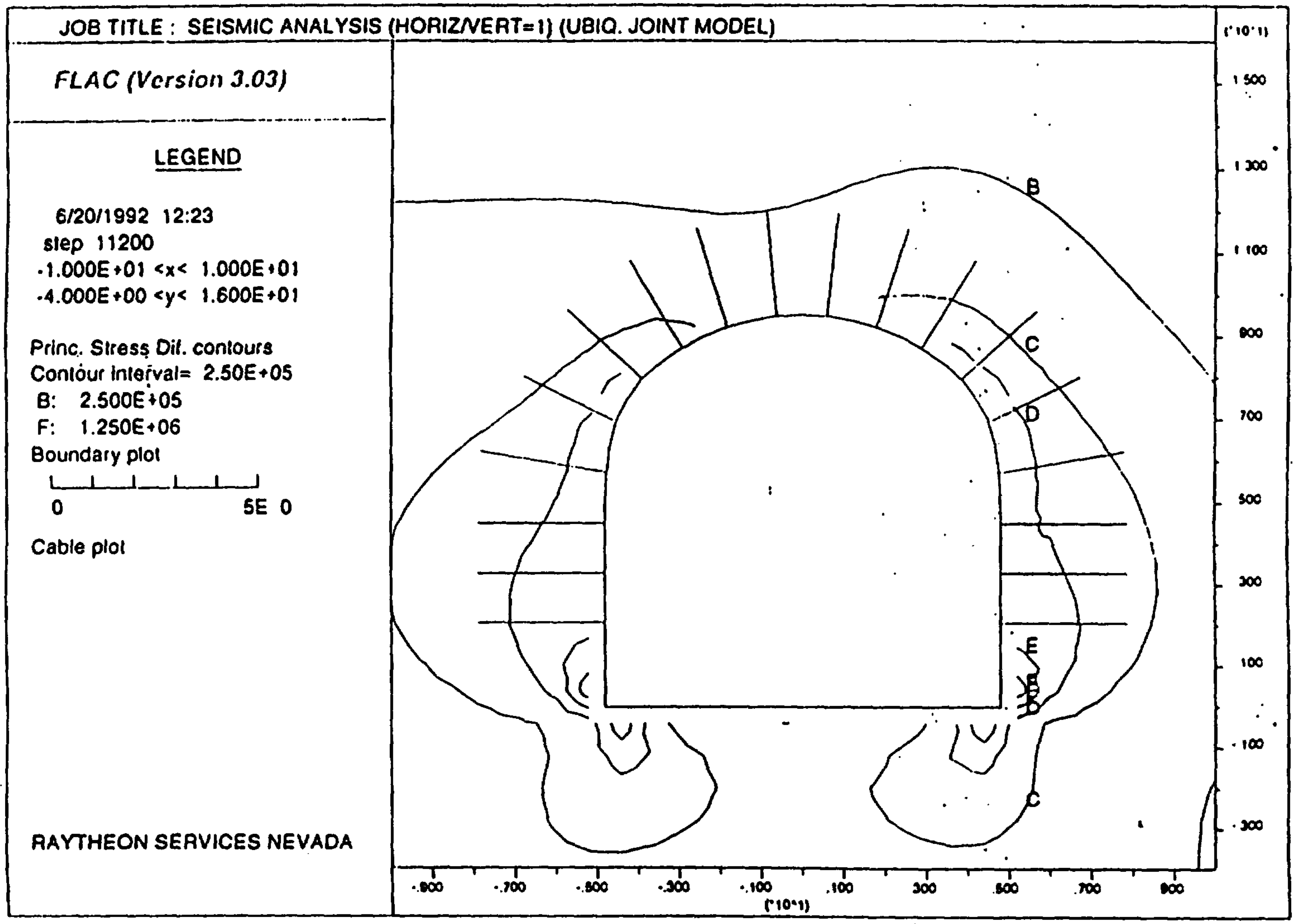

Fig. 63 Principal Stress Difference Contours around the Tunnel Opening at Seismic Event with Horizontal and Vertical Components of Acceleration of 0.5g, Ubiquitous Joint Model (Case 1). Compression is Negative. Stresses are in Pascal.

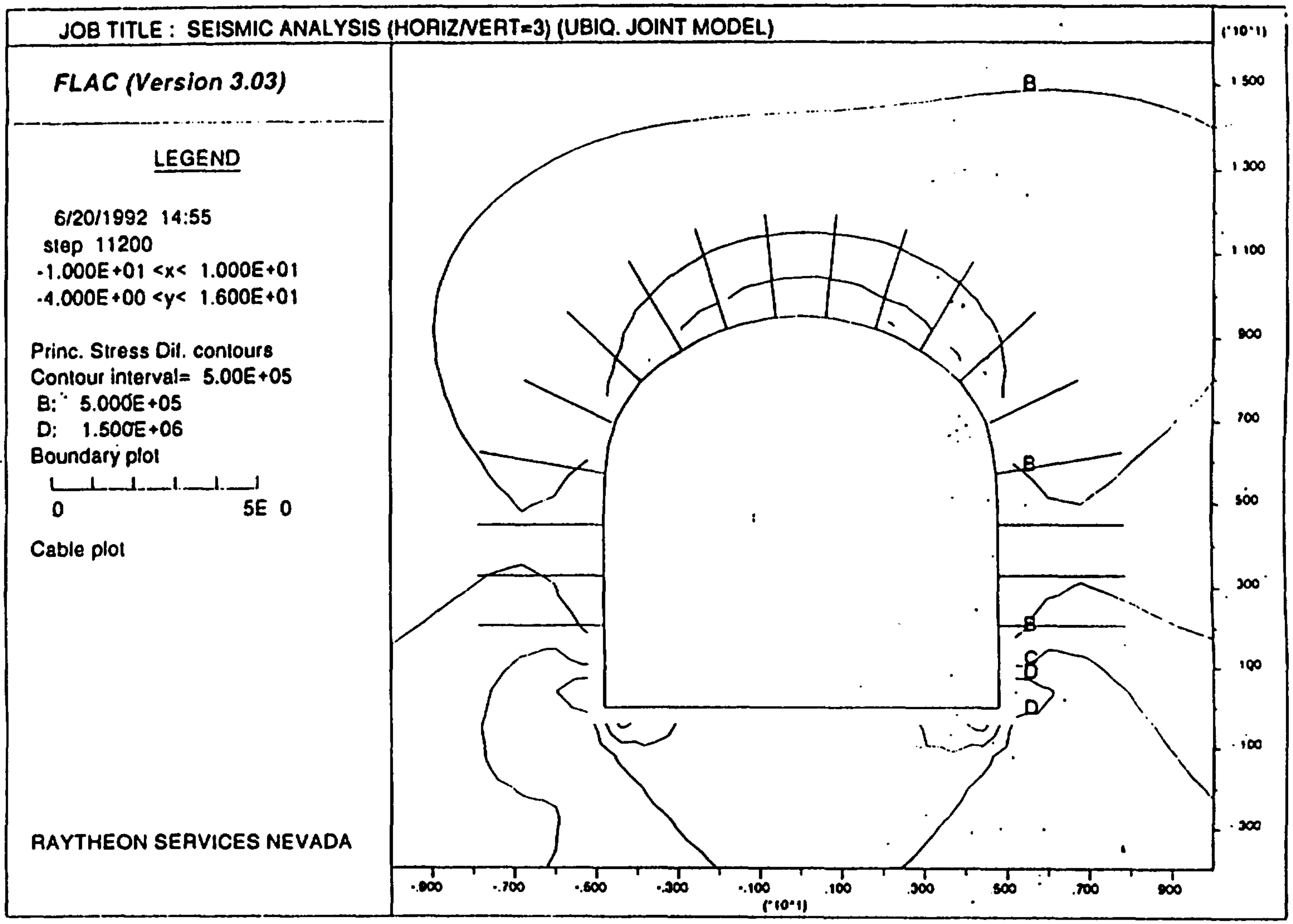

Fig. 64 Principal Stress Difference Contours around the Tunnel Opening at Seismic Event with Horizontal and Vertical Components of Acceleration of 0.5g, Ubiquitous Joint Model (Case 2). Compression is Negative. Stresses are in Pascal.

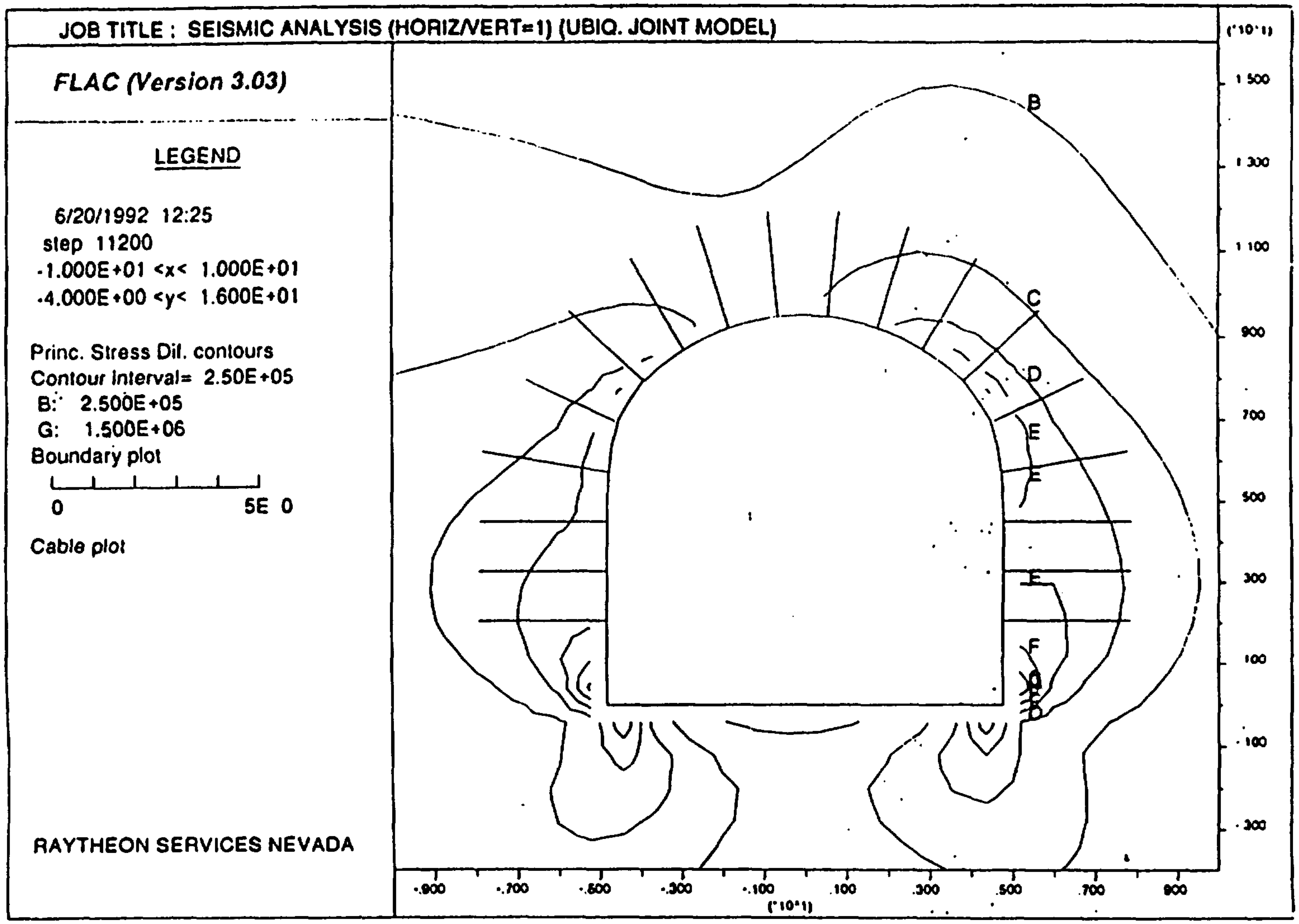

Fig. 65 Principal Stress Difference Contours around the Tunnel Opening at Seismic Event with Horizontal and Vertical Components of Acceleration of 0.75g, Ubiquitous Joint Model (Case 1). Compression is Negative, Stresses are in Pascal.

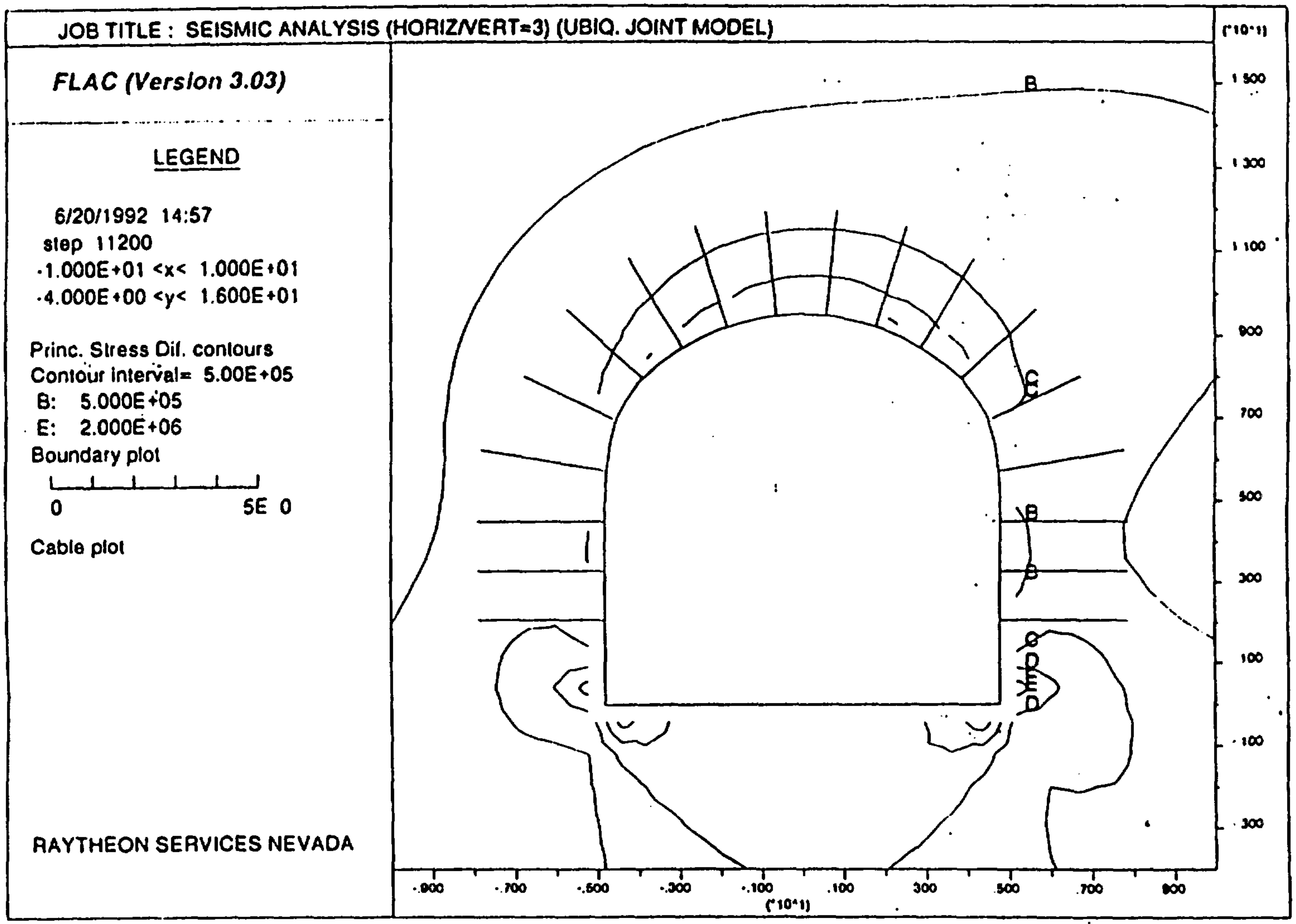

Fig. 66 Principal Stress Difference Contours around the Tunnel Opening at Seismic Event with Horizontal and Vertical Components of Acceleration of 0.75g, Ubiquitous Joint Model (Case 2). Compression is Negative. Stresses are in Pascal.

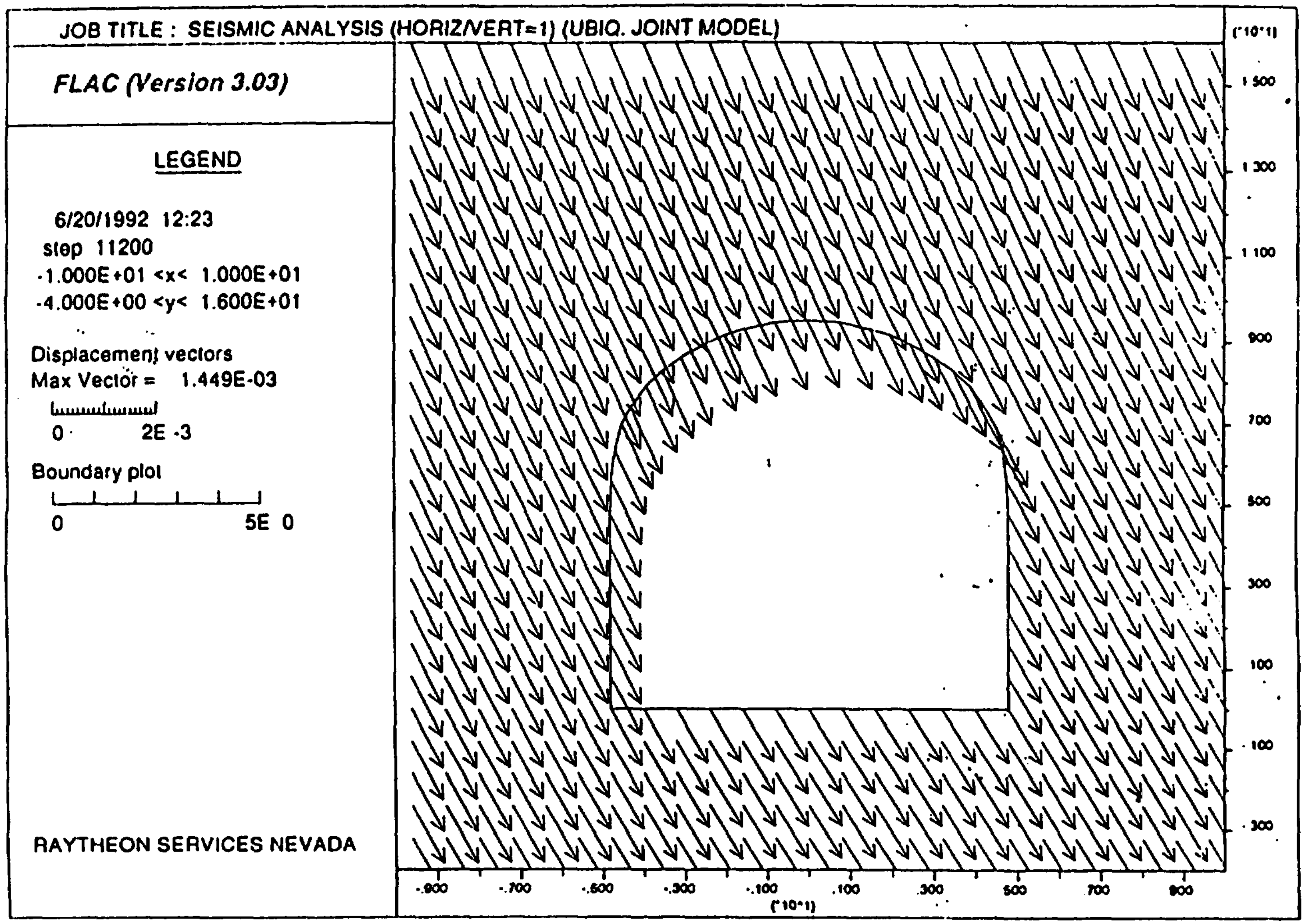

Fig. 67 Displacement Vectors around the Tunnel Opening at Seismic Event with Horizontal and Vertical Components of Acceleration of 0.5g, Ubiquitous Joint Model (Case 1). Compression is Negative.

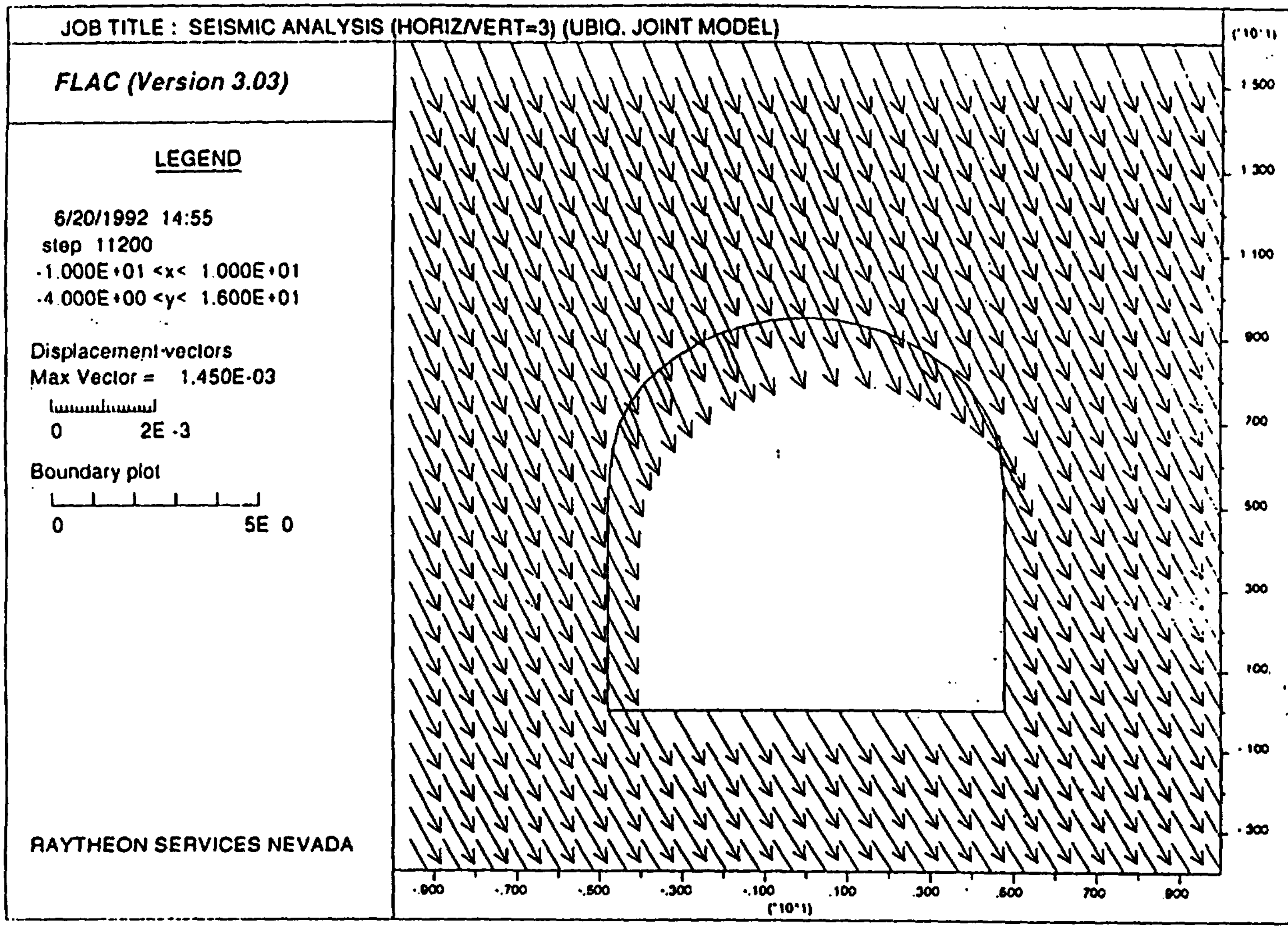

Fig. 68 Displacement Vectors around the Tunnel Opening at Seismic Event with Horizontal and Vertical Components of Acceleration of 0.5g, Ubiquitous Joint Model (Case 2). Compression is Negative.

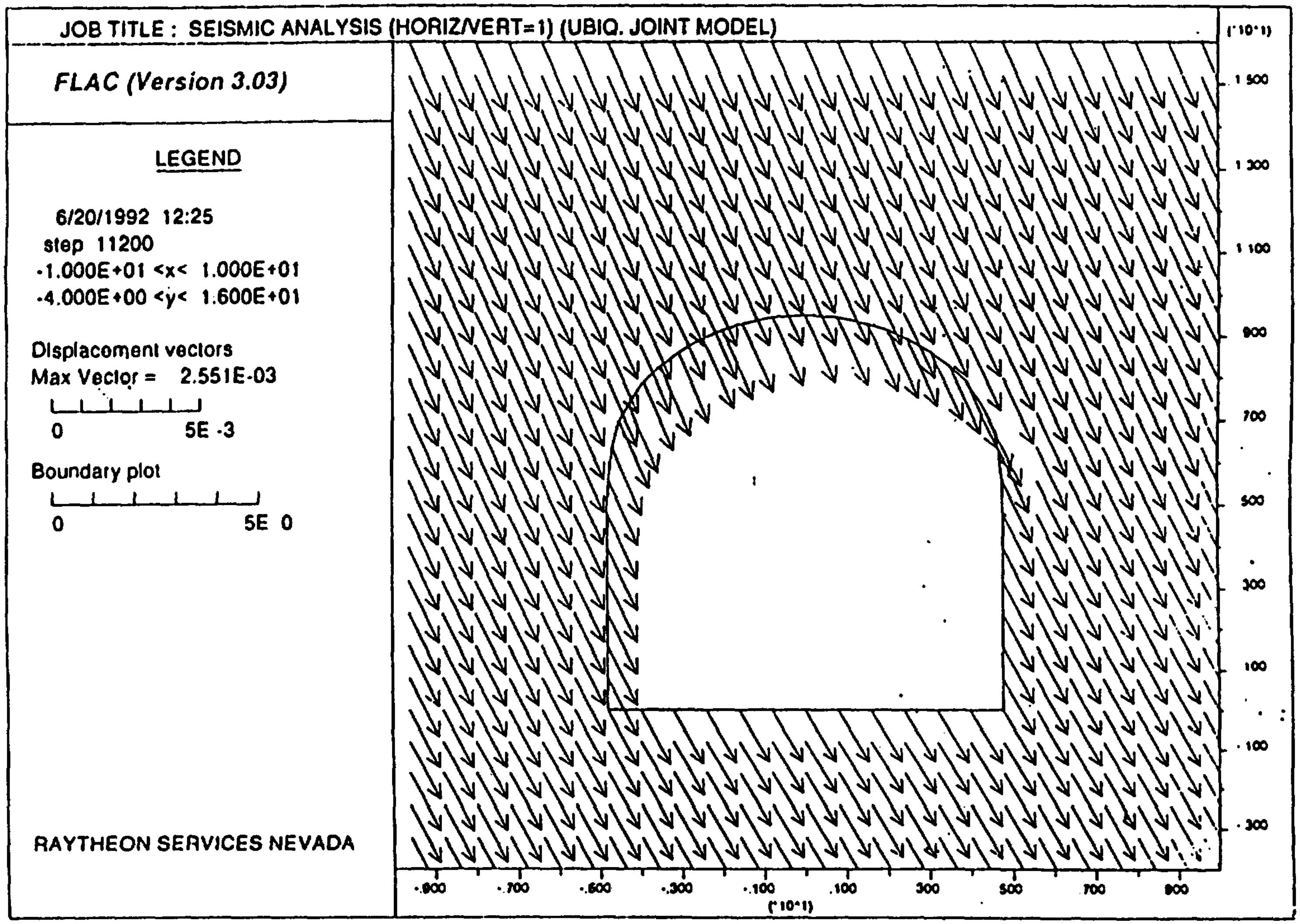

Fig. 69 Displacement Vectors around the Tunnel Opening at Seismic Event with Horizontal and Vertical Components of Acceleration of 0.75g, Ubiquitous Joint Model (Case 1). Compression is Negative.

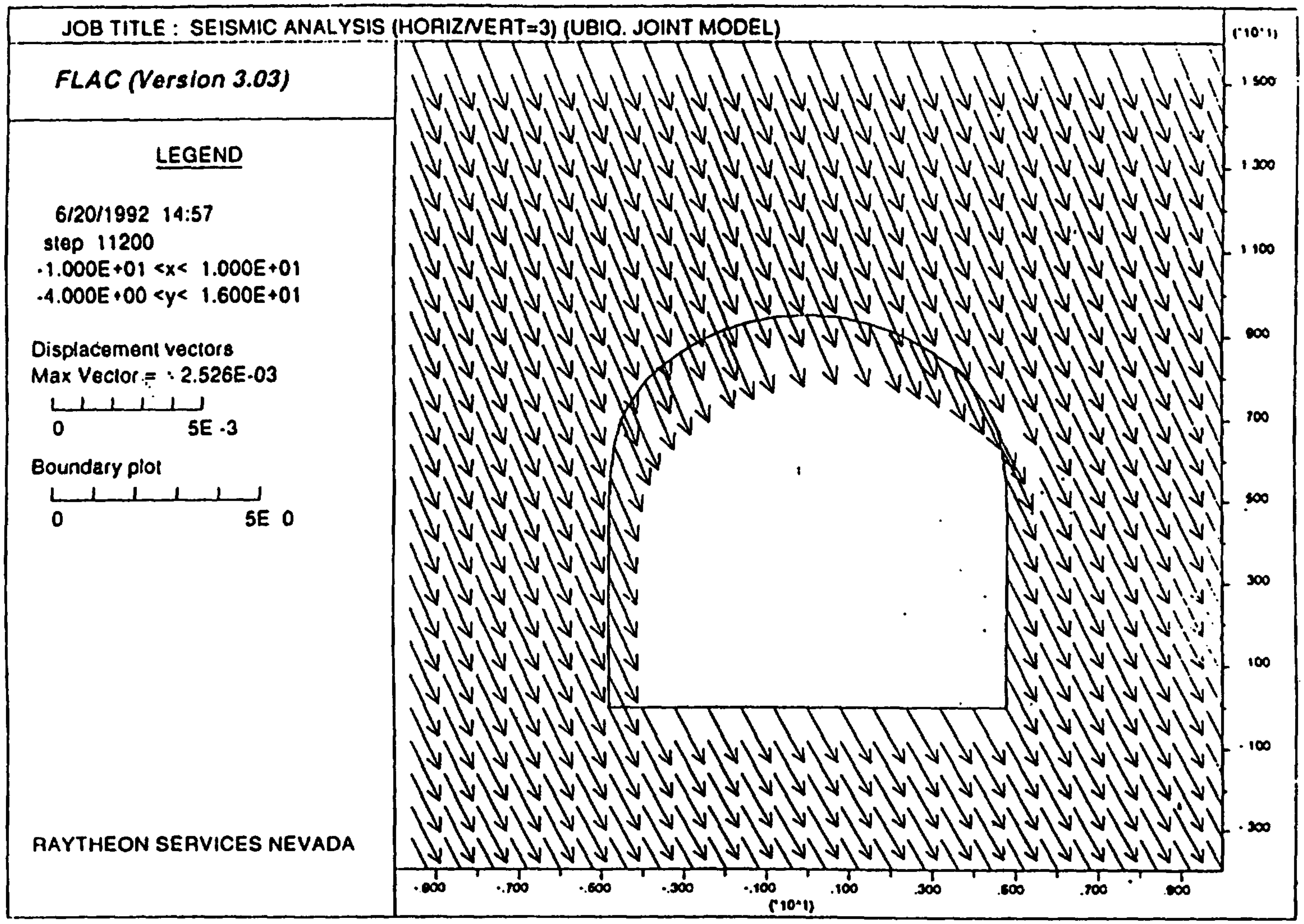

Fig. 70 Displacement Vectors around the Tunnel Opening at Seismic Event with Horizontal and Vertical Components of Acceleration of 0.75g, Ubiquitous Joint Model (Case 2). Compression is Negative.

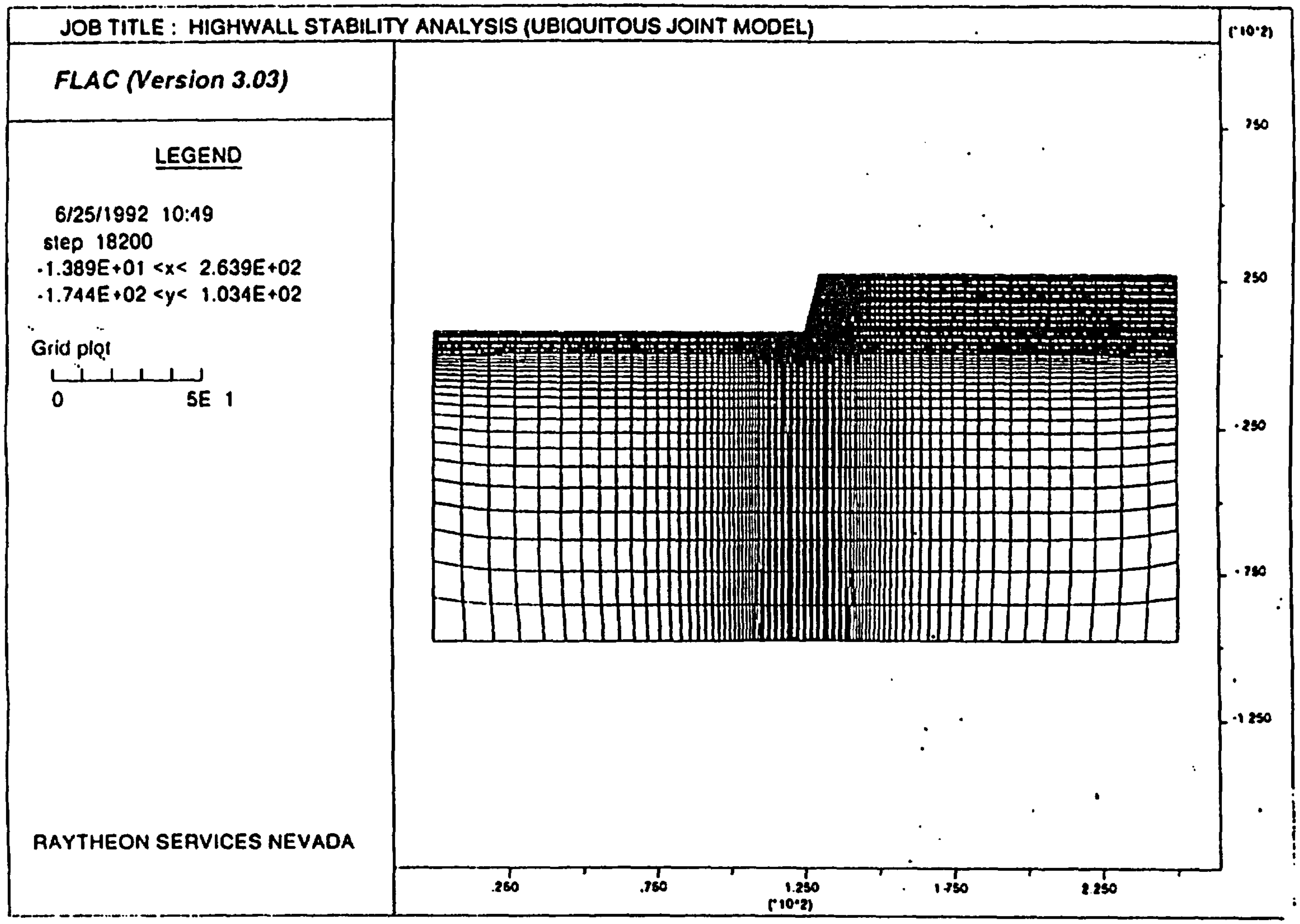

Fig. 71 Finite Difference Mesh Used for the Highwall Seismic Analyses.

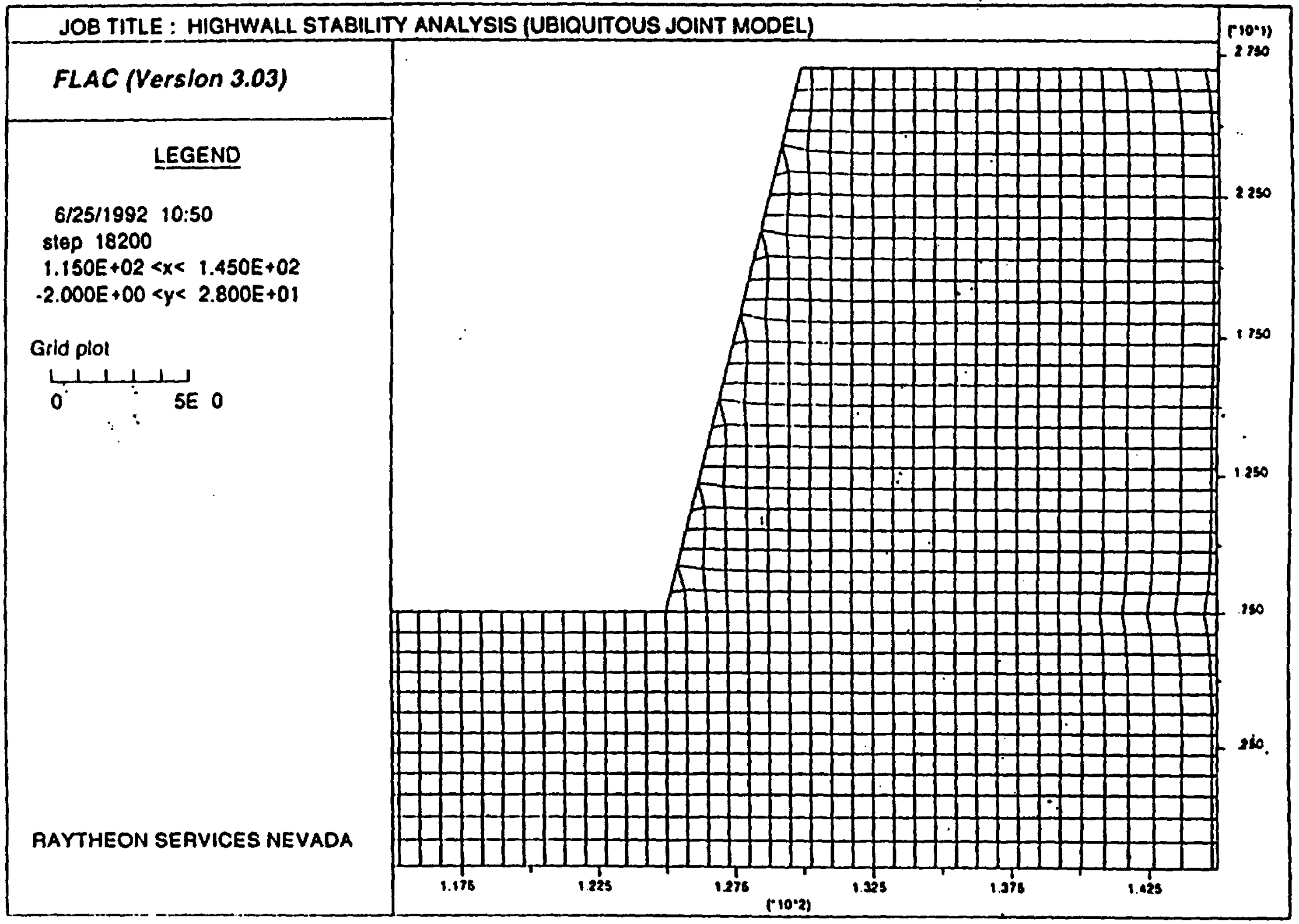

Fig. 72 Close-up of the Grid for the Highwall.

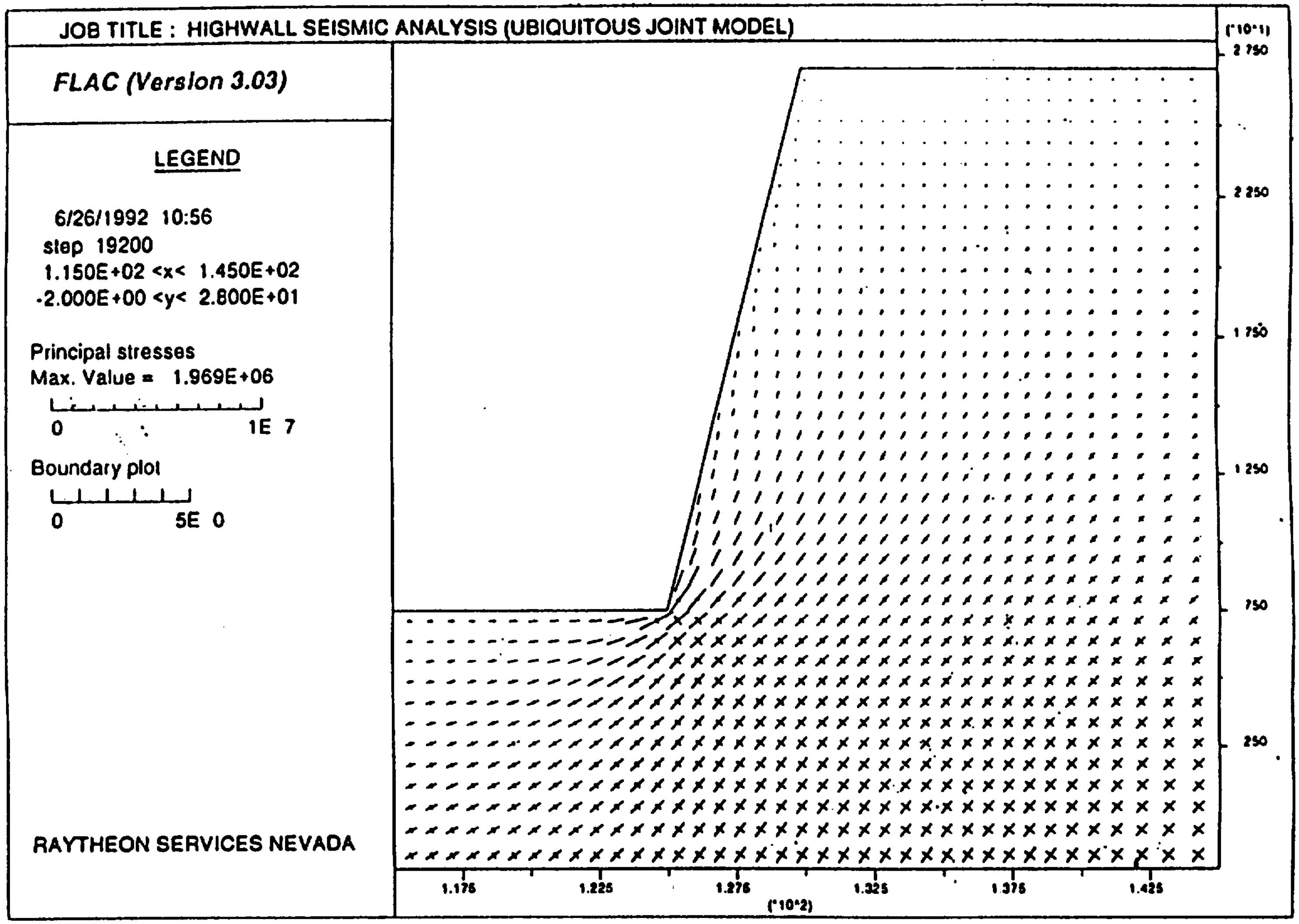

Fig. 73 Principal Stress Vectors along the Highwall at Seismic Event with Horizontal and Vertical Components of Acceleration of 0.5g, Ubiquitous Joint Model (Case 1). Compression Is Negative. Stresses are in Pascal.

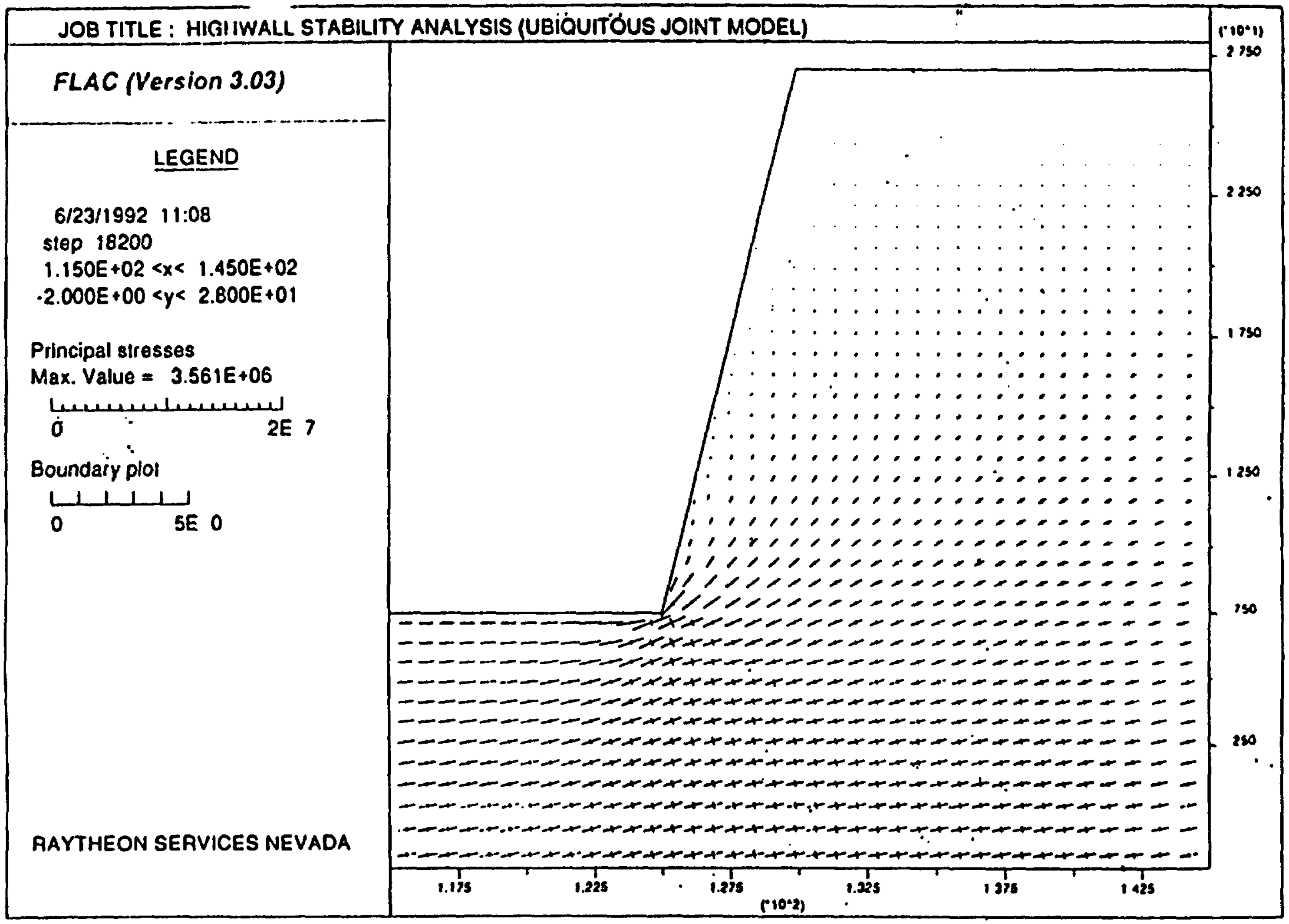

Fig. 74 Principal Stress Vectors along the Highwall at Seismic Event with Horizontal and Vertical Components of Acceleration of 0.5g, Ubiquitous Joint Model (Case 2). Compression Is Negative. Stresses are in Pascal.

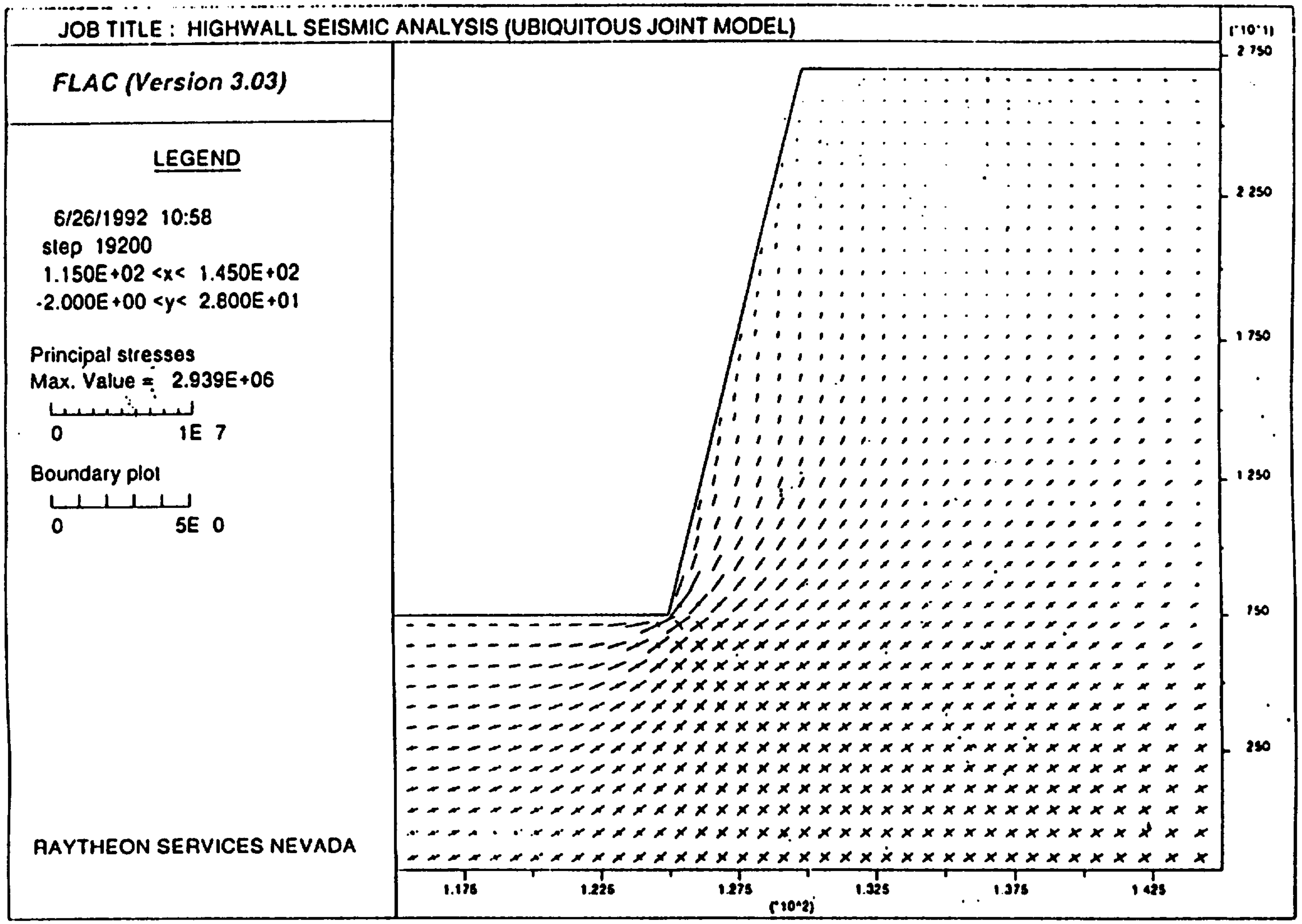

Fig. 75 Principal Stress Vectors along the Highwall at Seismic Event with Horizontal and Vertical Components of Acceleration of 0.75g, Ubiquitous Joint Model (Case 1). Compression Is Negative. Stresses are in Pascal.

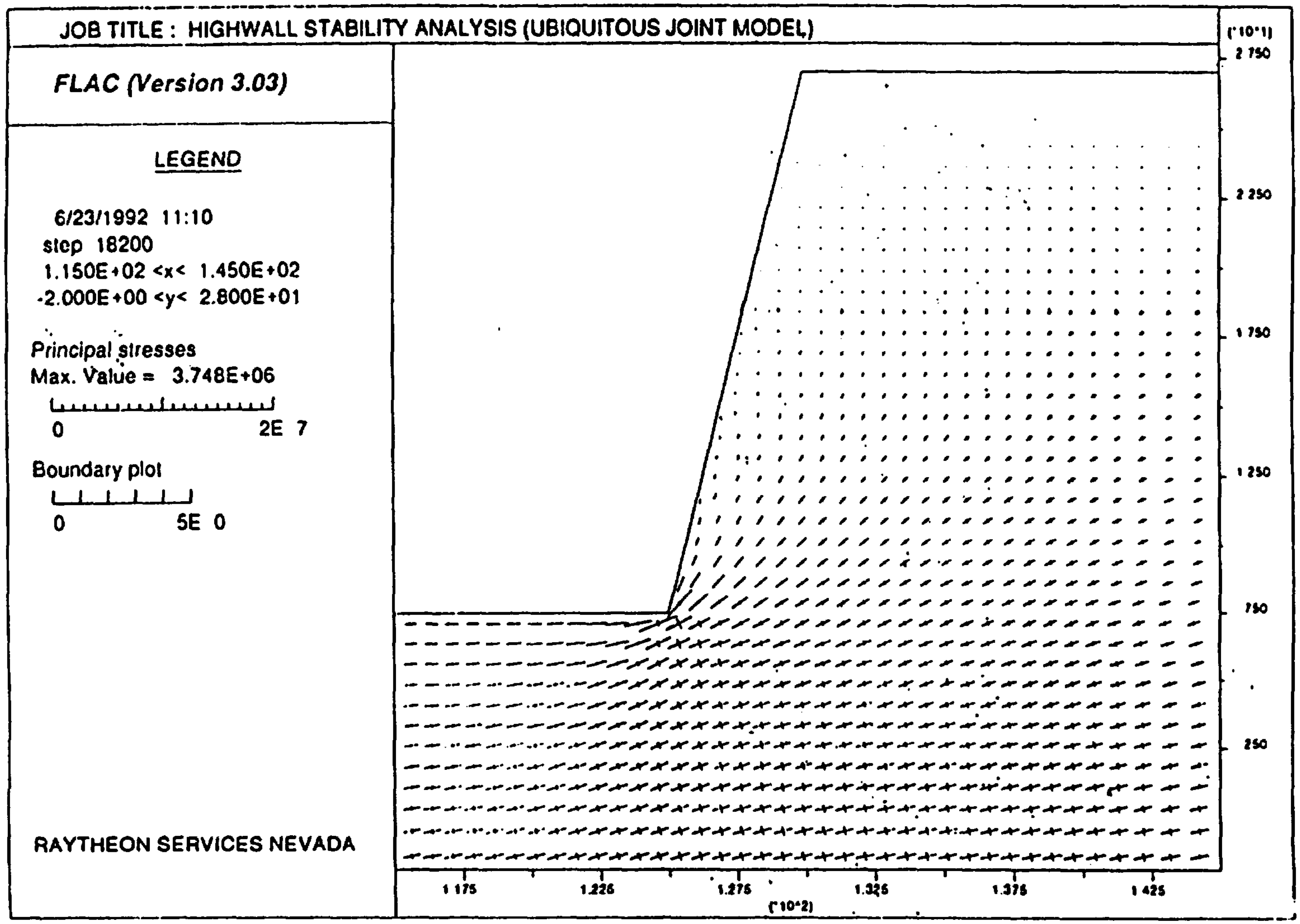

Fig. 76 Principal Stress Vectors along the Highwall at Seismic Event with Horizontal and Vertical Components of Acceleration of 0.75g, Ubiquitous Joint Model (Case 2). Compression Is Negative. Stresses are in Pascal.

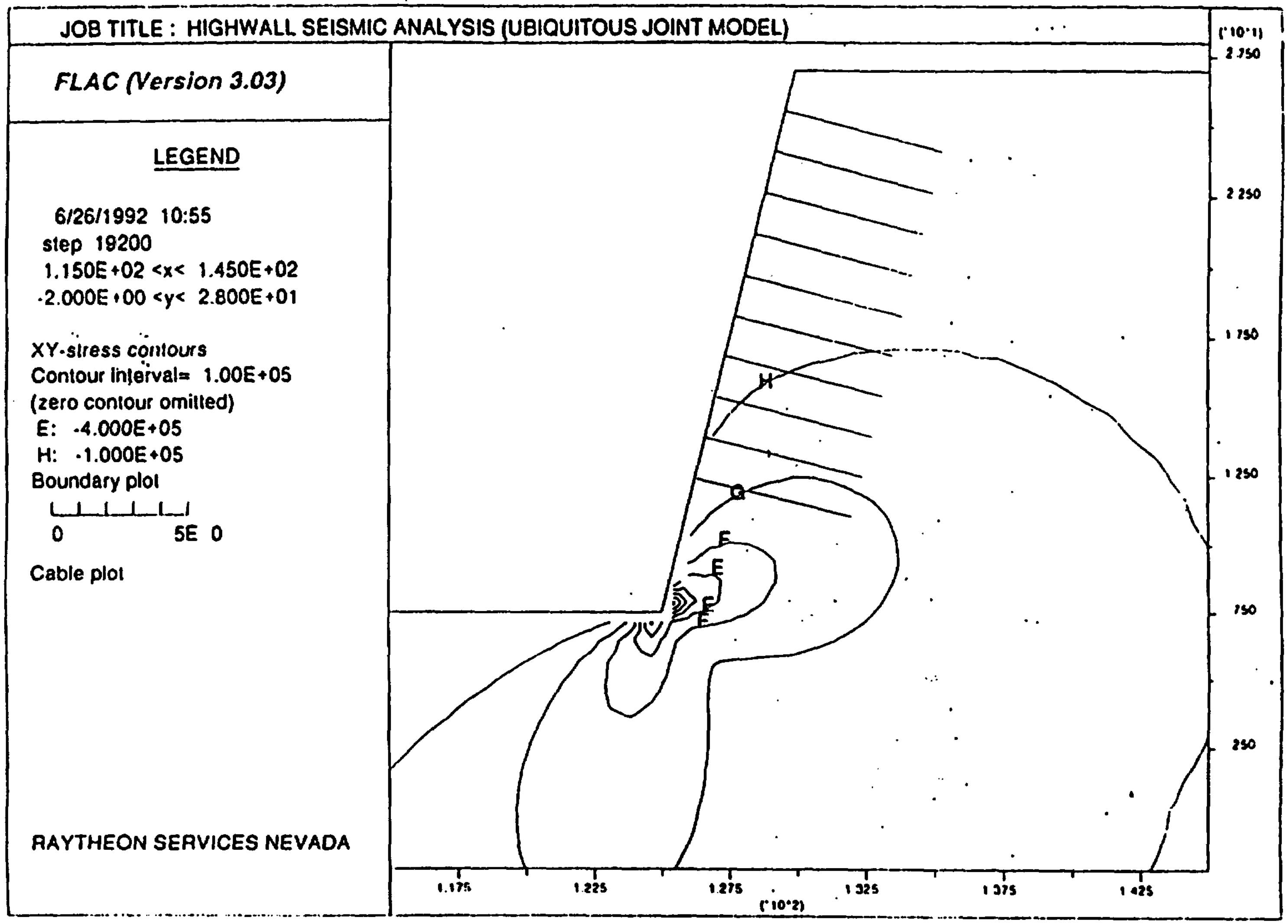

Fig. 77 Shear Stress Contours along the Highwall at Seismic Event with Horizontal and Vertical Components of Acceleration of 0.5g, Ubiquitous Joint Model (Case 1). Compression Is Negative. Stresses are in Pascal.

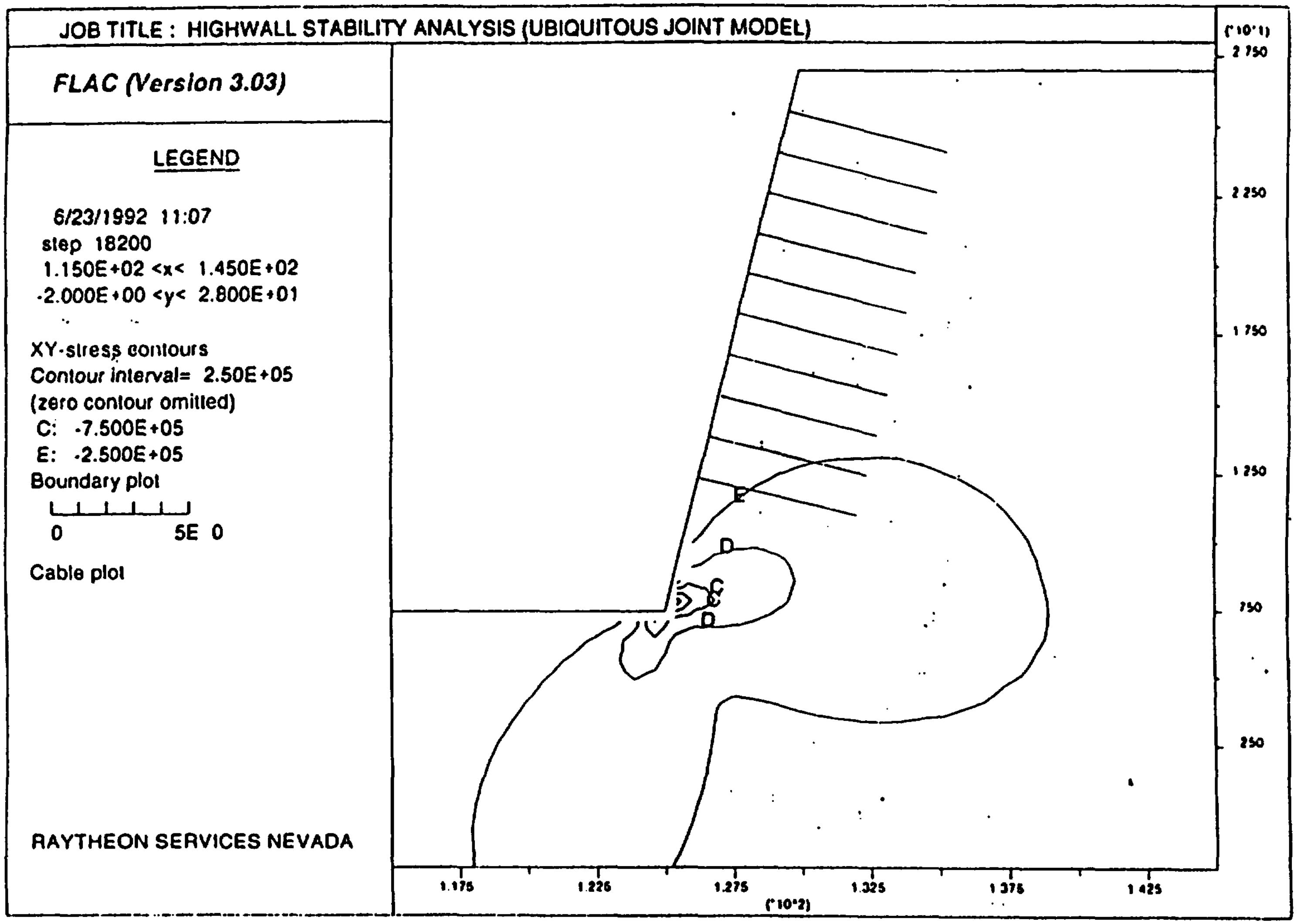

Fig. 78 Shear Stress Contours along the Highwall at Seismic Event with Horizontal and Vertical Components of Acceleration of 0.5g, Ubiquitous Joint Model (Case 2). Compression Is Negative. Stresses are in Pascal.

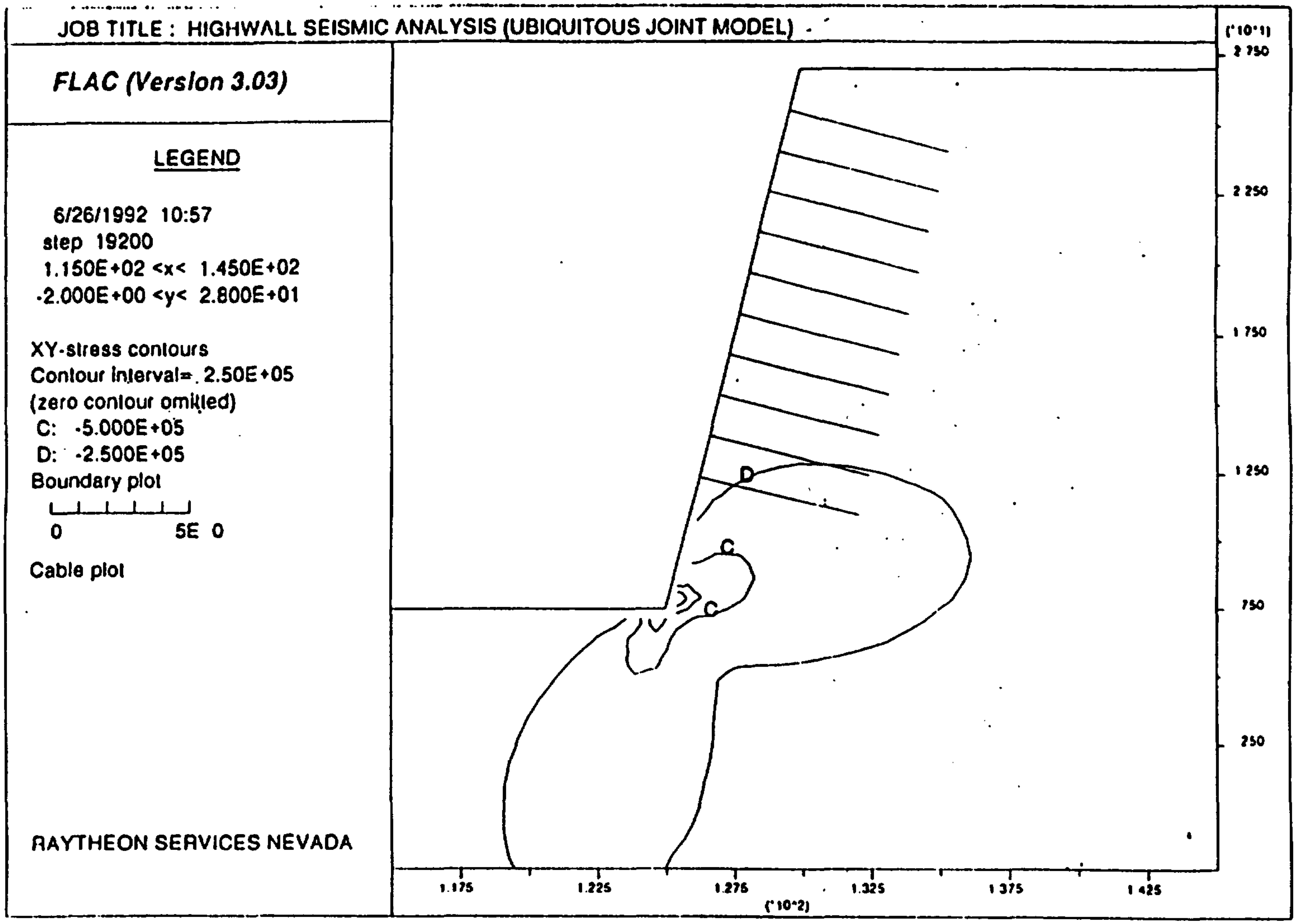

Fig. 79 Shear Stress Contours along the Highwall at Seismic Event with Horizontal and Vertical Components of Acceleration of 0.75g, Ubiquitous Joint Model (Case 1). Compression Is Negative. Stresses are in Pascal.

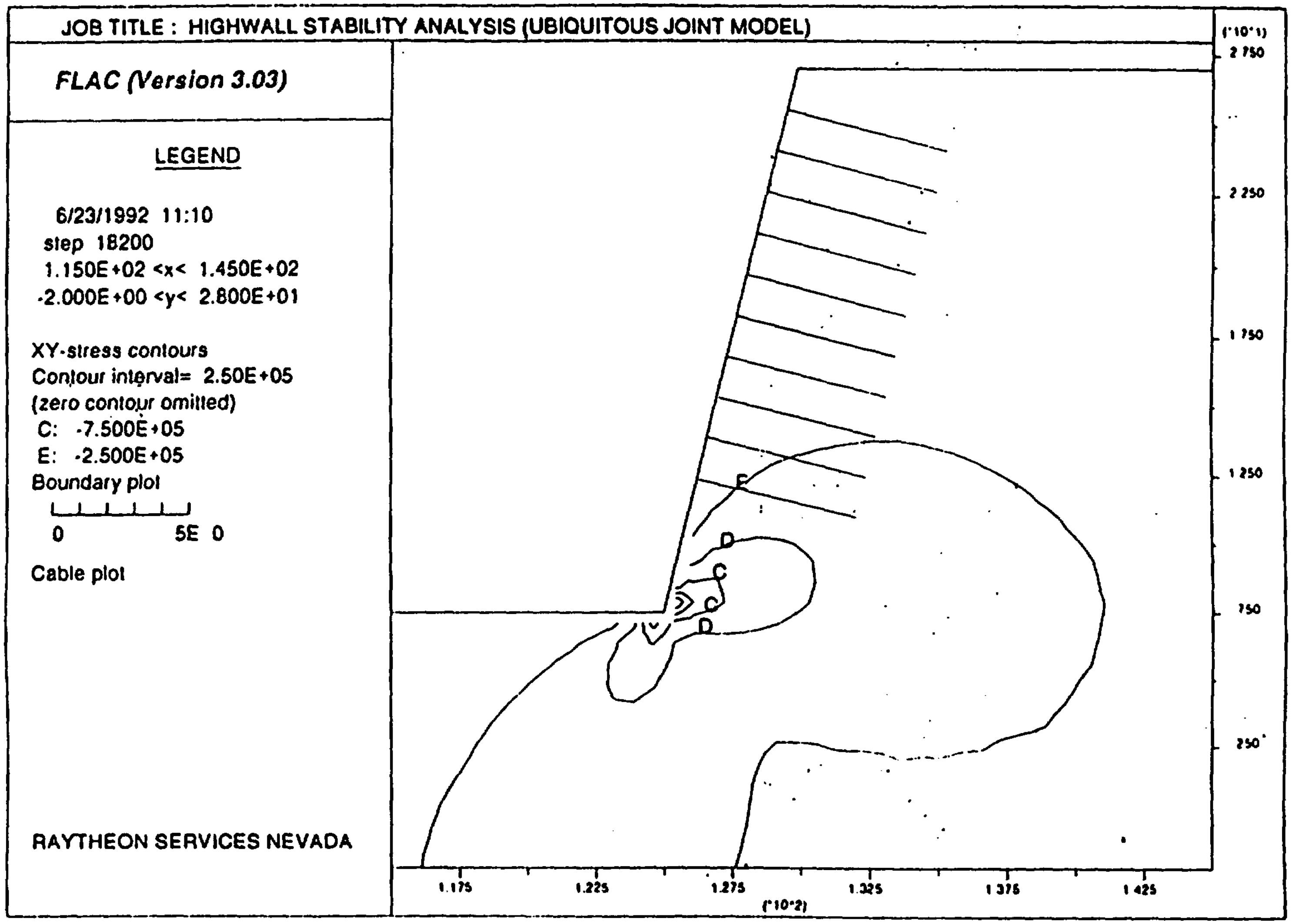

Fig. 80 Shear Stress Contours along the Highwall at Seismic Event with Horizontal and Vertical Components of Acceleration of 0.75g, Ubiquitous Joint Model (Case 2). Compression Is Negative. Stresses are in Pascal.

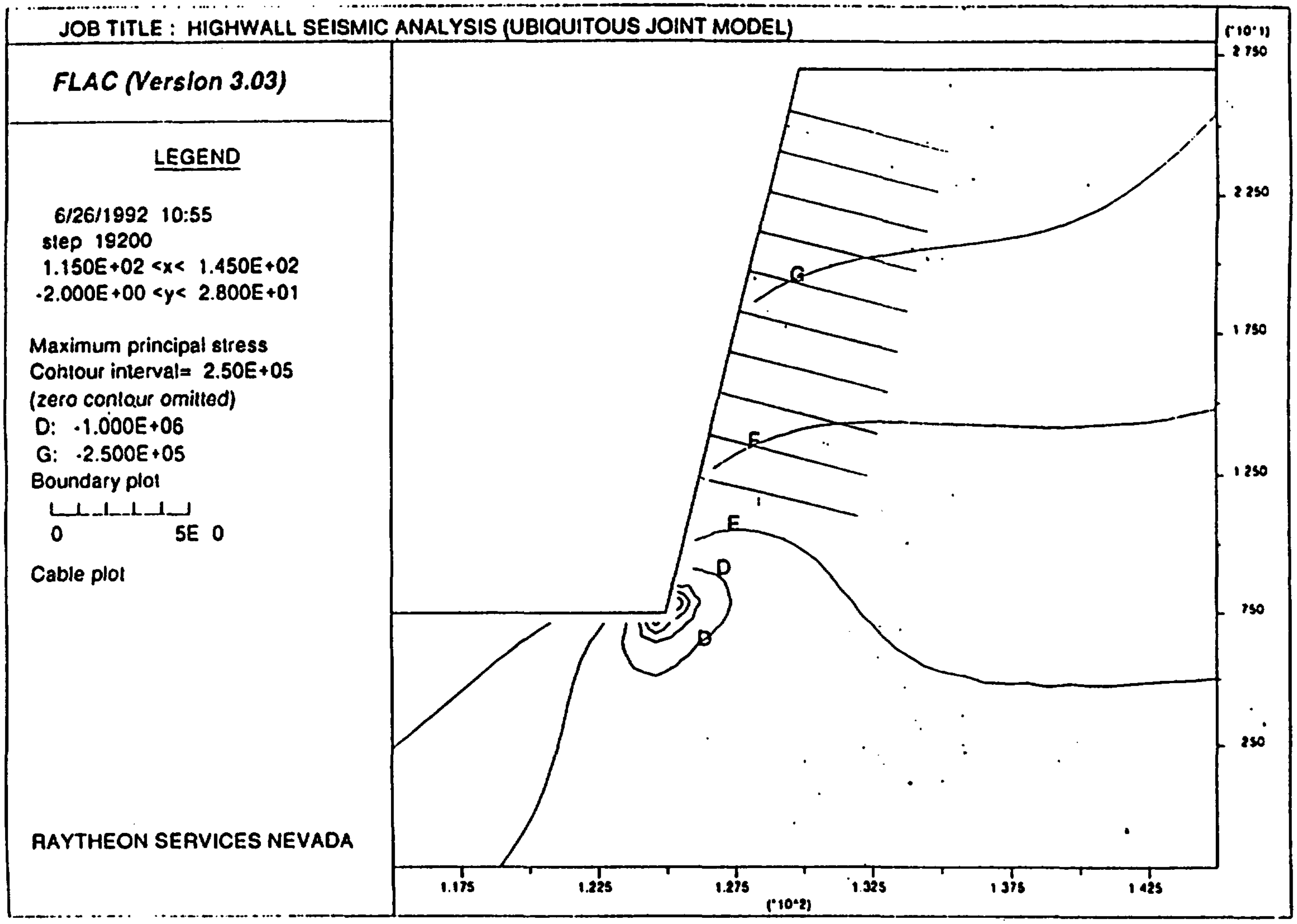

Fig. 81 Maximum Principal Stress Contours along the Highwall at Seismic Event with Horizontal and Vertical Components of Acceleration of 0.5g, Ubiquitous Joint Model (Case 1). Compression Is Negative. Stresses are in Pascal.

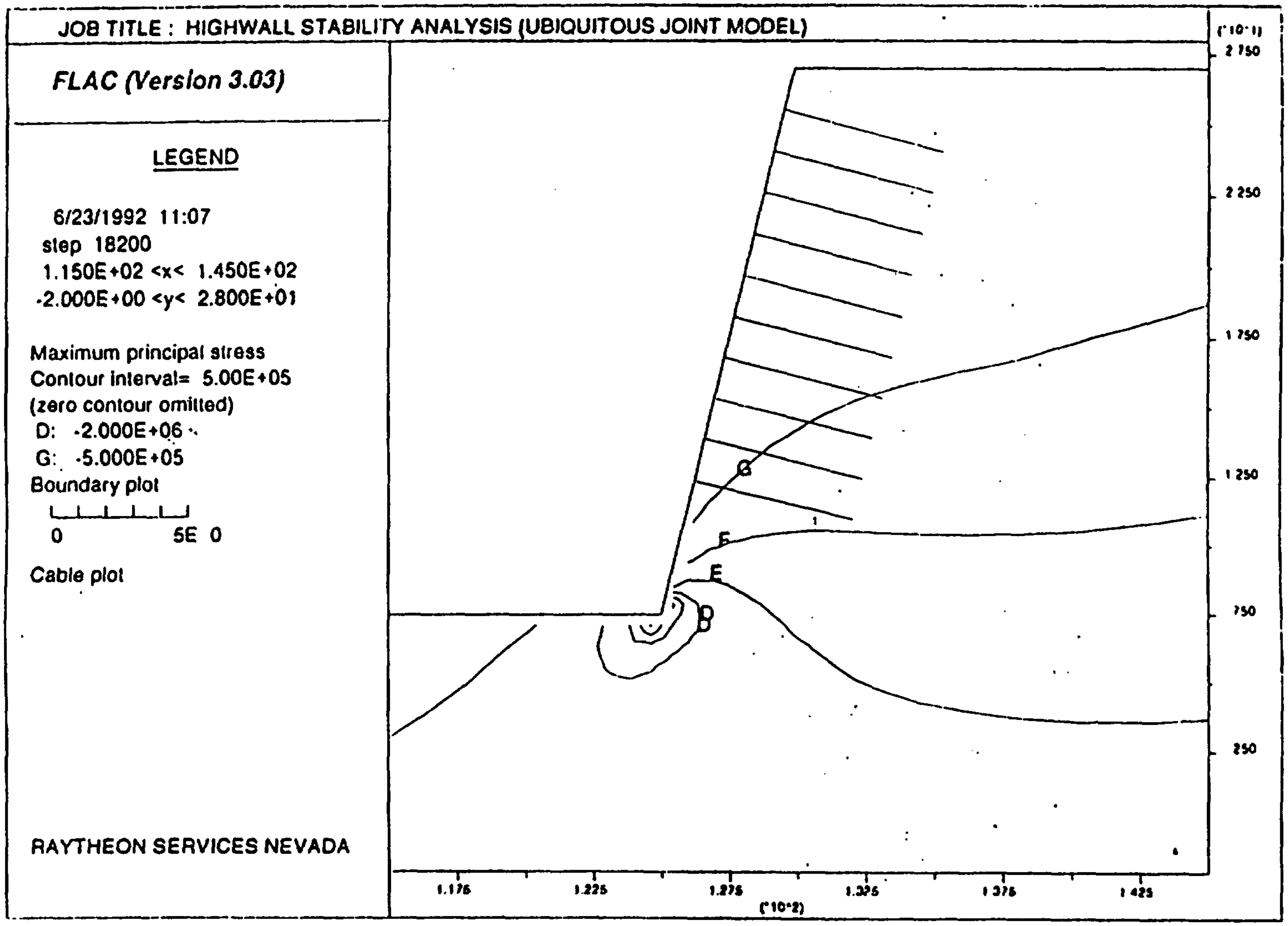

Fig. 82 Maximum Principal Stress Contours along the Highwall at Seismic Event with Horizontal and Vertical Components of Acceleration of 0.5g, Ubiquitous Joint Model (Case 2). Compression Is Negative. Stresses are in Pascal.

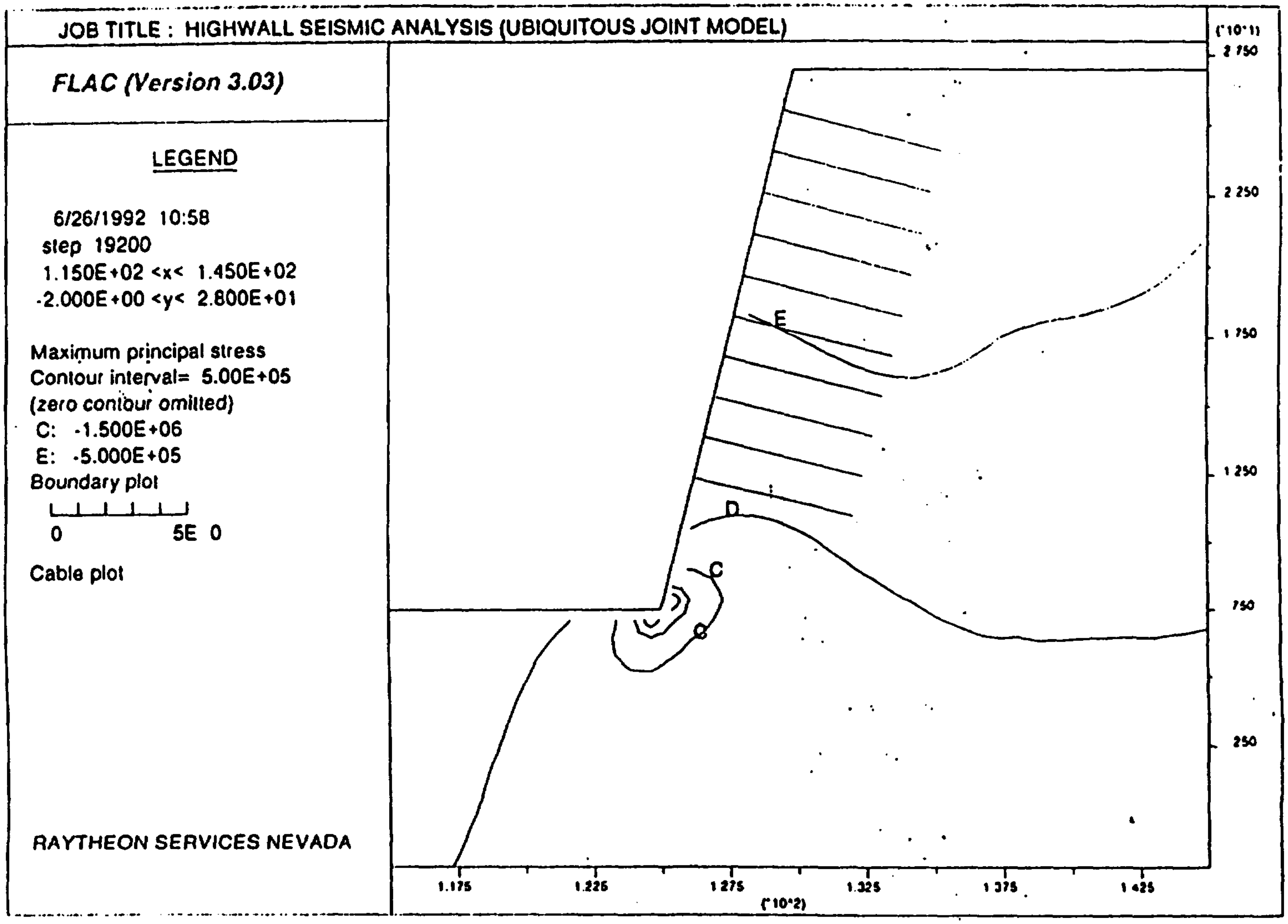

Fig. 83 Maximum Principal Stress Contours along the Highwall at Seismic Event with Horizontal and Vertical Components of Acceleration of 0.75g, Ubiquitous Joint Model (Case 1). Compression Is Negative. Stresses are in Pascal.

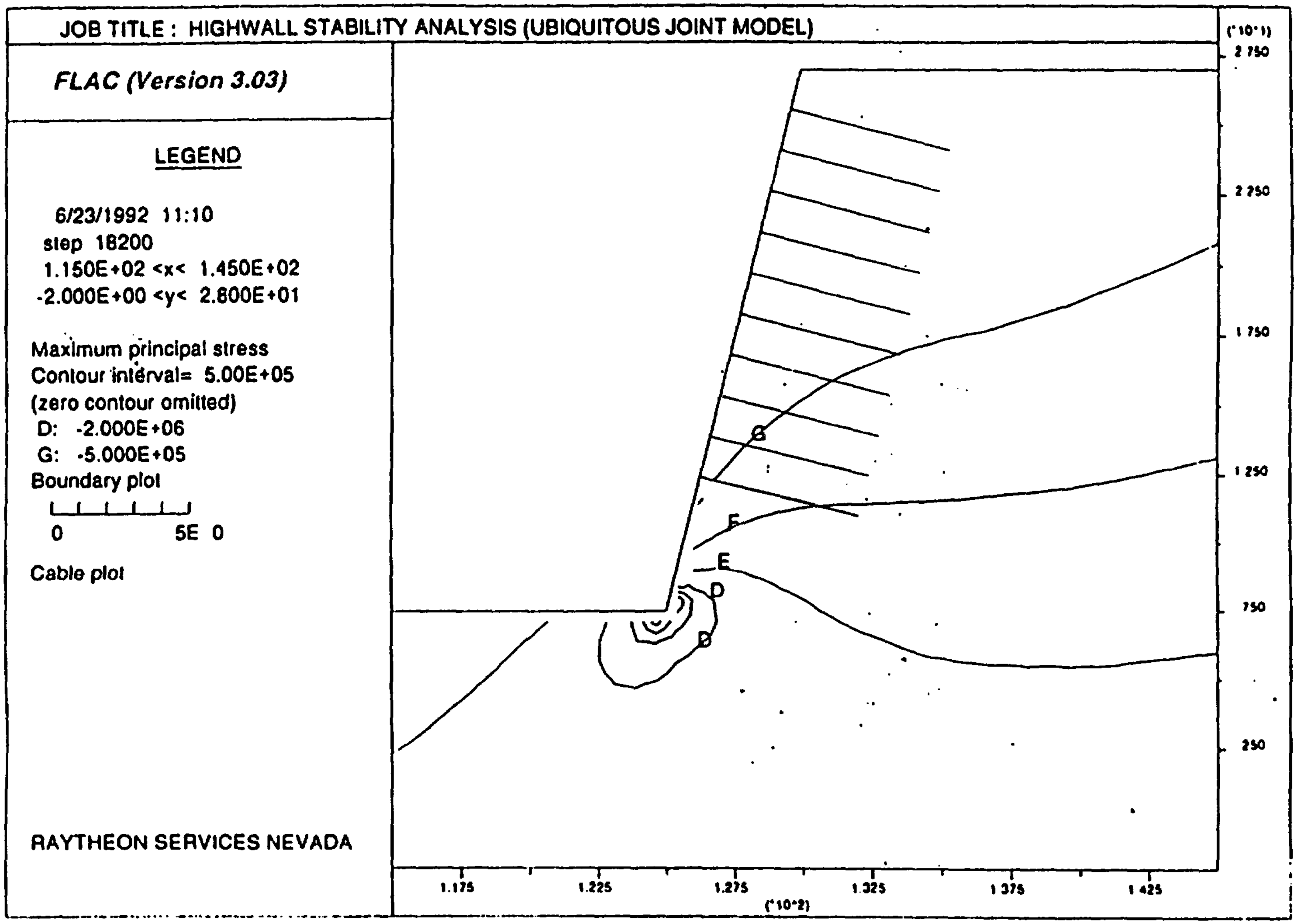

Fig. 84 Maximum Principal Stress Contours along the Highwall at Seismic Event with Horizontal and Vertical Components of Acceleration of 0.75g, Ubiquitous Joint Model (Case 2). Compression Is Negative. Stresses are in Pascal.

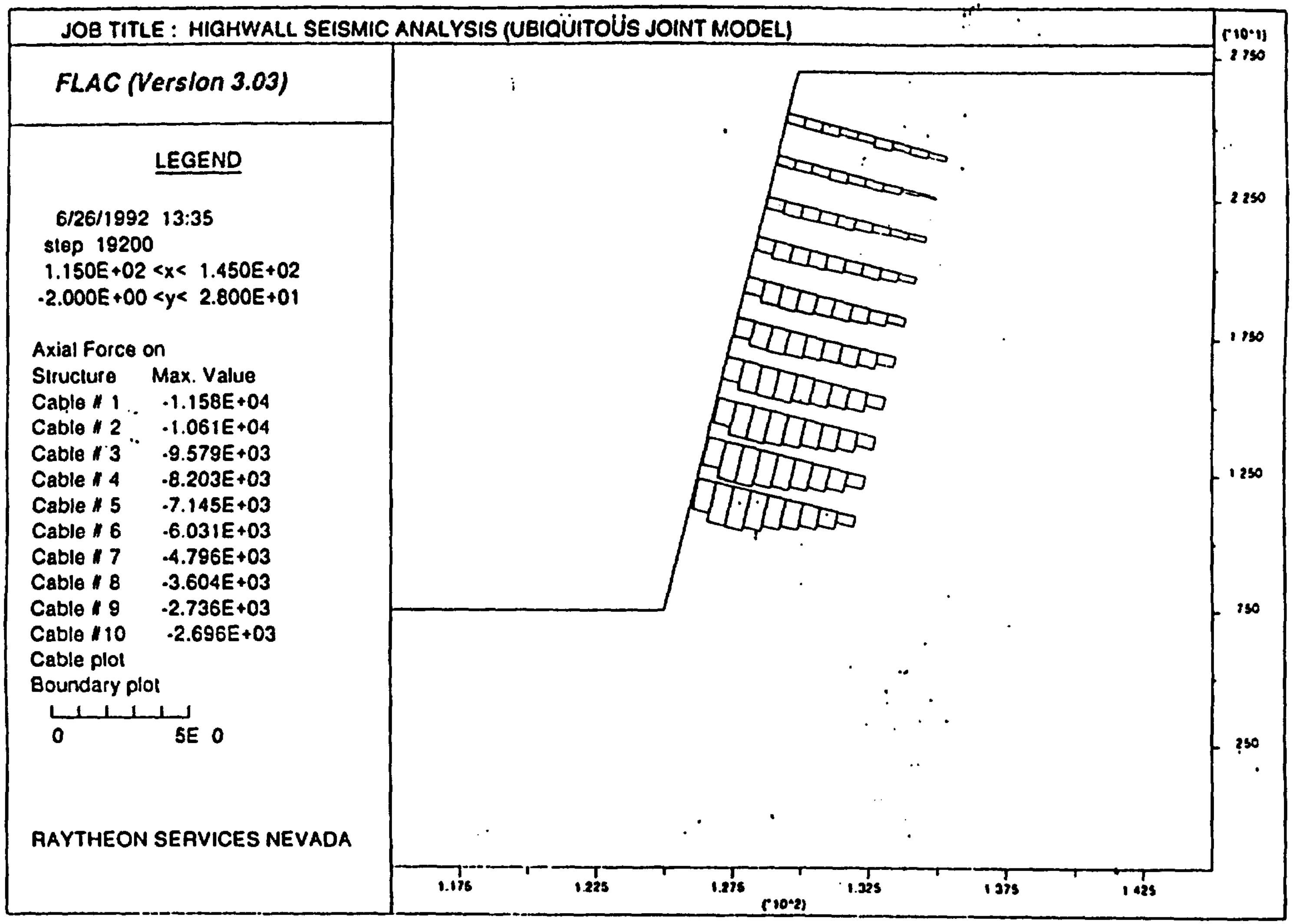

Fig. 85 Axial Force in Bolts at Seismic Event with Horizontal and Vertical Components of Acceleration of 0.5g, Ubiquitous Joint Model (Case 1). Forces are in Newton. Bolts are Numbered from Bottom to Top.

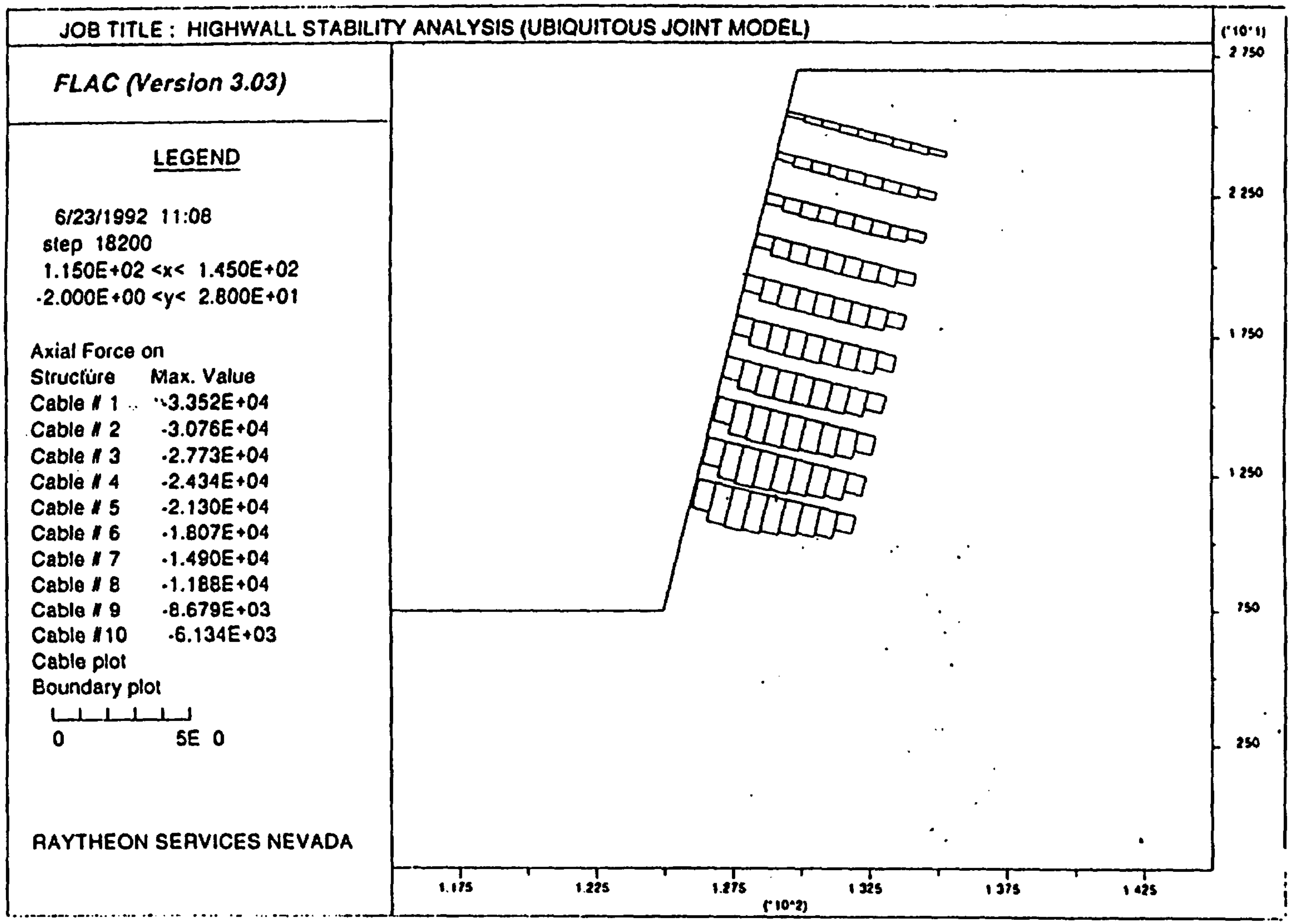

Fig. 86 Axial Force in Bolts at Seismic Event with Horizontal and Vertical Components of Acceleration of 0.5g, Ubiquitous Joint Model (Case 2). Forces are in Newton. Bolts are Numbered from Bottom to Top.

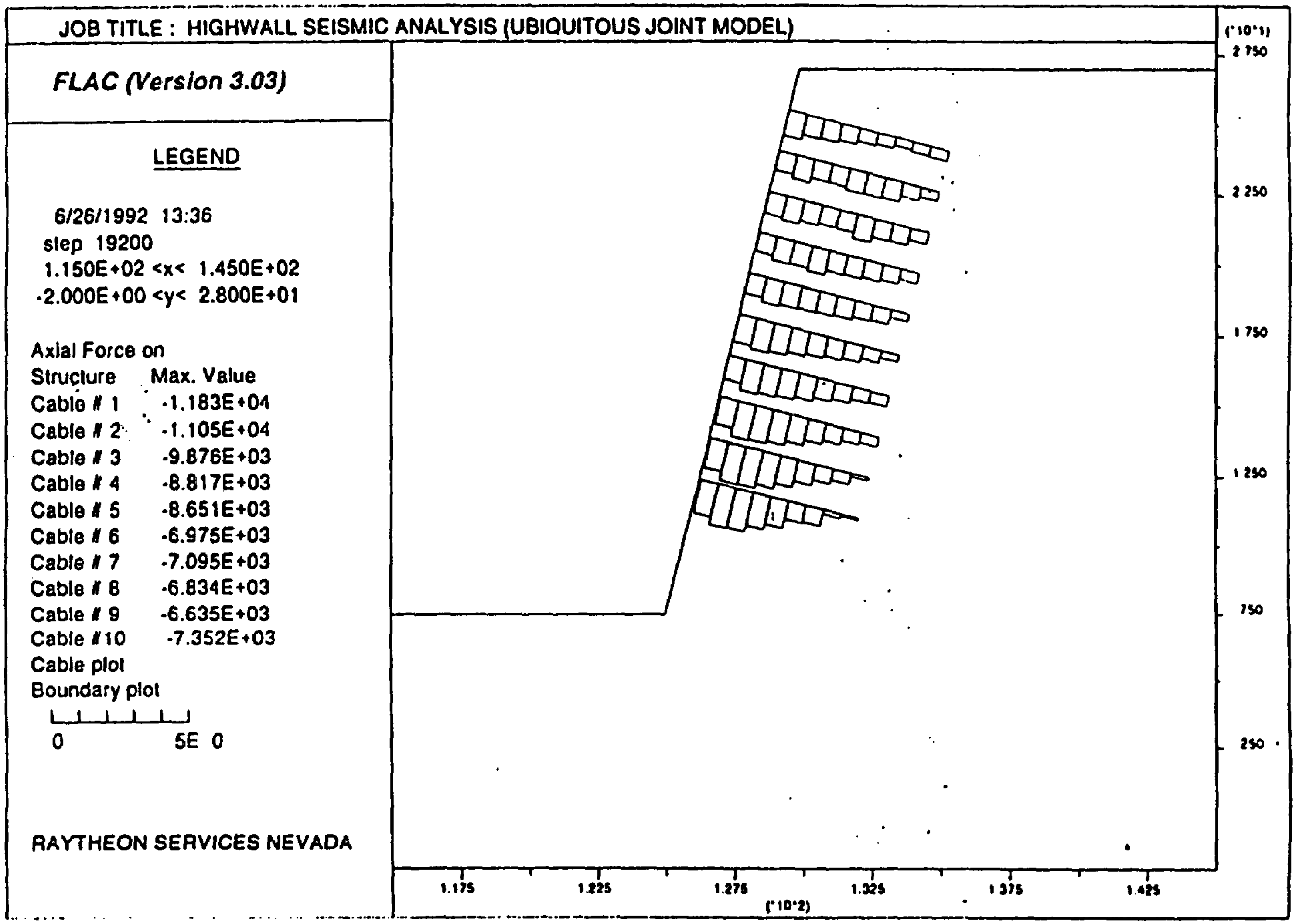

Fig. 87 Axial Force in Bolts at Seismic Event with Horizontal and Vertical Components of Acceleration of 0.75g, Ubiquitous Joint Model (Case 1). Forces are in Newton. Bolts are Numbered from Bottom to Top.

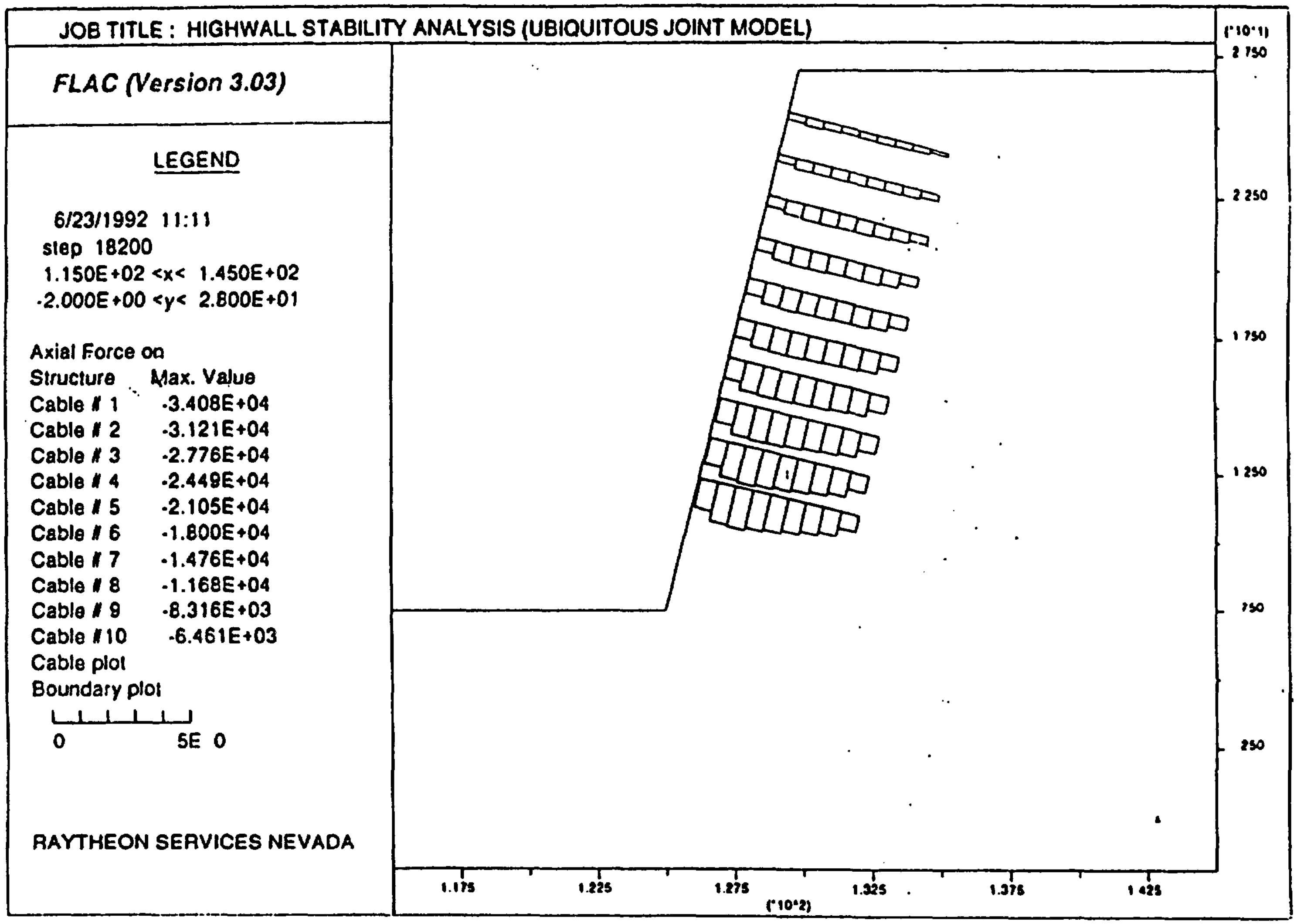

Fig. 88 Axial Force in Bolts at Seismic Event with Horizontal and Vertical Components of Acceleration of 0.75g, Ubiquitous Joint Model (Case 2). Forces are in Newton. Bolts are Numbered from Bottom to Top.

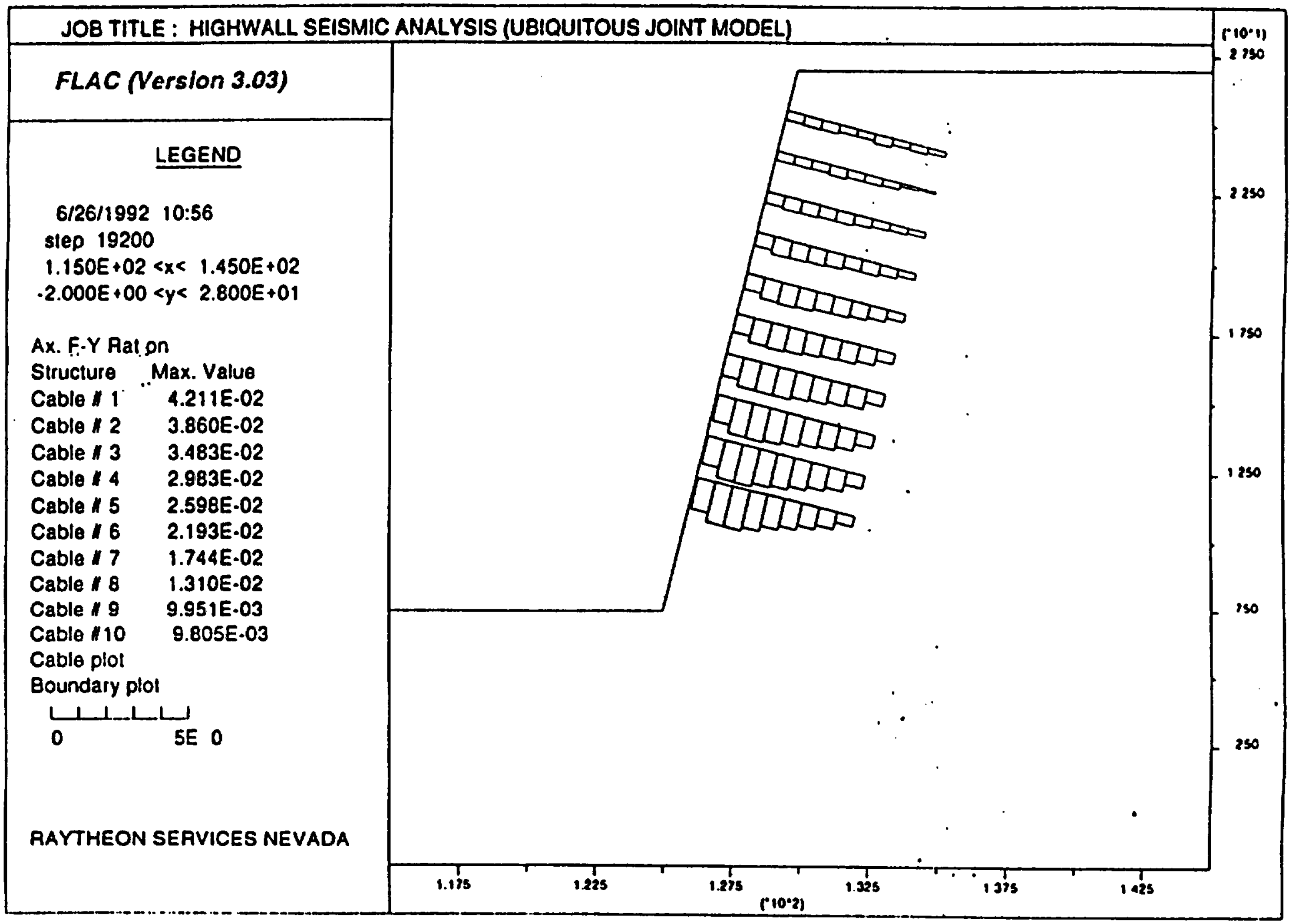

Fig. 89 Ratio of Axial Load to Yield Strength of Bolts at Seismic Event with Horizontal and Vertical Components of Acceleration of 0.5g, Ubiquitous Joint Model (Case 1). Bolts are Numbered from Bottom to Top.

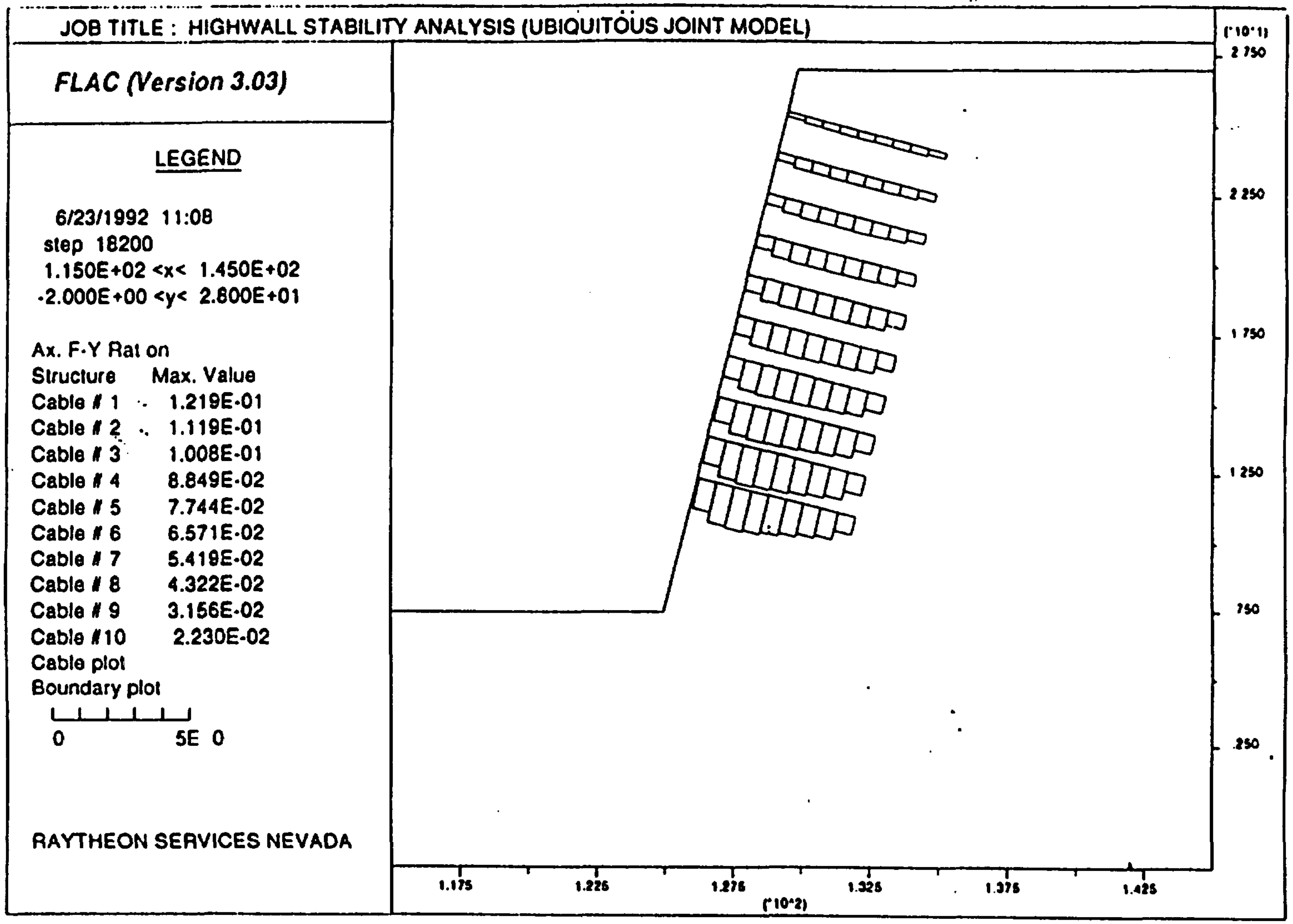

Fig. 90 Ratio of Axial Load to Yield Strength of Bolts at Seismic Event with Horizontal and Vertical Components of Acceleration of 0.5g, Ubiquitous Joint Model (Case 2). Bolts are Numbered from Bottom to Top.

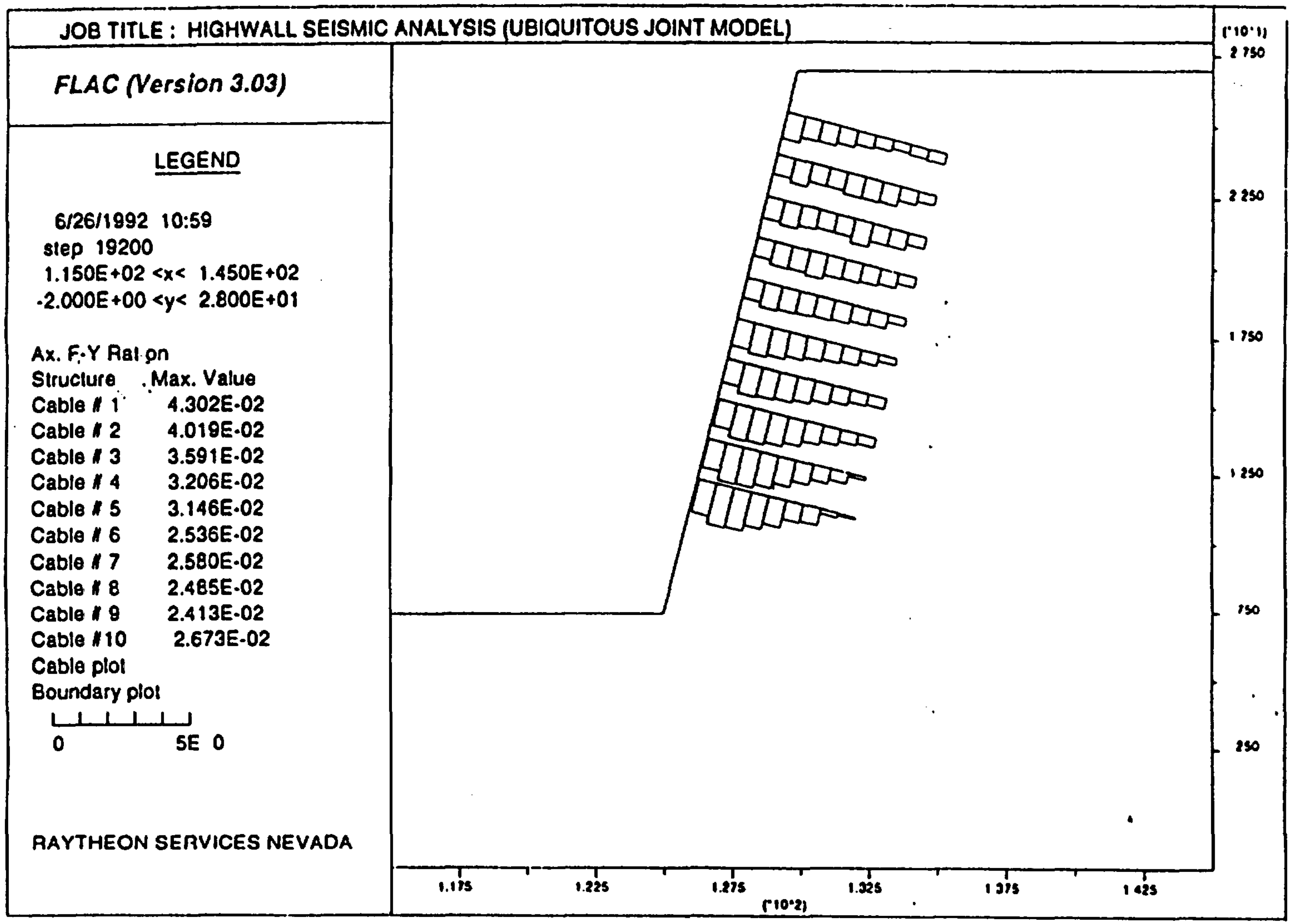

Fig. 91 Ratio of Axial Load to Yield Strength of Bolts at Seismic Event with Horizontal and Vertical Components of Acceleration of 0.75g, Ubiquitous Joint Model (Case 1). Bolts are Numbered from Bottom to Top.

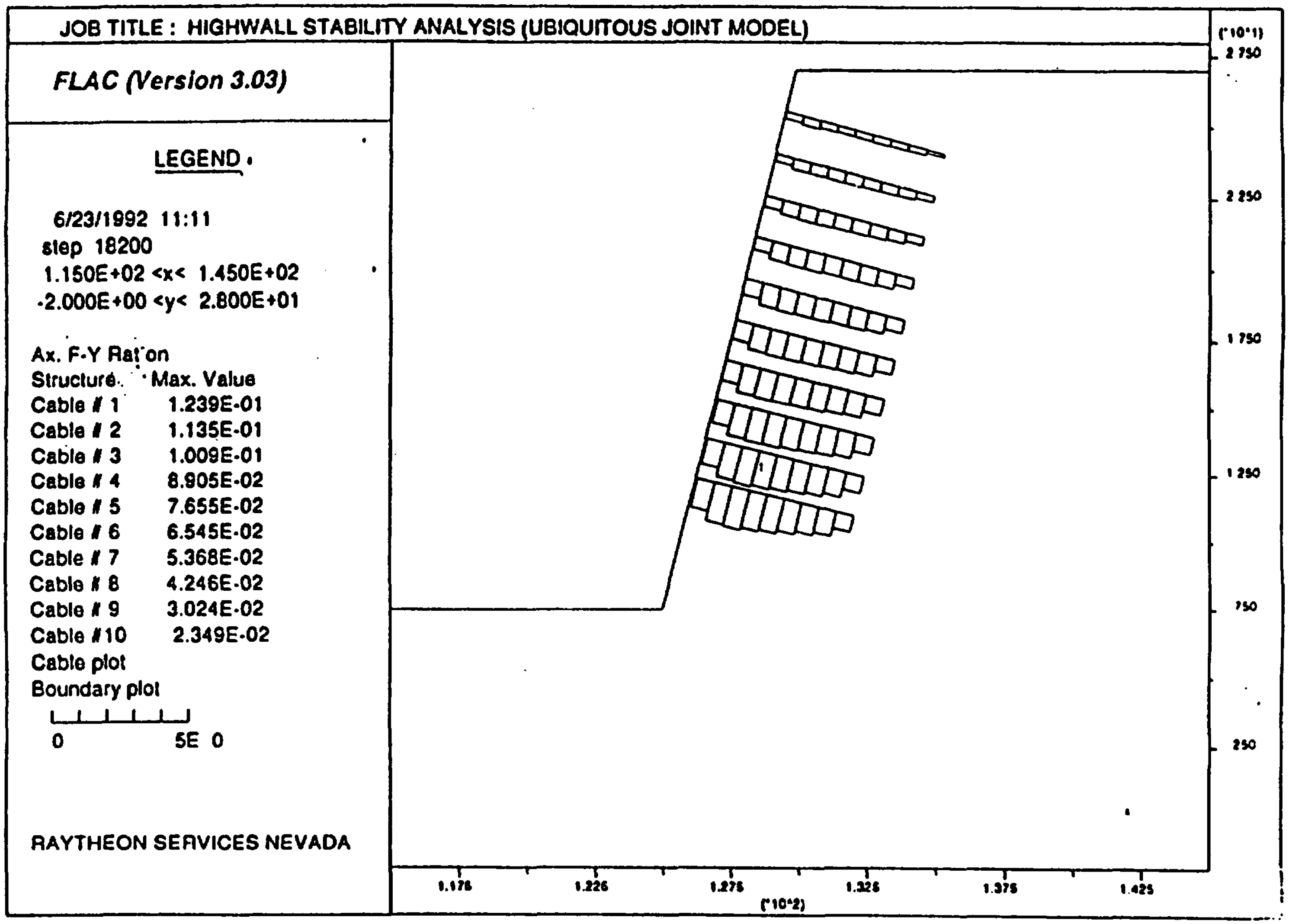

Fig. 92 Ratio of Axial Load to Yield Strength of Bolts at Seismic Event with Horizontal and Vertical Components of Acceleration of 0.75g, Ubiquitous Joint Model (Case 2). Bolts are Numbered from Bottom to Top.